UCRL - 76207
PREPRINT
Conf-741131--3

LAWRENCE LIVERMORE LABORATORY
University of California/Livermore, California

RECENT DEVELOPMENTS IN THE DESCRIPTION OF ODD-MASS NUCLEI

R. A. Meyer

November 4, 1974

This paper was prepared for submittal to Proceedings of the International Conference on Gamma-Ray Transition Probabilities, Delhi, India, Nov. 11-15, 1974, Vol. I: Invited Lectures

RECENT DEVELOPMENTS IN THE DESCRIPTION OF ODD-MASS NUCLEI*

R. A. Meyer
Lawrence Livermore Laboratory, University of California
Livermore, California 94550

ABSTRACT

A detailed survey of the medium-mass region ($60 < A < 140$) of the nuclear chart has been made to compare a number of recent theoretical calculations with the significant body of experimental information coming into the published literature. A comparison of the level properties of the $Z = 51$ antimony nuclei shows very good agreement with the recent calculations of Vanden Berghe, who includes two-particle one-hole configurations. The level structure and electromagnetic properties of the Z or $N = 53$ nuclei are not predicted so well as the antimony nuclei. Inclusion of three-particle clustering has improved the agreement between calculated and experimental electromagnetic transition rates for the low-lying levels in odd-mass nuclei. More recent calculations using a dressed quasi-particle formalism are shown to have some success. The detailed experimental study of odd-mass iodine near the neutron shell closure at $N = 82$ suggests that the particle-core interaction can account for a majority of the levels observed, if one uses an even-even core that includes known low-lying two-proton states.

*Work performed under the auspices of the U. S. Atomic Energy Commission.

The nonnormal parity states in a given shell have higher J values than the normal parity states (e.g., $h_{11/2}$ in the g-d-s shell). This can cause significant deviations from the expected vibrational character. Studies of the odd-mass Z = 57 lanthanum nuclei suggest that the Coriolis force and its effect on high-J state coupling to the core can be used to account for the excess negative-parity states observed in the lathanum nuclei and their electromagnetic decay properties. The deformability of the cadmium (Z = 48) core and the Coriolis force may be the causes of apparent rotationlike level structure observed in the experimental studies of the odd-mass indium nuclei. These results suggest that more attention should be paid to the inclusion of a dynamic rather than static core and that the Coriolis force should be included as part of any complete, effective interaction.

INTRODUCTION

A number of improvements have been made in the description of vibrationlike nuclei in the past few years. Several of these improvements have been suggested by experimental studies of electromagnetic transitions in nuclei either alone or in conjunction with reaction spectroscopy studies. A number of these can be illustrated by a discussion of the odd-mass nuclei in the region of the nuclear chart bounded by Z of approximately 50 and $N < 82$.

The inclusion of three-quasi-particle effects can provide a model that is consistent with the results of various experimental studies. We will consider three examples. First, how incorporation of two-particle, one-hole (2p 1h) states can lead to a good description of the odd-mass antimony nuclei. Second, how the recognition of three-particle clustering or alternately dressed n-quasi-particle configurations may lead to an understanding of odd-mass nuclei such as iodine. Third, how recent gamma-ray spectroscopy studies may explain the apparent deviation from vibrationlike character of the $N = 81$ nuclei.

The recognition of the role of the Coriolis force in soft vibrational nuclei may lead to a better description of a large class of nuclei. To illustrate this, we will discuss the recent evidence for the triaxial rotation-aligned bands in the lanthanum nuclei.

There are a large number of new experimental techniques and equipment that have been developed in the past few years. Some mention should be made of devices such as the Compton Suppression Spectrometer,

the LLL PDP-9/disc megachannel gamma-gamma coincidence spectrometer, and the new microcomputor-controlled fast-chemistry system that has been developed at LLL.* Although it is not the purpose of this presentation to cover experimental techniques, I have included a discussion of the above and other techniques in Appendix I.

TWO-PARTICLE, ONE-HOLE STATES

The low-energy-level structure systematics for the odd-mass antimony (Z = 51) nuclei are shown in Fig. 1, where the insert shows the rapid decrease in energy for all levels with respect to the $g_{7/2}$ orbital as neutron number is decreased.[1-3] A simple, weak-coupling model of single particle and single particle plus phonon cannot adequately account for all of the levels that are observed below the pairing gap in these nuclei. However, reaction spectroscopy studies have suggested that the excess states have strong two-particle, one-hole character (2p 1h).[4] Recently Vanden Berghe and Degrieck[5] have attempted to calculate the structure of the antimony nuclei, taking into account the 2p-1h states and their interaction with the single-particle and phonon-coupled states.

The ^{121}Sb nucleus is an ideal case for studying the nature of the high-spin, positive-parity levels, since both 2p-1h and particle-phonon levels occur within a few hundred keV of each other, as seen in Fig. 2.

*Reference to a company or product name does not imply approval or recommendation of the product by the University of California or the U. S. Atomic Energy Commission to the exclusion of others that may be suitable.

These levels are populated by decay, as well as by Coulomb-excitation techniques. Thus any theoretical calculation is put to a stringent test, for it must not only properly predict the proximity of these levels, but also yield the measured transition moments [B(E2)↑ in particular].

The results of recent gamma-ray spectroscopy studies[6,7] are shown in Fig. 3. The $11/2^+$ level and all four high-spin levels observed in excitation studies are populated in the beta decay of $^{121}Te^m$. Also, the branching ratios for the decay of the three $9/2^+$ levels are quite distinct from each other. The 1035-keV level has only seven parts per thousand populating the ground state, while the 1145-keV decays 73% and the 947-keV level decays 10% of the time to the $5/2^+$ ground state.

The calculations of Vanden Berghe and Degrieck[5] predict all three $9/2^+$, the $7/2^+$, and the $11/2^+$ levels at approximately 1 MeV. The branching ratios from the three $9/2^+$ levels to the ground and first excited states are consistent with their wave functions. The near lack of branching of the 1035-keV level to the $5/2^+$ ground state is understood in terms of a very small $|d_{5/2}\ 12\rangle$ component,* while the preference of decay to the ground state for the 1145-keV level comes from the dominance of the $|d_{5/2}\ 12\rangle$ configuration.[5] The more stringent test of predicting the electric quadrupole transitions is also moderately successful. The experimental vs calculated B(E2)↑ values are listed in Table 1, given in italics on the appropriate transition in Fig. 3,[8-12] and compared graphically in Fig. 4.

The qualitative features of the three $9/2^+$ levels are explained by

*$|j\ N\rangle$ means the j-shell model state coupled to the N^{th} phonon of spin j: thus, $|d_{5/2}\ 12\rangle$ represents the configuration: $d_{5/2}$ on the first 2^+ phonon.

the predicted major configurations. The branching ratios from the three $9/2^+$ levels to the ground and first excited states are consistent with their wave functions. Their results are presented in modified form in Table 2. The near lack of branching of the 1035-keV level to the $5/2^+$ ground state is understood in terms of the lack of the $|d_{5/2}\ 12>$ configuration, while the preference of decay to the ground state for the 1145-keV level comes from the dominance of that configuration.

The other levels that remain unexplained in the simple particle-plus-vibration picture are the $1/2^-$ and $3/2^-$ levels. They occur at a decreasing energy of excitation as the nucleus considered is closer to midshell, and exhibit large 2p-1h strength in reaction cross-section measurements.[4] They have been treated by Vanden Berghe and Degreick in their calculations.[5] The electromagnetic deexcitation of these levels can best be studied in the beta decay of ^{119}Te. The deexcitation of the $1/2^-$ and $3/2^-$ levels in ^{119}Sb[13] are shown in Fig. 5, where the numbers in parentheses represent the relative transition intensities/rates. The results of gamma-ray spectroscopy studies performed on ^{119}Te activity are shown in Figs. 6 and 7. The sources were made by the ^{120}Te $(\gamma, n)^{119}$Te^{m+g} reaction at the LLL electron linac.[14,15] Although no lifetime measurements are available, the relative decay rates are consistent with the predictions of Vanden Berghe and Degrieck.[5] The apparent hindrance of the M1 transition between the two negative-parity levels is explained by a cancellation of the 2p-1h matrix elements, which provide the only allowed transitions between these two levels. For the decay of the $1/2^-$ level, an E3 rate of one single-particle unit (SPU)* is not inconsistent with E-3

*See Appendix II.

transitions in this region of the nuclear chart,[1] while the highly hindered M2 transition is to be expected because of the different nature of the two levels it occurs between.[1]

THREE-PARTICLE EFFECTS

For the structure of iodine nuclei, the simple particle-vibration model used by Kisslinger and Sorenson[16, 17] failed on several points. First, it did not account for the systematic occurrence of a second low-lying $5/2^+$ level in all of the odd-mass iodine nuclei (see Fig. 8); second, it did not account for the large B(E2) observed in the $5/2_1^+ \rightarrow 7/2_1^+$ transition such as that reported by Bemis and Fransson[18]; and third, it did not account for the large number of levels observed at an excitation energy of 1 to 3 MeV. The situation was improved when calculations based on the suggestions of Alaga, Paar, and coworkers[19-21] were undertaken. These calculations introduce the effects of three-particle clustering in nuclei such as iodine.

The magnitude of the electric quadrupole transition for the $5/2_1^+ \rightarrow 7/2_1^+$ transition in ^{129}I is not predicted correctly by either a particle- or quasi-particle-phonon description.[16, 17] These models predict values of 1.1 and 2.5, respectively, while the measured value[18] is $7.3 \times 10^{-50} e^2 cm^4$. However, Almar and coworkers[22] predict a value of $6.7 \times 10^{-50} e^2 cm^4$, which is in good agreement with experimental data. Their work gives a description of the low-lying states of odd-mass iodine nuclei in terms of a three-proton cluster coupled to a vibrational

core. Their predictions for the B(E2) values from other low-lying levels can be compared with experimental values taken from recent Coulomb-excitation,[23] angular-correlation,[24] and decay-scheme studies.[25] These are (in units of $10^{-50}e^2cm^4$):

$2J_i/2J_f$	$5_1/7_1$	$9_1/5_1$	$3_1/7_1$	$5_2/7_1$	$7_2/7_1$	$9_1/7_1$	$11_1/7_1$
Exptl.	7.3	≤ 0.4	3.5	1.6	1.1	7.8	12.2
Almar	6.7	2.6	12.9	5.3	0.24	3.8	9.7
Reehal	1.1	4.6	11.6	0.11	0.48	0.21	15.4
Sorensen	2.5	–	12.5	–	–	–	–

Although there is close agreement in the B(E2) value for the $5/2_1^+ \rightarrow 7/2_1^+$ transition, most other values have the correct relative magnitude. The $3/2_1^+ \rightarrow 7/2_1^+$ transition has also been measured in ^{125}I and ^{127}I, where the values are 14.4 and $11.2 \times 10^{-50}e^2cm^4$, respectively,[26] and are more in agreement with the predictions.

The level structure of ^{129}I from a few hundred to 1500 keV is more dense than would be expected from a simple particle-vibration picture. The inclusion of three-particle clustering in the Z = 53 nuclei improves the agreement between theory and experiment. The recent decay-scheme studies of Mann et al.,[25,27,28] in conjuction with other studies,[23,24,26,29,30] have given a fairly complete picture of the level structure of ^{129}I (Figs. 9 and 10). In Fig. 11 a comparison of the ^{129}I level structure is shown between experimental values and two calculations: one by Almar et al.[22] and the other by Vanden Berghe.[31]

Three-particle effects are also observed in the odd-neutron nuclei. This can be seen in the impressive change in level density when one considers the odd-neutron nuclei of molybdenum, as shown in Fig. 12. Recently, we investigated the decay properties of the ^{95}Tc isomers in detail; our results are shown in Figs. 13 and 14. Besides the level-decay properties, the most interesting feature of this set of decay schemes is the log ft values deduced from gamma-ray intensity-balance techniques. The beta decay of the $g_{9/2}$ ground state of ^{95}Tc proceeds at an expected allowed rate with log ft values of 5 to 6. However, the $p_{1/2}$ isomer of ^{95}Tc decays by highly hindered, first-forbidden beta decay. Presumably this is a reflection of the lack of single-particle character of these levels in ^{95}Mo. An example of this would be the $1/2^+$ level known from reaction studies at 1301 keV. For this we are only able to set a limit of 11 on the log ft value.

The unique, first-forbidden beta decay of the $1/2^-$ isomer to the $5/2^+$ levels in these nuclei is also in line with a multiparticle nature for these levels. Values in this system range from 10 to 11.4 instead of from 8.5 to 9.5. In this case we can more confidently infer a difference in structure, since only one matrix element ($\langle\sigma\cdot\tau\,\frac{1}{2}\rangle$) contributes to the beta decay and we do not have the possibility of cancellation of matrix elements, which might be possible for the first-forbidden beta decays.

The properties of the low-lying levels of odd-mass nuclei have also recently been treated by Marumori and coworkers. Their new microscopic theory for describing collective excitations in spherical odd-mass nuclei[32,33] treats low-lying anomalous coupling states as

a new kind of fermion collective mode.[34-38] This dressed three-quasi-particle (3QP) formalism is used to describe the odd-mass nuclei with 53 to 59 protons or neutrons.

The energy levels, main amplitudes of the dressed 3QP mode, and transition probabilities in the iodine, cesium, and lanthanum nuclei with 74 to 76 neutrons have been calculated by Marumori and coworkers.[38] The general trend of the lowest $7/2^+$, $3/2^+$ and two $5/2^+$ levels in the odd-proton nuclei are replicated well by their calculations. The transition probabilities generally agree within a factor of 2 to 4. This can be seen for the $5/2_2^+$ to $7/2_1^+$ transition when compared to experimental values[38]:

Nucleus	^{129}I	^{131}Cs	^{133}Cs	^{135}La
Calc.	6.8	10.7	8.8	8.2
Expt.	2.1 ± 0.4	23	10.4 ± 1.2	26

For the deexcitation of the $3/2_1^+$ level to the first $5/2^+$ in the molybdenum and ruthenium nuclei, the values are[38]:

Nucleus	^{95}Mo	^{97}Ru	^{99}Ru	^{101}Ru
(N)	(53)	(53)	(57)	(59)
Calc.	2.0	4.9	11.3	13.9
Expt.	5.3	7.4	13.1	5.7

In our studies of the properties of the odd-mass lanthanum nuclei,[39-41] we were able to identify the trends of the low-lying levels shown in Fig. 15. Of particular interest are out results for the $^{137}Ce^{m}$, $^{137}Ce^{g}$, and ^{135}Ce decay shown in Figs. 16 through 19. The downward trend of the $5/2_2^+$ and $3/2_2^+$ levels as neutron pairs are decreased in the lanthanum nuclei is reproduced by the Marumori calculations.[38] However, the relative B(E2) ratios do not fully agree:

Ratio	Theory	Experiment
$\frac{B(E2:\ 5/2_2^+ \rightarrow 7/2^+)}{B(E2:\ 3/2_1^+ \rightarrow 5/2_1^+)}$	20.5	7.5
$\frac{B(E2:\ 3/2_1^+ \rightarrow 5/2_1^+)}{B(E2:\ 3/2_1^+ \rightarrow 7/2_1^+)}$	10.2	48

Similar trends can be seen when one compares the M1 hindrances and E2 enhancements for nuclei with 78 neutrons, listed in Table 3. The low-lying levels of these odd-proton N = 78 nuclei are shown in Fig. 20.

The systematics of the low-lying levels of odd-mass lanthanum nuclei were shown in Fig. 15. The heavy marks to the left of each level scheme indicate the energy difference between the 2_1^+ level and the ground state of the core nucleus (barium). The systematics suggest that the weak-coupling model may be applicable in explaining these positive-parity levels, at least down to ^{131}La. Comfort and students

have also attempted to calculate these levels.[47] They can calculate the correct number of levels using a Coriolis coupling model; however, they do not find good agreement.[48]

ONE-PROTON, TWO-NEUTRON CONFIGURATIONS

A large number of negative-parity states have been observed at about 2 MeV of excitation in the Z = 53 iodine nuclei. Their origin can be best understood if we first consider the even-even Z = 52 tellurium core, where 5^- and 7^- levels have been identified in ^{122}Te to ^{134}Te, as well as several N = 80 nuclei.[49] The electric dipole transition that depopulates the levels in the even-even nucleus has a hindrance of approximately 10^8 over the single-particle estimate. Such high hindrances have led to the suggestion that these levels are predominately made from the two-neutron configuration: $[2d_{3/2}\ 1h_{11/2}]$. For the odd-mass iodine nuclei, then, we should expect one-proton, two-neutron ($\pi\nu\nu$) states built on this configuration.[50]

The negative-parity levels that have been identified in ^{131}I and ^{133}I are shown in the center of Fig. 21, where the deexcitation of selected levels is shown in the outer portions[51-53]; the decay of levels in ^{133}I up to 2 MeV[53] is shown in Fig. 22. The decrease in energy of excitation in the odd-mass iodine nuclei is similar to that of the negative-parity levels in the even-mass tellurium-core nuclei. The appearance of the known 9-sec, $19/2^-$ isomer of ^{133}I can be understood as the $\pi\nu\nu$ level with configuration $[\pi g_{7/2}\ \nu(d_{3/2}\ h_{11/2})_{7^-}]_{19/2^-}$. The hindrance of approximately a million for the M2 deexcitation arises from

the lack of any such $\pi\nu\nu$ components in the $15, 2^+$ vibrational state to which the level decays. The 7^- configuration, upon which the $19, 2^-$ is built, occurs at an excitation higher than the 5^- in ^{130}Te. Correspondingly, the $19/2^-$ level would be expected to be at an excitation energy above the $15/2^-$ level in ^{131}Te, and its deexcitation could occur through an E2 transition to the $15/2^-$ level.

The deexcitation of the $15/2^-$ level at 1797 keV in ^{131}I is by a highly hindered E1 transition to the lower lying, single-particle, vibration-coupled levels and by an E2 to the single-particle $h_{11/2}$ level. The latter transition is not expected if the 1797-keV level has a pure configuration: $[\pi g_{7/2}\ \nu(d_{3/2}\ h_{11/2})_5^-]$. However, the apparent hindrance factor of this E2 transition is 14 and may represent a small amount of the $|h_{11/2}\ 12>$ configuration in the 1797-keV level. A similar explanation may be appropriate for the deexcitation of the $15/2^-$ level in ^{133}I.

Two possible $13/2^-$ levels in ^{133}I at 1776 and 1990 keV should be commented on. The lower energy level has deexcitation characteristics similar to the 1899-keV level in ^{131}I and may have the configuration: $[\pi\ d_{3/2}\ \nu(d_{3/2}\ h_{11/2})_5^-]$. This configuration would be expected a few hundred keV above the $[\pi g_{7/2}\ \nu(d_{3/2}\ h_{11/2})_5^-]$ levels and would be expected to decay predominately to the lower levels with $\pi\nu\nu$ configurations.

OCCURRENCE OF ROTATIONLIKE STRUCTURE

One of the deviations from vibrationlike character occurs for the nonnormal-parity, $h_{11/2}$ coupled states in nuclei. Recently we have

given evidence for the existence of all particle-plus-rotor levels predicted at low energy in the odd-mass lanthanum nuclei.[54-56] The particle-plus-rotor model was suggested to explain the results of (HI, $x n\gamma$) reaction experiments by Leigh et al.,[57,58] who have established the systematics of an yrast band with level spins of j, j + 2, j + 4 . . . built on the lowest $11/2^-$ level in light, odd-mass lanthanum nuclei. A stretched, E2, gamma-ray cascade was observed in these nuclei with transition energies very close to those of the ground-state band in the even-even barium-core nucleus. Neither strong-coupling nor weak-coupling models appear to explain adequately these bands.

Leigh et al. showed that the character of the yrast bands is consistent with a particle-plus-rotor coupling scheme[57,59-62] with an intermediate prolate deformation of $0.1 < \beta < 0.3$. In this coupling scheme, the single-particle and Coriolis terms of the Hamiltonian are of comparable size for intermediate deformation.[63] When the rotation axes of the core and odd particle are aligned, the angular momentum of the nucleus is more equally shared between the core and the odd particle, minimizing the Coriolis force and decoupling the particle from the core. This results in a rotation-aligned band with the observation of a stretched, E2, gamma-ray cascade, $\rightarrow j + 4 \rightarrow j + 2 \rightarrow j$, similar to that of the ground band of the barium-core nucleus.

In addition to the yrast band, the lower spin levels not populated in (HI, $x n\gamma$) experiments are predicted by the particle-plus-rotor model, including levels with j = 7/2, 9/2, 3/2, 13/2, 11/2, and 5/2. For

example, for intermediate prolate deformation, the energy of the $7/2^-$ level in light lanthanum nuclei is predicted to be about midway between that of the $15/2^-$ and $11/2^-$ levels, the $9/2^-$ level to be between the $19/2^-$ and the $15/2^-$ levels, and the second $11/2^-$ level to rise sharply with increasing β.[59] These lower spin levels provide a critical test for the particle-plus-rotor model in this region and for the conclusion of Leigh et al. that the light lanthanum nuclei have a prolate deformation. In order to study these we have performed gamma-ray spectroscopy studies on the decay of mass-separated cerium to lanthanum from ^{133}Ce to shell closure at ^{139}Ca. All of these studies were possible because of the high-yield isotope-separation techniques developed at LLL by P. Johnson.[64]

The electromagnetic decay properties of the ^{133}La levels best serve to illustrate the decay of the rotation-aligned levels. In Fig. 23, we present the decay of some of the levels we have observed; the decay scheme is shown in more detail in Figs. 24-27. On the right-hand side of the Fig. 23 is a comparison between the levels we have identified and the results of a calculation with no free parameters by Meyer ter Vehn[59] for ^{133}La using an asymmetric rotor model (Theory A). The value of β in this calculation is determined to be 0.201 from the energy of the 2_1^+ level of ^{132}Ba.[65] The value of the asymmetry parameter, γ, is determined to be 23.5° from the ratio of the energies of the 2_2^+ and 4_1^+ levels of ^{132}Ba.

A comparison of the level ordering and relative spacing shows a very good agreement between Meyer ter Vehn's calculation, the experimental levels determined in our beta-decay study, and the (HI, χnγ) results of Leigh et al. The larger absolute-energy differences

in the calculation than in the experiments may be due to the fact that the theory used by Meyer ter Vehn uses a rigid rotor. Allowing for rotor softness leads to a compression of the calculated spectrum.[55,59,66] The $5/2^-$ level is above the $19/2^-$ level in Meyer ter Vehn's calculation, while experimentally it is probably below.

The inclusion of pairing (shown as Theory B in Fig. 23) will bring the $5/2^-$ level below the $19/2^-$ level. Inclusion of pairing also depresses other lower spin levels relative to high-spin levels. Of some importance is the energy of the second $11/2^-$ level. A more recent calculation of Meyer ter Vehn includes the effect of a Fermi energy, λ, and pairing. This provides a lowering of the levels[59,65]; as seen in the center portion of Fig. 23, a number of the levels are brought down sharply in agreement with experiment. The branching ratio can be calculated by first adjusting λ to the relative energy of the $9/2^-$ level with respect to the $11/2_1^-$ and then using a deformation parameter of $\beta = 0.21$ and asymmetry parameter of $\gamma = 24°$ (these values are taken from the adjacent even-even nuclei ^{132}Ba and ^{134}Ce).[65] The branching ratios are:

Transition	Theory B[59]	Experiment[55]
$\frac{9/2_1 \rightarrow 11/2_1}{9/2_1 \rightarrow 7/2_1}$	~7	12
$\frac{11/2_2 \rightarrow 11/2_1}{11/2_2 \rightarrow 9/2_1}$	3.9	3.2

The lifetime of the $7/2^-$ level at 785 keV is unknown. However, if we take the enhancement of the E2 transitions in the even-even barium-core nuclei as an upper limit for the enhancement of the 249-keV gamma ray (cf., the $2_1^+ \rightarrow 0_{gs}^+$ transition in ^{134}Ba has an enhancement of 35), then we calculate the following hindrances:

Transition	Type	Hindrance
$7/2 \rightarrow 11/2^-$	E2	$\equiv 1/35$
$7/2^- \rightarrow 5/2_1^+$	E1	1.1×10^5
$7/2^- \rightarrow 7/2_1^+$	E1	1.4×10^6
$7/2^- \rightarrow 9/2_1^+$	E1	6.7×10^4

Used strictly, these hindrances should be taken as a lower limit. We find the E1 transitions are highly hindered, as would be expected from such a rotation-aligned configuration. The decay of the $11/2^-$ band-head level at 536 keV is more in line with what would be expected of an $h_{11/2}$ level. The lifetime of this level has been measured at 65 nsec. Using this value and the gamma-ray intensities, we find hindrances of 0.9 for the 536-keV E3, 82 for the 405-keV M2, and 1.6×10^5 for the 58-keV E1. These are consistent with transitions from $h_{11/2}$ levels known in this region.[1]

There are an increasing number of cases where nonyrast members of the rotation-aligned bands can be observed. The higher spin members of these bands can be found in the odd-proton iridium and gold nuclei, such as ^{187}Ir[67] and ^{195}Au.[68, 69] There is also some evidence for

lower spin members in the odd-neutron nuclei, such as that observed by Nowicki in ^{137}Nd.[70,71]

COEXISTENCE OF PARTICLE-CORE AND HOLE-CORE STATES

The indium nuclei also exhibit significant deviations from a simple vibrational picture. The expected single-hole and hole-vibration excitations have been identified[72,73] in the indium nuclei. The electric quadrupole strength to the hole-core states has been measured by heavy-ion Coulomb excitation and agrees with simple hole-core calculations.[72] However, early decay-scheme studies showed many more levels than expected were present at the hole-core excitation energies,[74] having positive parity andlarge, electric, quadrupole, transition moments between them.[75] Various mechanisms have been proposed to explain the occurrence of these states. Bäcklin et al.[75] have studied several of the nuclei and suggest the existence of a deformed band based on the $1/2^+$ [431] Nilsson orbital. We have considered these nuclei[76] and have suggested that calculations more in the framework of the rotation-aligned scheme would better account for these levels.[77]

In our spectroscopy studies of the odd-mass nuclei,[78-82] it has been possible to study the decay of several of the low-spin positive-parity levels. The first and second members of the positive-parity band have been observed in the beta decay of ^{111}Sn[78] and (p, xnγ) experiments.[83, 84] They have been observed in ^{113}In by (p,xnγ) [83,84]; and as shown in Fig. 26. we have observed the $1/2^+$ level at 1029 keV

populated in the beta decay of ^{113}Sn.[79] In the case of ^{115}In, we can identify at least two low-spin bands.[80,81] The bands are observed in ^{117}In[81,84] and ^{119}In[84] as well. In all of these the main electromagnetic decay features are the highly hindered, electric dipole transitions to the known hole states and strong, intraband, M1 and E2 transitions.

The best case to discuss is ^{115}In, for it has been studied with the largest number of varied techniques. Besides the decay-scheme[75,76] (see Figs. 29 and 30) and Coulomb-excitation[72,73,85,86] studies, reaction studies have identified the hole states[87-89] of ^{115}In. The (^{3}He, d) reaction studies[90] have shown strong 1p-2h strength in the ^{115}In levels that are thought to have particle-cadmium-core character.[77] Also, the quadrupole moment of the lowest $3/2^+$ level has been measured by Haas and Shirley[91] as 0.60 ± 0.08b. Unfortunately, most theoretical work has been on the calculations of the hole-vibration states,[92-94] while only one attempt has been made to calculate simultaneously the hole-tin-core and particle-cadmium-core states and their possible mixing.[95]

The electromagnetic decay of the 1p-2h states is consistent with a configuration quite different from a simple hole-core picture. The E2 transition between the $1/2^+$ and $3/2^+$ level has been shown to be collective[75] with a speed similar to the cadmium core, while the E1 transitions are hindered by factors of 10^6 to 10^7. The higher energy, low-spin, positive-parity levels decay predominately to the lower 1p-2h levels, while the E1 transitions to the known $1/2^-$ and $3/2^-$ hole states are hindered by 10^4. Recent Compton-suppression spectroscopy results[81] show that the relative intraband E2 transition from the $9/2^+$

member of the 1p-2h band is highly favored, while the ground-state transition is hindered by at least a factor of 4000. The first $9/2^+$ hole-tin-core level lies 30 keV above the $9/2^+$ particle-cadmium-core level. Here our studies have been able to identify the E2 transitions to the two lower $5/2^+$ levels. We find that the E2 to the particle-cadmium-core state is hindered by a factor of 10 over that to the $5/2^+$ hole-cadmium level.

A multiple-band structure is predicted by Meyer ter Vehn's calculations, where succeedingly higher energy bands decay into the next lower band.[59] In our studies of ^{111}In levels populated by decay of ^{111}Sn, we observe levels (Fig. 31) that decay in this manner (Figs. 32 and 33). Of particular interest is the level at 2212 keV, which has a strong decay to the lowest $3/2^+$ level while decay to the ground state is hindered by approximately 10^4.

All of the observed properties of the 1p-2h levels in ^{115}In are consistent with a deformed configuration, and it is tempting to ascribe the 1p-2h band to a 1/2 [431] Nilsson orbital. However, a more quantitative explanation should encompass an extensive Coriolis calculation as a function of deformation, much in the spirit of Diamond, Stevens, and coworkers.[57-60]

OTHER LOW-LYING CONFIGURATIONS

The effect of low-lying 2- and 4-proton configurations in the core can be seen in the systematics of the N = 81 nuclei shown in Fig. 34.

These data come from reaction[96,97] and gamma-ray[98-103] spectroscopy studies. The three lowest-lying levels with J^{π} of $3/2^{-}$, $1/2^{+}$, and $11/2^{-}$ have been shown to have nearly all the $d_{3/2}$, $s_{1/2}$, and $h_{11/2}$ strength,[84-86] while the $g_{7/2}$ and $d_{5/2}$ strength has been shown to be fragmented over several levels.[96, 97] The beta-decay studies have shown the presence of many more levels below 2 MeV in ^{133}Te[103] and ^{135}Xe[98-102] than observed in the beta decay to levels of ^{139}Ce,[99-101] ^{141}Nd,[101] and ^{143}Sm.[104] These excess levels are unaccounted for in the calculations of Heyde and coworkers,[105-108] who couple the single-neutron-hole motion to the quadrupole vibrations of the nuclear surface.

The results of our recent experiments on the decay of ^{139}Pr made by the ^{140}Pr (γ, n) ^{139}Pr reaction at the LLL electron linac[101] are shown in Fig. 35. The decay of most of these levels can be described by Heyde and coworkers,[95-98] but there remains an extra set of levels. Presumably it can be accounted for by the coupling of the known 0^{+} level in ^{140}Pr to the neutron hole. The electromagnetic decay of the 1907-keV level is one such candidate. Its branching to the known first vibrational state at 1320 keV suggests such a configuration.

The level structure of ^{135}Xe becomes understandable when the detailed electromagnetic decay properties of the ^{135}Xe levels are considered along with the recent studies of the ^{136}Xe core.[109-111] In Fig. 36, the level structure of ^{135}Xe is shown and compared to a simple ^{136}Xe experimental core-hole-coupling picture. The energy and decay properties of the first three levels above 1 MeV agree well with the hole-vibration calculations of Heyde and Brussaard.[105] However,

some of the higher-lying levels decay in a manner consistent with the decay characteristics expected from coupling a neutron hole to the known ^{136}Xe core. An example of this is the 1968-keV $5/2^+$ level shown in Figs. 37-39. Here, the E2 transition to ground state is hindered by a factor of 5×10^3 over the transition to the $7/2^+$ level at 1131 keV. Such a hindrance is consistent with the coupling of the $d_{3/2}$ ground state to the known 4_1^+ level of ^{136}Xe. Similar states are observed in ^{133}Te, as shown in Fig. 40.[112]

OTHER MULTIPARTICLE STATES

The effect of five-quasi-particle (5QP) configurations may be seen in the odd-proton nuclei of the $g_{9/2}$ shell. Recently, Marumori[113,114] pointed out that one would expect the dressed 5QP mode to give an extra low-lying level with J-2. That is, for the $g_{9/2}$ nuclei, we should expect a $5/2^+$ level to be low lying. Such an effect has been observed in the odd-mass technetium (Z = 43) nuclei; $5/2^+$ and $7/2^+$ levels have been observed in ^{99}Tc, as illustrated by our recent work on ^{99}Mo decay[115] (see Fig. 41) and on ^{101}Tc (see Fig. 42),[116] where the $9/2^+$, $7/2^+$ and $5/2^+$ form a triplet at 0, 9, and 15 keV.[117] This is contrasted with the Z = 45 rodium nuclei, as shown in Fig. 43, where only the $7/2^+$ level is low-lying.

Detailed studies of the odd-proton nuclei in the technetium and rhodium regions, such as the one performed on ^{103}Rh levels[118] shown in Fig. 44, have demonstrated that the electric quadrupole (E2)

transition is highly collective. This can be seen in Table 4 by the relatively high-percentage E2 in the $7/2^+ \rightarrow 9/2^+$ transition for Z = 43 and 45 nuclei.

It should be noted that Kuriyama et al. have considered these transitions,[125] and in nuclei such as ^{99}Tc find good agreement when they use a dressed 3QP formation:

Transition	Theory	Experiment[126]
B(E2) $5/2^+ \rightarrow 9/2^+$	4.2	4.5 ± 1.5
$7/2^+ \rightarrow 9/2^+$	11.7	13.5 ± 1.5
B(M1) $7/2^+ \rightarrow 9/2^+$	0.044	0.076 ± 0.009

However, they do not examine ^{101}Tc where a 5QP configuration should be considered.

The 3QP and 5QP configurations are apparent in all regions of the nuclear chart and deserve theoretical treatment in the manner of Murumori and coworkers.[33-38] A good example of this is the region where the orbital of the $g_{9/2}$ shell model occurs. We observe levels with positive-parity J values less than $9/2^+$ at energies lower than the pairing gap, or lower than would be expected from simple phonon coupling. This is shown for the odd-neutron nuclei in Fig. 45 and in more detail for the Z = 30 zinc nuclei in Fig. 46. The electromagnetic decay of these levels can be studied in cases such as ^{67}Ga decay,[127] shown in Fig. 47, where the major branching of a $5/2^+$ level is by E2 decay to the known $g_{9/2}$ level.

The levels of the odd-proton nuclei in the light $g_{9/2}$, Z = N shell are shown in Fig. 48. In this case, low-lying J^+ levels have not been observed until the Z = 33 arsenic nuclei. However, Betts et al.[128] have identified positive-parity levels in arsenic, as shown in Fig. 49; for comparison, all known levels of ^{75}As are shown in Fig. 50. Here, again, we can study the electromagnetic decay properties of these levels, and in Figs. 51 and 52 we show the decay of ^{75}Ge and ^{75}Se to ^{75}As levels respectively.[129,130] The electromagnetic decay of the $5/2^+$ and $1/2^+$ levels (Fig. 51)[129,130] are in line with what would be expected for decay of levels with predominately dressed 3QP and 5QP configurations. This is an area where further theoretical work would be welcome.

HIGHER-ORDER MULTIPOLARITIES

The magnetic transitions with orders higher than one are rarely observed. The M2 transitions have been reviewed by Kurath and Lawson.[131] When the M2 transition occurs between predominately single-particle levels, they are found to be hindered by a factor of 50 over simple single-particle estimates for nuclei in the tin region (Fig. 53). An example of this is in the odd-mass tellurium nuclei, where two $7/2^+$ levels are known; one arises from the $d_{3/2}$ coupled to the first 2^+ phonon and the other is a $g_{7/2}$ hole state. As the systematics show in Fig. 54, the two $7/2^+$ levels are within 6 keV of each other. The M2 transition has been recently identified in the ^{125}Te nucleus (Fig. 55).[132] Its measurement by Compton-suppression techniques allowed the assignment of the $g_{7/2}$ hole state in the nucleus.[133] The M4 transitions occur in the tin region

between the low-lying $h_{11/2}$ and $d_{3/2}$ levels. The calculation of their absolute rate has been a good test of several nuclear models.[16,134]

The electric octupole transition has now been observed in a number of tin-region nuclei. These transitions are observed to compete with M2 transitions from the known $h_{11/2}$ single-particle states. Presumably the enhancement of one to two times the single-particle rate reflects the influence of the octupole state identified at about 3 MeV in many of the core nuclei.[135]

THREE-PARTICLE EFFECTS AND THE $h_{11/2} \rightarrow g_{7/2}$, UNIQUE, FIRST-FORBIDDEN BETA DECAY

It is often possible to obtain information about the rates of beta decay by performing detailed balances of gamma-ray intensities populating and depopulating the levels of a nucleus. This information, in conjunction with half-life values, yields log ft values. Since the unique, first-forbidden, beta-decay process has only one matrix element governing it $\left(<\sigma \cdot \tau \frac{1}{2}>\right)$, the log f_1t values in a related series of nuclei can be used as a measure of changes in the nuclear structure of the states involved. The $7/2^+ \rightarrow 11/2^-$ beta transitions in the odd-mass nuclei in the tellurium-xenon region are a good example, and we discuss them next.

The data in the literature for the log f_1t value of the odd-mass iodine nuclei are shown in Fig. 56. Except for the $^{137}Cs \rightarrow {}^{137}Ba$ value, at best these values are highly suspect. Therefore, we performed precision spectroscopy on all of the odd-mass iodine nuclei that beta decay to xenon. The ^{135}I case is most interesting since its old log f_1t value of 12 suggests quite a surprising change in the structure of the iodine or xenon. To obtain a consistent value for this, we had to separate

iodine from fission products, seal it in quartz, and then freeze it to liquid nitrogen (LN_2) temperatures. Then, while the source was kept at LN_2 temperature, we took spectra over several half-lives of the $^{135}Xe^m$ daughter. This measurement, combined with our other ^{135}I (Figs. 37-39) and ^{135}Xe (Figs. 57 and 58) decay data, gave the value of 10.06 for the log f_1t. This and our $^{133}I \rightarrow {}^{133}Xe$ results (see Fig. 59) are shown in Fig. 60, where they are compared with other values we have measured.

The variation of the log f_1t value among the odd-mass iodine to xenon nuclei can be understood if pairing is included; however, the variation with atomic number is not readily apparent until we take into account the three-particle correlations in these nuclei. First, though, we note that the $11/2^-$ level in all these nuclei is fairly well behaved. This can be seen in Fig. 61, where the B(M4) value from the $11/2^-$ to the $3/2^+$ level is compared with theory. The values are consistent with a fairly pure $h_{11/2}$ configuration. Therefore, the $7/2^+$ ground state of the parent is suspect. We note that three-particle correlations should be strongest in the Z = 53 iodine nuclei, and thus have the greatest influence on the availability of a single $g_{7/2}$ nucleon for beta decay. Conversely, we would expect the fastest decay from the Z = 51 antimony nuclei, as there is only one proton. The trend shown in Fig. 50 agrees with this, suggesting that there are substantial three-particle correlations even in the ground state of the nuclei with atomic number 53 and greater.

SUMMARY

The electromagnetic decay properties of odd-mass nuclei have been discussed. These data and complementary information have been used to show how multiparticle and high-j shell-model states can account for the observed deviation of nuclear properties from a simple vibration-coupled picture. Of the three major effects discussed, the first was the inclusion of three quasi-particle configurations: 2p-1h configurations described the odd-mass antimony nuclei, three-particle effects improved the description of the 51 to 59 odd-neutron and odd-proton nuclei, and $\pi\nu\nu$ states could account for the negative-parity levels of iodine near the N = 82 shell closure. Second, the occurrence of rotationlike bands in otherwise vibrationlike nuclei were discussed. Lastly, the levels and their electromagnetic decay properties of some N = 81 nuclei were compared to the known states in the even-even core nuclei to explain the observed deviation of the level structure from a purely vibrational picture. In conclusion, I would like to point out that a number of the multiparticle effects may be accounted for when calculations of the type done by Immele and Struble[136] become available for the vibrational class of nuclei.

APPENDIX I

Experimental Techniques and Equipment

Often the critical test of a nuclear model involves measurement of a gamma ray that represents a transition far less probable than others. In the past few years, the development of a number of experimental devices for detecting low-intensity gamma rays has allowed us to probe the nucleus further than thought possible before. A large body of data on electromagnetic transition probabilities is obtained from the measurement of gamma rays from radioactivity. Consequently, the discussion here will be limited to current techniques used in the attainment of radioactive sources, their measurement, and the analysis of raw data. Where possible, I will illustrate these with equipment available at LLL.

Current Techniques

A pure isotopic species is the most ideal radioactive source. To isolate isotopically pure sources with short half-lives from the fission process, the fission-fragment analyzer, developed by P. C. Stevenson,[137] is best; devices such as "Tristan und Isolde" at Ames, Iowa, U.S.A.,[138] and CERN[139] are useful for extracting gaseous fission products and spallation products, respectively. For longer-lived radioactive sources, off-line isotope separators can be used. The high yield attained by P. Johnson[64] on the LLL isotope separator has allowed the collection of up to 99% of the original isotopic radioactivity.

Prior chemical purification is necessary for sources that are to be mass separated with off-line devices. There are numerous chemical purification techniques[140]; however, two recent developments should be mentioned. The first concerns the separation of rare earth elements. Mode and coworkers[141] have developed high-pressure resin columns in which they have attained single-element separation within 30 min to 1 hr. The second development involves separating gases by gas-chromatographic techniques. Interfacing a small computer with this technique allows the automatic separation of xenon from all other fission-product gases.[66]

A number of the critical studies discussed in the text depend on the rapid isolation of a particular element from the products of thermal fission. For this, we have developed a microcomputer-controlled system that automatically controls the irradiation, delivery, and chemical separation of selected fission products. For example, we can separate antimony within 29 sec after the end of irradiation[112] (see next section). The swift separation of fission products has benefited in the past few years by the excellent work of Prof. G. Herrmann and his coworkers at Mainz.[142]

There are numerous discussions on current gamma-ray spectroscopy techniques.[143] However, mention should be made of a key device in the measurement of very low-abundance gamma rays present in radioactive decay: the Compton Suppression Spectrometer as designed by D. C. Camp[144] (see Fig. 62). In all germanium detectors, the Compton distribution from higher energy gamma rays may mask less intense lower energy gamma rays; however, in the Compton Suppression

Spectrometer, the Compton events are significantly reduced in the final spectra. This spectrometer allows detection of gamma rays tens-to-hundreds-of-thousands times less intense than higher energy gamma rays. Such a technique is particularly significant when searching for gamma rays that are forbidden by a nuclear theory or model.

Generally, gamma-gamma coincidence experiments are performed using a memory buffer with magnetic tape readout. An extension of the system to three parameters allows measurement of the time interval between pairs of gamma rays. This technique is useful in measuring lifetimes in the range of nanoseconds to milliseconds. A more sophisticated gamma-gamma spectrometer has been developed by L. G. Mann and coworkers at the Radiochemistry Division of LLL.[145] This megachannel system uses a small computer-based coincidence spectrometer with a disc memory. Such a device permits on-line analysis of coincidence data.

Measurement of conversion electrons is most readily made with Si(Li) detector systems. However, this technique is limited by the fact that Si(Li) detectors are very sensitive to the Compton process and, hence, produce large backgrounds. To overcome such a difficulty, we have developed a unique instrument incorporating a magnetic field that bends the electrons in a trochoidal path, focusing them on a silicon detector shielded from the source and its gamma rays.

The analysis of raw gamma-ray spectroscopy data involves the reduction of multichannel spectra. The computer code GAMMANL has been developed by R. Gunnink and coworkers[146] for use on the

LLL CDC-7600 and other types of computers.[147] This technique uses a realistic sigmoidal background for photopeaks and fits the photopeak shape with a skewed Gaussian.[146] The program SAMPO is superior for reducing conversion electron spectra, particularly when used in the VISTA interactive mode.[148] A newer integrated concept combines a small disc-computer system with a gamma-ray spectrometer system and modified GAMMAN routine.[149]

Application of Current Techniques: Study of $^{133}Te^{m}$

Some of these techniques, as well as the development of our microprocessor, controlled, fast-chemistry facility, can be well illustrated by our study of ^{133}I levels. The difficulty of isolating fairly pure $^{133}Te^{m}$ from fission products for spectroscopy studies is mainly due to the fact that most techniques that isolate $^{133}Te^{m}$ also produce ^{134}Te. This latter activity in turn produces ^{134}I in equilibrium and masks the measurement of $^{133}Te^{m}$ (^{134}Te and ^{134}I have similar half-lives). The best way to isolate the ^{133}Te is first to produce 2.45-min ^{133}Sb and then milk the ^{133}Te daughter. This avoids the ^{134}Te, because ^{134}Sb is known to have a half-life of 0.17 sec.[3] However, it has the disadvantage of requiring the handling of large amounts of radioactivity.

We have developed a microcomputer-controlled system based on an INTEL-8008, CPU-pin integrated circuit. This system allows automatic handling of a rabbit into the reactor, irradiation, and delivery of the rabbit to one of four external stations. Once the rabbit is delivered to

the fast-chemistry station, a second microcomputer takes over. This chip, which can contain up to 2000 programmable steps, controls the extraction and processing of the sample. In the case of isolating the ^{133}Te, a solution of enriched ^{235}U was irradiated in the Livermore Pool Type Reactor (LPTR) and extracted after 1 to 30 sec. After extraction of the solution, the antimony carrier was automatically added and the mixture dropped into hot sodium borohydride, which produced stibene gas (SbH_3). The stibene gas was then bubbled through HCl and mixed in a slurry of resin. The slurry was dropped into a catcher and rinsed with acid. After a delay time of 2 to 3 min, the resin was washed with dilute acid to strip off the ^{133}Te that had grown in. This ended the automatic phase of the separation.

The sources were either counted for measurement of the 12.4-min ground state or stored for about 1 hr and repurified to give nearly pure $^{133}Te^{m}$. The automatic part of the separation was completed in 29 to 40 sec, and the system was ready to process a subsequent irradiation within a minimum of 1 min 30 sec.

The spectroscopy measurements used several different techniques. The singles' spectra were taken by using several Ge(Li) detector systems in succession; that is, one source was counted on detector A for one half-life. The first source was then moved to detector B and a new source was put on detector A. Repetition of this sequence with numerous sources and several detectors allowed us to collect high counting statistics for several time periods. The detectors used included large-volume Ge(Li) detectors and Ge(Li)-LEPS (low-energy photon spectrometer); the latter allowed measurement of gamma rays with energies of from 10 to 200 keV.

The gamma-gamma coincidence experiments were performed on two types of instruments. The first was the LLL megachannel analyzer. Use of this system allowed easy access to the data, for as described earlier, all data is stored on a two-million-word disk. The second gamma-gamma coincidence experiment was performed through a collaboration of LLL and University of Maryland workers at the NBS reactor. In this experiment a $^{133\text{-}134}$Te source was produced from fission once every hour. The tellurium was adhered to a resin and the iodine daughter products were continuously eluted away by concentrated HCl. The analysis of the buffer-tape gamma-gamma coincidence studies were performed on the LLL CDC-7600 computers.

APPENDIX II

Transition Rates

Direct calculation of transition rates from a particular nuclear model is the best test of that model.[150] However, often these calculations are not available and we must resort to a standard estimate. For gamma-ray transitions, we can use the single-particle estimates given by Weisskopf[151-152] and modified by Moskowski.[153] These take the general form:

$$T^{\gamma}_{1/2:S.P.}(\mu\lambda) = \left\{ (\lambda, R)\, (E_{\gamma}^{2\gamma+1} S)^{-1} \right.,$$

where S is a statistical factor to account for the change in magnetic substates, E_{γ} is the gamma-ray energy, R is the nuclear radius, and λ is the multipole order of the transitions. The explicit form for specific multipole orders can be found in standard texts.[153]

References

1. R. A. Meyer, Proc. Conf. Vibrational Nuclei, Zagreb, Yugoslavia, 1974.
2. E. S. Macias and W. B. Walters, Nucl. Phys. A 160, 274 (1971).
3. S. Raman, R. L. Auble, and F. F. Dyer, Phys. Rev. C 9, 426 (1974)
4. R. L. Auble, J. B. Ball, and C. B. Fulmer, Phys. Rev. 169, 955 (1968).
5. G. Vanden Berghe and E. Degrieck, Z. Phys. 262, 25 (1973) and references quoted therein.
6. R. A. Meyer, Bull. Amer. Phys. Soc. 19, 501 (1974).
7. The experimentalist will note that a prime difficulty in identifying the population of the 1144-keV level for the first time is that the very intense 573-keV transition seems to produce a false peak in the gamma-ray spectra at approximately the same energy as the 1144.65-keV gamma ray. The final value resulted from use of absorbers, counting distance and differentiation of summing peaks and true photopeaks in the Compton Suppression Spectrometer Spectra.
8. The experimental data comes from Refs. 6 and 9-12.
9. E. Booth, R. Arnold, and W. Alston, Phys. Rev. C 7, 1500 (1973).
10. P. D. Forsyth, quoted in Ref. 5.
11. P. C. Barnes, C. Ellegaard, B. Herskind, and M. C. Joshi, Phys. Lett. 23, 266 (1966).
12. D. J. Horen, Nucl. Data Sect. B 67, 75 (1971).
13. R. Auble, Ph.D. Thesis, Michigan State University, Lansing, Mich. (1968).

14. J. T. Larsen, R. G. Lanier, and R. A. Meyer, Bull. Amer. Phys. Soc. 18, 679 (1973).

15. R. G. Lanier, J. T. Larsen, and R. A. Meyer, Bull. Amer. Phys. Soc. 18, 679 (1973).

16. L. S. Kisslinger and R. A. Sorenson, Rev. Mod. Phys. 35, 853 (1963).

17. B. S. Reehal and R. A. Sorenson, Phys. Rev. C 2, 819 (1970).

18. C. E. Bemis and K. Fransson, Phys. Lett. 19, 567 (1965).

19. G. Alaga and G. Ialongo, Nucl. Phys. A 97, 600 (1965).

20. V. Paar, Phys. Lett. B 39, 466 (1972).

21. Ibid, p. 587.

22. R. Almar, O. Civitarese, and F. Krmpotic, Phys. Rev. C 8, 1518 (1973).

23. B. W. Renwick, B. Byrne, D. A. Eastham, P. D. Forsyth, and D. G. E. Martin, Nucl. Phys. A 208, 574 (1973).

24. J. De Raedt, M. Rots, and H. Van de Voorde, Phys. Rev. C 9, 2391 (1974).

25. L. G. Mann, W. B. Walters, and R. A. Meyer, Bull. Amer. Phys. Soc. 18, 1425 (1973).

26. J. Kownacki, J. Ludziejewsky, and M. Moszynski, Nucl. Phys. A 107, 476 (1968).

27. L. G. Mann, W. B. Walters, and R. A. Meyer, to be submitted to Phys. Rev. (1974).

28. W. B. Walters and R. A. Meyer, Bull. Amer. Phys. Soc. 17, 902 (1972).

29. D. Horen, Nucl. Data Sect. B 8, (2) 123 (1972).

30. R. L. Auble, J. B. Ball, and C. B. Fulmer, Phys. Rev. 169, 955(1968).

31. G. Vanden Berghe, Z. Phys. 266, 266 (1974).

32. A. Kuriyama, T. Marumori, and K. Matsuyanagi, Progr. Theor. Phys. 45, 784 (1971).

33. A. Kuriyama, T. Marumori, K. Matsuyanagi, and R. Okamoto, INS Rept. 217, Institute for Nuclear Study, University of Tokyo, Tokyo, Japan (1974).

34. A. Kuriyama, T. Marumori and K. Matsuyanagi, Progr. Theor. Phys. 47, 489 (1972).

35. A. Kuriyama, T. Marumori and K. Matsuyanagi, Progr. Theor. Phys. 51, 779, (1974).

36. A. Kuriyama, T. Marumori and K. Matsuyanagi, R. Okamoto, and T. Suzuki, to be published.

37. T. Marumori, Institute for Nuclear Study, University of Tokyo, Tokyo, Japan, private communication (1974).

38. A. Kuriyama, T. Marumori, K. Matsuyanagi, and R. Okamoto, INS Rept. 220, Institute for Nuclear Study, University of Tokyo, Tokyo, Japan (1974) and experimental references quoted therein.

39. E. A. Henry and R. A. Meyer, "Structure of Odd-Mass Lanthanum Nuclei, II: ^{135}La," to be submitted to Phys. Rev. (1974).

40. E. A. Henry, P. J. Johnson, and R. A. Meyer, "Structure of Odd-Mass Lanthanum Nuclei, I: ^{137}La," to be submitted to Phys. Rev. (1974).

41. E. A. Henry and R. A. Meyer, "Structure of Odd-Mass Lanthanum Nuclei, III: ^{133}La," to be submitted to Phys. Rev. (1974).

42. M. Conjeaud, S. Harar, M. Caballero, and N. Cindro, Nucl. Phys. A 215, 383 (1973).

43. R. L. Auble, J. B. Ball, and C. B. Fulmer, Phys. Rev. 169, 955 (1968).

44. E. Macias and W. B. Walters, Nucl. Phys. A 161, 471 (1971).

45. S. V. Jackson, W. B. Walters, and R. A. Meyer, submitted to Phys. Rev. (1974).

46. E. A. Henry, Nucl. Data 11, 495 (1974).

47. J. R. Comfort and K. R. S. Devan, Bull. Amer. Phys. Soc. 19, 61 (1974).

48. J. R. Comfort, Kernfysich Versneller Instituut, Rijksuniversiteit, Groningen, The Netherlands (1974-75 address), private communication (Nov. 1974).

49. A. Kerek, P. Carle, and S. Borg, Nucl. Phys. A 224, 367 (1974).

50. L. V. Peker, Multiparticle States, Winter School for Nuclear Theory and High Energy Physics (1969), Lawrence Berkeley Laboratory, UCRL-Trans. 1399.

51. S. V. Jackson, W. B. Walters, and R. A. Meyer, submitted to Phys. Rev. C (1974).

52. W. B. Walters, S. V. Jackson, and R. A. Meyer, in Proc. Conf. Vibrational Nuclei, Zagreb, Yugoslavia, 1974.

53. R. A. Meyer, J. H. Landrum, and S. C. Bourret, Spectroscopy Investigation of the Fission Precursors of ^{131,133,135}Xe, Lawrence Livermore Laboratory, Final Rept., 1974 (in preparation).

54. E. A. Henry and R. A. Meyer, Bull. Amer. Phys. Soc. 19, 502 (1974).

55. E. A. Henry and R. A. Meyer, Z. Phys. (1974) (in press).

56. E. A. Henry, C. Gatrousis, and R. A. Meyer, Bull. Amer. Phys. Soc. 18, 680 (1973).

57. J. R. Leigh, K. Nakai, K. H. Maier, F. Puhlhofer, F. S. Stephens, and R. M. Diamond, Nucl. Phys. A 213, 1 (1973).

58. For a recent review of the results of (HI, γn) reaction states at Lawrence Berkeley Laboratory and München, see D. Proetel, "High Spin Excitation Modes in Transitional Nuclei Studied with (Hl, γn) Reactions," Proc. Conf. Vibrational Nuclei, Zagreb, Yugoslavia, 1974).

59. J. Meyer ter Vehn, Lawrence Berkeley Laboratory, private communication (April 1974).

60. F. S. Stephens, R. M. Diamond, and S. G. Nilsson, Phys. Lett. B 44, 429 (1973).

61. K. Nakai, P. Kleinheinz, J. R. Leigh, K. H. Maier, F. S. Stephens, R. M. Diamond, and G. L. Løvhøiden, Phys. Lett. B 44, 443 (1973).

62. F. S. Stephens, R. M. Diamond, J. R. Leigh, T. Kammuri, and K. Nakai, Phys. Rev. Lett. 29, 438 (1972).

63. For a good review of Coriolis effects in nuclei, see F. S. Stevens, Coriolis Effects in Nuclei, Lawrence Berkeley Laboratory, Rept. LBL-1251, presented at 5th Nucl. Phys. Summer School, Ruczíska, Poland (1972).

64. P. Johnson, Lawrence Livermore Laboratory, private communication (1974).

65. See, e. g., M. Sakai, Nucl. Data Tables 10, 511 (1972), and J. F. Wild and R. A. Meyer, in Proc. Am. Chem. Soc. Meeting, Los Angeles, 1974.

66. C. F. Smith, in Proc. Noble Gases Symp. (1973), Lawrence Livermore Laboratory, Rept. UCRL-74710.

67. S. André et al. (Grenoble-Swierk collaboration), quoted in J. Meyer ter Vehn, Lawrence Berkeley Laboratory, Rept. LBL-3416 (1974).

68. M. J. Martin, Nucl. Data Sect. B 8, 431 (1972).

69. P. O. Tjøm, M. Maier, D. Benson, Jr., F. S. Stephens, and R. M. Diamond, to be published in Nucl. Phys. (1974).

70. G. Nowicki, KFK 2017 (1974), Ges. für Kernforschung, Karlsruhe, Germany.

71. G. Nowicki, Ges. für Kernforschung, Karlsruhe, Germany, private communication (1974).

72. F. S. Dietrich et al., Nucl. Phys. A 155, 209 (1970).

73. J. McDonald, D. Parter, and D. T. Stewart, Nucl. Phys. A 104, 177 (1967).

74. G. Graffee, C. W. Tang, C. D. Coryell, and G. E. Gordon, Phys. Rev. 149, 884 (1966).

75. A. Bäcklin, B. Fogelberg, and S. G. Malinskog, Nucl. Phys. A 96, 539 (1967).

76. R. A. Meyer and G. L. Struble, J. Phys. Soc. Japan, 34, 418 (1973).

77. R. A. Meyer, J. T. Larsen, and R. G. Lanier, in Proc. Intern. Conf. Nucl. Phys., Munich, 1973.

78. J. Brownlee and R. A. Meyer, Bull. Amer. Phys. Soc. 18, 703 (1973).

79. A. A. Delucchi and R. A. Meyer, Bull. Amer. Phys. Soc. 18, 703 (1973).

80. N. Smith and R. A. Meyer, Bull. Amer. Phys. Soc. 17, 586 (1972).

81. S. V. Jackson, W. B. Walters, and R. A. Meyer, to be published (1974).

82. E. S. Macias, R. E. Head, H. C. Hseuh, and M. R. Zalutsky, Nucl. Instr. Methods to be published (1974).

83. H. J. Kim and R. L. Robinson, Phys. Rev. C 9, 767 (1974).

84. A. Bäcklin, Institute for Nuclear Physics, Stockholm, private communication (1974).

85. E. M. Bernstein, G. G. Seamon, and J. M. Palms, Nucl. Phys. A 141, 67 (1970).

86. A. Marcinkowski, A. Bäcklin, and I. Bergquist, Nucl. Phys. 179, 781 (1972).

87. E. V. Weiffenbach and R. Tickle, Phys. Rev. C 3, 1668 (1971).

88. M. Conjeaud, S. Harar, and E. Thuriere, Nucl. Phys. A 129, 10 (1969).

89. W. H. Hasselink, B. R. Kooistra, L. W. Put, R. H. Siemssen, and S. van der Werf, Nucl. Phys. A 226, 229 (1974).

90. M. Conjeaud, S. Harar, and E. Thuriere, Commissariat a l'Energie Atomique, Rept. CEA-N-1232 (1969), p. 36.

91. H. Haas and P. A. Shirley, Lawrence Berkeley Laboratory, Rept. UCRL-20426 (1970).

92. A. Covello, V. R. Manfredi, and N. Azziz, Nucl. Phys. A 201, 215 (1973).

93. B. I. Atalay and L. W. Chiao-Yap, Phys. Rev. C 5, 369 (1972).

94. S. Sen, Nucl. Phys. A 191, 29 (1972).

95. H. J. Mang, F. Krmpotic, and S. M. Abecasis, Z. Phys. 262, 39 (1973).

96. R. K. Jolly and E. Kashy, Phys. Rev. C 4, 1398 (1971).

97. A. Chaumeaux, G. Brugge, H. Faraggi, and J. Picard, Nucl. Phys. A 164, 176 (1971).

98. E. S. Macias, J. P. OpDeBeech, and W. B. Walters, Nucl. Phys. A 147, 513 (1970).

99. J. D. King, N. Neff, and H. W. Taylor, Nucl. Phys. A 99, 433 (1967).

100. D. B. Berry, W. H. Kelly, and W. C. McHarris, Phys. Rev. 188, 1875 (1969).

101. M Zalutsky, E. S. Macias, and R. A. Meyer, to be published (1974).

102. R. A. Meyer, J. H. Landrum, and W. B. Walters, to be published (1974).

103. R. A. Meyer, J. H. Landrum, and J. T. Larsen, to be published (1974).

104. C. M. Lederer, Lawrence Berkeley Laboratory, private communication (1974).

105. K. Heyde and P. J. Brussaard, Z. Phys. 259, 15 (1973).

106. K. Heyde and P. J. Brussaard, Nucl. Phys. A 104, 81 (1967).

107. K. Heyde and P. J. Brussaard, Nucl. Phys. A 112, 494 (1968).

108. H. Vanden Berghe and K. Heyde, Nucl. Phys. A 163, 478 (1970).

109. S. Sen, P. J. Riley, and T. Udagawa, Phys. Rev. C 6, 2201 (1972).

110. R. Bunting, Nucl. Data Sect. B, to be published, and private communication (1974).

111. A. Kerek, J. Kownacki, A. Marelins, and J. Pihl, Nucl. Phys. A 194, 64 (1972).

112. R. A. Meyer, S. C. Bourret, and J. H. Landrum, Spectroscopy Studies of the Odd Mass Xe Precursors, Lawrence Livermore Laboratory, DARPA Final Rept., 1974 (in preparation).

113. T. Marumori, Proc. Conf. Vibrational Nuclei, Zagreb, Yugoslovia, 1974.

114. T. Marumori, University of Tokyo, Tokyo, Japan, private communication (1974).

115. R. A. Meyer, K. V. Marsh, and H. Easterday, Bull. Amer. Phys. Soc. 50, 1510 (1972).

116. J. F. Wright, W. Talbert, and R. A. Meyer, to be submitted to Phys. Rev. (1974).

117. W. B. Cook, M. W. Johns, J. S. Geiger, and R. L. Graham, Can. J. Phys. 50, 1511 (1972).

118. E. S. Macias, M. E. Phelps, D. G. Sarentites, and R. A. Meyer, submitted to Phys. Rev. (1974).

119. R. S. Hager and E. C. Seltzer, Nucl. Data Sect. A 4, 1 (1968).

120. M. E. Phelps and D. G. Sarantites, Nucl. Phys. A 159, 113 (1970).

121. G. Graeff, Nucl. Phys. A 127, 65 (1969).

122. C. W. E. Van Eijk, B. Van Nooijin, F. Schutte, S. M. Brahmavor, J. H. Hamilton, and J. J. Pinajian, Nucl. Phys. A 121, 440 (1968).

123. S. O. Schriber and M. W. Johns, Nucl. Phys. A 96, 337 (1967).

124. G. Graeffe and G. E. Gordon, Nucl. Phys. A 107, 67 (1967).

125. A. Kuriyama, T. Marumori, and K. Matsuyanagi, INS Rept. 204, Institute for Nuclear Study, University of Tokyo, Tokyo, Japan (1973).

126. M. Marelius et al., Nucl Phys. A 148, 433 (1970).

127. W. Myers, A. L. Prindle, and R. A. Meyer, to be published.

128. R. Betts et al., Phys. Rev. Lett. 26, 1576 (1971).

129. A. Partridge and R. A. Meyer, Bull. Amer. Phys. Soc. 16, 506 (1971).

130. R. A. Meyer, A. Delucci, and A. Partridge, to be submitted for publication (1975).

131. D. Kurath and R. D. Lawson, Phys. Rev. 161, 915 (1967).

132. R. A. Meyer and W. B. Walters, to be submitted to Phys. Rev. (1974).

133. R. L. Auble, Nucl. Data Sect. B 7, 465 (1972).

134. See, e.g., Refs. 105 and 106.

135. I am indebted to C. M. Lederer of Lawence Berkeley Laboratory and his staff for making available to me the data in their forthcoming compilation of nuclear data (Table of Isotopes, 7th Ed.).

136. See, e.g., J. D. Immele and G. L. Struble, Phys. Rev. C 9, 460 (1974).

137. P. C. Stevenson, J. T. Larsen, and J. J. Leary, In Proc. Intern. Conf. Prop. Nuc. Far From Region Beta Stability (Leysin, 1970, CERN 70-30), vol. 1, p. 143.

138. W. L. Talbert, Jr. and J. R. McConnell, Ark. Fys. 36, 99 (1966).

139. For references on these devices see Proc. Intern. Conf. Prop. Nuc. Far From Region Beta Stability (Leysin, 1970, CERN 70-30).

140. Radiochemical Procedures Used in the Radiochemistry Division, H. Hicks, Ed., Lawrence Livermore Laboratory (unpublished manual).

141. B. M. Morris, V. A. Mode, and D. H. Sisson, J. Chromatogr. 71, 389 (1972) and references quoted therein.

142. G. Herrmann, University of Mainz, private communication (1974). See, e.g., N. Trautmann, N. Kaffrell, H. W. Behlich, G. Herrmann, and D. Hübscher, Radiochim. Acta 18, 86 (1972).

143. See, e.g., Proc. Intern. Conf. Radioactivity Nucl. Phys., J. H. Hamilton and J. C. Manthuruthil, Eds. (Gordon and Breach, New York, 1972).

144. D. C. Camp, in Proc. Intern. Conf. Radioactivity Nucl. Phys. (Gordon and Breach, New York, 1972), p. 135.

145. J. B. Niday and L. G. Mann, in Proc. Intern. Conf. Radioactivity Nucl. Phys. (Gordon and Breach, New York, 1972), p. 313.

146. R. Gunnink and J. B. Niday, Lawrence Livermore Laboratory, Rept. UCRL-51061 (1971).

147. S. V. Jackson, University of Maryland, private communication (1974).

148. C. M. Lederer, Lawrence Berkeley Laboratory, private communication (1974).

149. R. Gunnink, J. B. Niday, and P. D. Siemens, Lawrence Livermore Laboratory, Rept. UCRL-51577 (1974).

150. W. Heitler, The Quantum Theory of Radiation (Oxford Press, London, 1957).

151. J. M. Blatt and V. F. Weisskopf, Theoretical Nuclear Physics (J. Wiley, New York, 1953).

152. F. Weisskopf, Phys. Rev. 83, 1073 (1951).

153. S. A. Moskowski in Alpha, Beta, and Gamma Ray Spectroscopy, K. Siegbahn, Ed. (North Holland Publishing Co., Amsterdam, 1966), vol. 2, p. 863.

JKP/cb

Table 1. Experimental vs calculated B(E2)↓ values

Level (in keV)	(J^{π})	B(E2)↓ ($100\ e^2b^2$) Experiment[8]	Theory
507	$(3/2^+)$	12	12
573	$(1/2^+)$	81	90
947	$(9/2^+)$	0.6	14
1024	$(7/2^+)$	66	65
1035	$(9/2^+)$	3	0.6
1145	$(9/2^+)$	62	50

Table 2. Calculated configurations for $9/2^+$ levels in ^{121}Sb.

$9/2^-$ level	Percent of configuration				
in keV	$\|5/2, 12\rangle$	$\|7/2, 12\rangle$	$\|2p\ 1h\rangle$	$\|2p\ 1h, 12\rangle$	Other
948	12	3	74	8	—
1035	<1	79	—	1	$4\|7/2, 22\rangle$ $10\|7/2, 24\rangle$
1144	69	—	12	—	$2\|5/2, 22\rangle$ $7\|5/2, 24\rangle$ $1\|7/2, 22\rangle$ $4\|1/2, 24\rangle$

Table 3. M1 hindrances and E2 enhancement for nuclei with 78 neutrons.

Transition		^{131}I[a]	^{133}Cs[b]	^{135}La[c]	^{137}Pr[d]
$7/2^+ \rightleftarrows 5/2^+$	H(M1)	140	430	540	30
	E(E 2)		5.9		
$5/2_2^+ \rightarrow 7/2^+$	H(M1)		260 to 410[e, f]	670	
	E(E 2)		17 to 65[e, f]	33	5.0
$5/2_2^+ \rightarrow 5/2_1^+$	H(M1)		7 to 14[e]	280	
	E(E 2)		120 to 240[e]	4.4	8.2
$3/2^+ \rightarrow 5/2_2^+$	H(M1)		840	≤1530	
	E(E 2)		0.18		
$3/2^+ \rightarrow 7/2^+$	E(E 2)		19	≥0.25	
$3/2^+ \rightarrow 5/2_1^+$	H(M1)		54	≤81	
	E(E 2)		3.3	≥12	
$1/2^+ \rightarrow 3/2^+$	H(M1)		≤40	≤2.6	
	E(E 2)		≥73	≥56	
$1/2^+ \rightarrow 5/2_1^+$	E(E 2)		≥12	≥52	

[a] Data from Refs. 42 and 43.

[b] Data from Ref. 44.

[c] Data from present work and Ref. 45.

[d] Data from Ref. 46.

[e] $T_{1/2}$ of $5/2_2^+$ level is uncertain; see Ref. 44.

[f] $\delta^2 = 1.08$ from internal conversion data and 0.35 from angular correction results; see Ref. 44.

Table 4. Percentage of E2 in various odd-proton nuclei.

Isotope	Transitions[a]	E_γ keV	Multipolary		Method of determination[b]
^{95}Tc	$7/2^+(1) \rightarrow 9/2^+(1)$	336	M1 + (11 ± 9)%	E2	α_K, K/L + M[120]
^{97}Tc	$7/2^+(1) \rightarrow 9/2^+(1)$	215	M1 + (7 ± 6)%	E2	α_K, K/L + M[121]
			M1 + (10 ± 4)%	E2	α_K, K/L + M[120]
^{99}Tc	$7/2^+(1) \rightarrow 9/2^+(1)$	141	M1 + (7 ± 3)%	E2	α_K, K/L + M[122]
^{99}Rh	$7/2^+(1) \rightarrow 9/2^+(1)$	136	M1 + (13 ± 4)%	E2	α_K, K/L + M[120]
^{101}Rh	$7/2^+(1) \rightarrow 9/2^+(1)$	25	M1 + (3.8 ± 1.5)%	E2	α_T[120]
^{105}Rh	$7/2^+(1) \rightarrow 9/2^+(1)$	53	M1 + (1.8 ± 1.7)%	E2	α_K[118]
^{105}Rh	$9/2^+(1) \rightarrow 7/2^+(1)$	149	M1 + (19 ± 8)%	E2	α_L[123]
^{109}Rh	$9/2^+(1) \rightarrow 7/2^+(1)$	45	M1 + (16)%	E2	α_T[124]

[a]The number in parentheses is the number of the level with this J value.

[b]The theoretical conversion coefficients from Ref. 119 have been used to calculate the E2 admixture. The data on α_K and K/L + M ratios are from references sited.

FIGURE CAPTIONS

Fig. 1. Systematics of odd-mass antimony nuclei.

Fig. 2. Systematics of ^{119}Sb to ^{125}Sb showing trend of the three $9/2^+$ levels.

Fig. 3. Decay sheme of $^{121}Te^m$ and $^{121}Te^g$.

Fig. 4. Comparison of calculated and experimental B(E2) values in ^{121}Sb.

Fig. 5. Decay of selected levels in ^{119}Sb.

Fig. 6. Decay of $^{119}Te^g$.

Fig. 7. Decay of $^{119}Te^m$.

Fig. 8. Systematics of odd-mass iodine nuclei.

Fig. 9. Decay of $^{129}Te^g$.

Fig. 10. Decay of $^{129}Te^m$.

Fig. 11. Comparison of theory and experimentally observed levels of ^{129}I.

Fig. 12. Systematics of levels in odd-mass molybdenum nuclei.

Fig. 13. Decay of $^{95}Te^m$.

Fig. 14. Decay of $^{95}Te^g$.

Fig. 15. Systematics of low-lying levels of odd-mass lanthanum nuclei.

Fig. 16. Decay of $^{137}Ce^m$.

Fig. 17. Decay of $^{137}Ce^g$.

Fig. 18. Decay of ^{135}Ce (low energy levels).

Fig. 19. Decay of ^{135}Ce (high energy levels).

Fig. 20. Systematics of odd-proton N = 78 nuclei.

Fig. 21. Selected levels and level-decay properties of ^{131}I and ^{133}I.

Fig. 22. Levels to 2 MeV in ^{133}I populated in ^{133}Te^{m} decay.

Fig. 23. (Left) Comparison of experimentally observed levels with theoretical calculations; Theory A: rigid rotor; Theory B: effect of pairing inclusion in a triaxial rotor. (Right) Decay properties of selected levels of ^{133}La.

Fig. 24. Decay of ^{133}Ce to levels in ^{133}La (0 to 1.5 MeV).

Fig. 25. Decay of ^{133}Ce to levels in ^{133}La (1.5 to 1.9 MeV).

Fig. 26. Decay of ^{133}Ce to levels in ^{133}La (1.9 to 2.1 MeV).

Fig. 27. Decay of ^{133}Ce t levels in ^{133}La (2.1 to 2.9 MeV).

Fig. 28. Decay of ^{113}Sn.

Fig. 29. Decay of ^{115}Cd^{g}.

Fig. 30. Decay of ^{115}Cd^{m}.

Fig. 31. Levels observed in ^{111}In.

Fig. 32. Decay of high-spin levels in ^{111}In.

Fig. 33. Decay of lower-spin levels in ^{111}In.

Fig. 34. Systematics of N = 81 nuclei.

Fig. 35. Decay of ^{139}Pr.

Fig. 36. Comparison of experimentally observed levels in ^{135}Xe with simple hole-core-coupling predictions.

Fig. 37. Decay of ^{135}I (0 to 2.0 MeV).

Fig. 38. Decay of ^{135}I (2.0 to 2.3 MeV).

Fig. 39. Decay of ^{135}I (2.3 to 2.5 MeV).

Fig. 40. Decay of selected levels in ^{133}Te populated in the decay of 2.45-min ^{133}Sb.

Fig. 41. Decay of ^{99}Mo.

Fig. 42. Low energy levels of ^{101}Tc populated in the decay of ^{101}Mo.

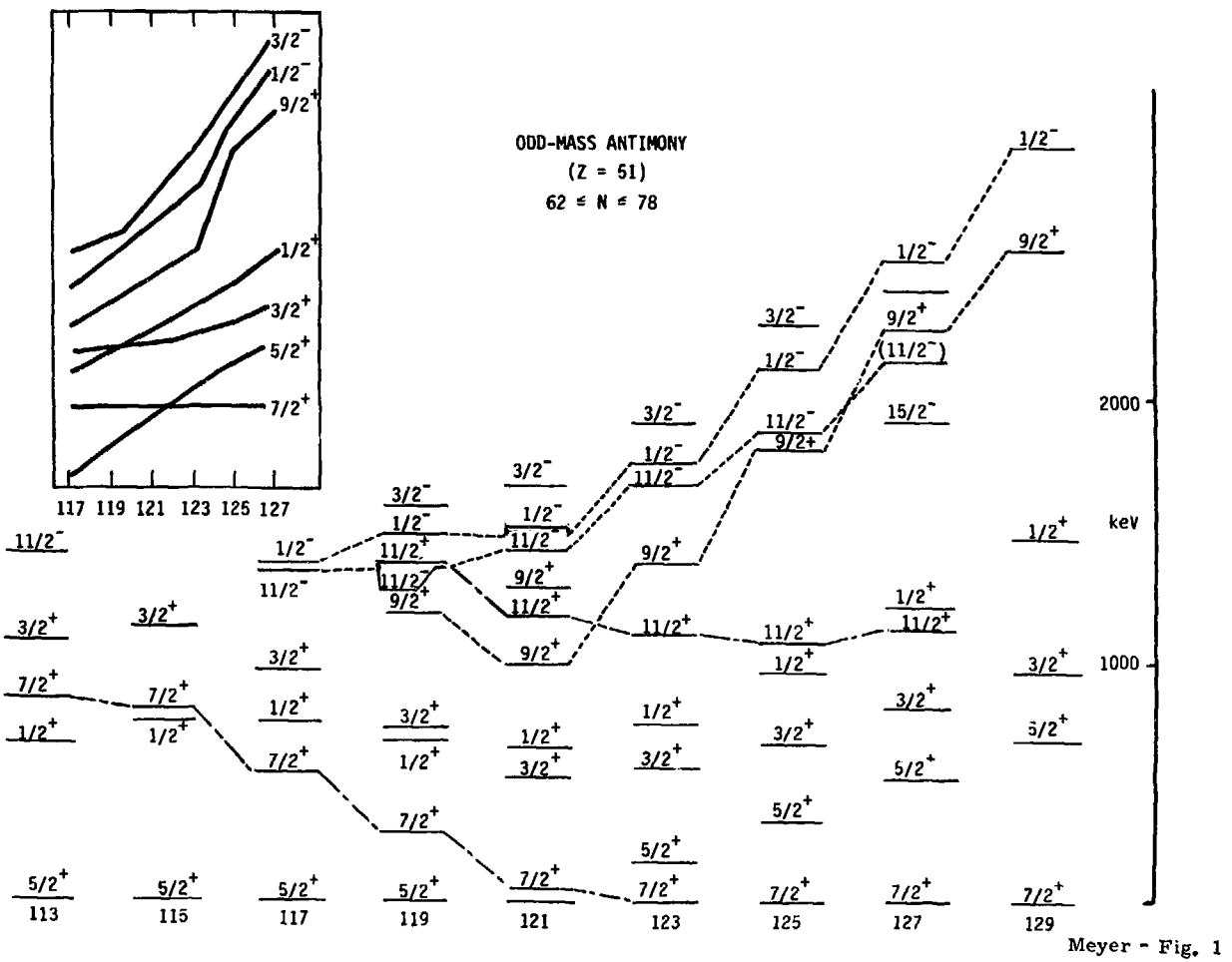
ODD-MASS ANTIMONY
(Z = 51)
62 ≤ N ≤ 78
3/2⁻
1/2⁻
9/2⁺
1/2⁺
3/2⁺
5/2⁺
7/2⁺
117 119 121 123 125 127
2000
1000
keV
11/2⁻
3/2⁺
7/2⁺
1/2⁺
5/2⁺
113
115
117
119
121
123
125
127
129
(11/2⁻)
15/2⁻
11/2⁺

Meyer - Fig. 1

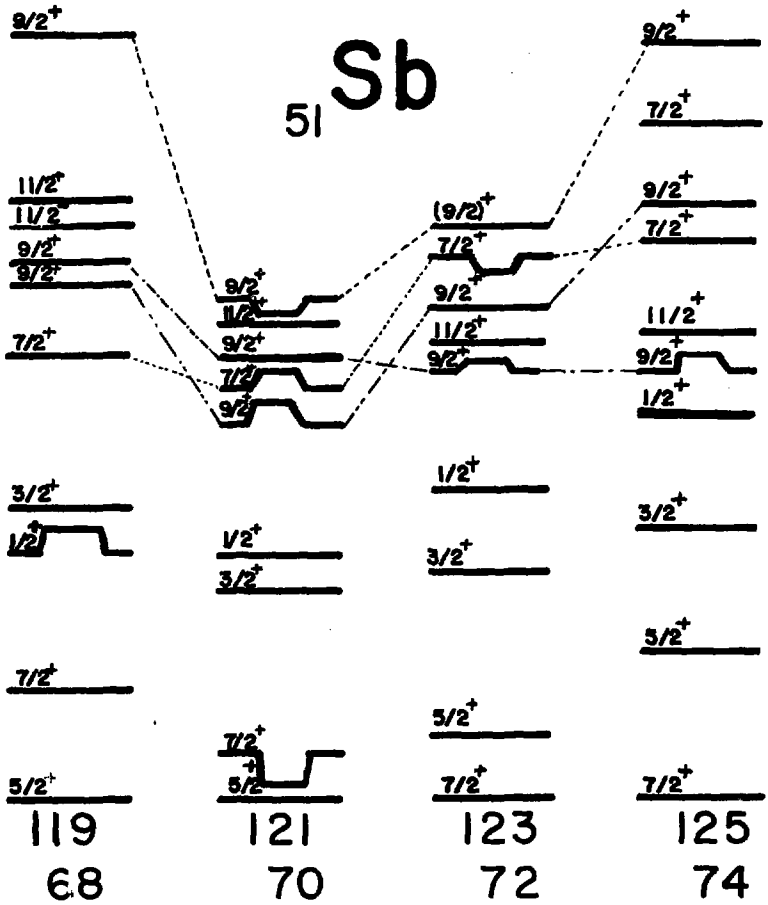
51 Sb
9/2+
11/2+
11/2+
9/2+
9/2+
7/2+
3/2+
1/2+
7/2+
5/2+
119
68
9/2+
11/2+
9/2+
7/2+
9/2+
1/2+
3/2+
7/2+
5/2+
121
70
(9/2)+
7/2+
9/2+
11/2+
9/2+
1/2+
3/2+
5/2+
7/2+
123
72
9/2+
7/2+
9/2+
7/2+
11/2+
9/2+
1/2+
3/2+
5/2+
7/2+
125
74

Meyer - Fig. 2

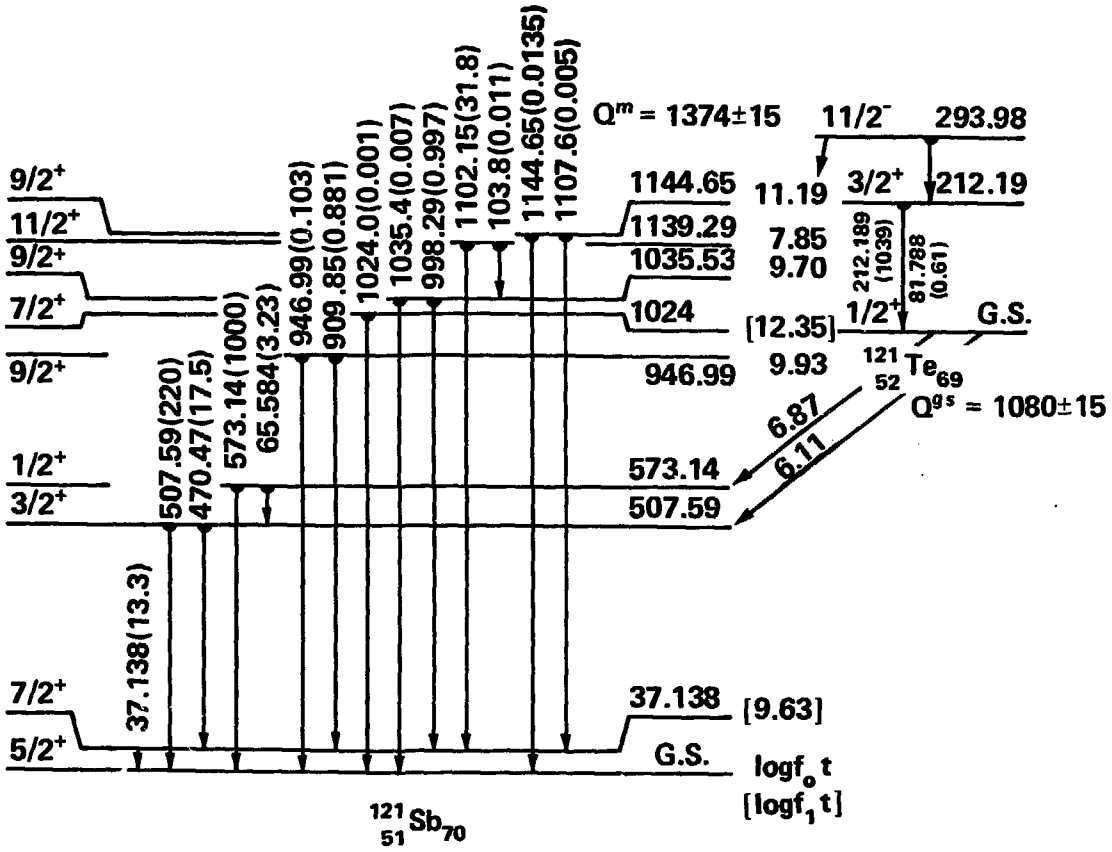
Q^m = 1374±15
11/2⁻ 293.98
3/2⁺ 212.19
11.19
212.189 (1039)
81.788 (0.61)
1/2⁺ G.S.
[12.35]
9.93
$^{121}_{52}Te_{69}$
Q^{gs} = 1080±15
6.87
6.11
9/2⁺
11/2⁺
9/2⁺
7/2⁺
9/2⁺
1/2⁺
3/2⁺
7/2⁺
5/2⁺
1144.65
1139.29
1035.53
1024
946.99
573.14
507.59
37.138
G.S.
946.99(0.103)
909.85(0.881)
1024.0(0.001)
1035.4(0.007)
998.29(0.997)
1102.15(31.8)
103.8(0.011)
1144.65(0.0135)
1107.6(0.005)
507.59(220)
470.47(17.5)
573.14(1000)
65.584(3.23)
37.138(13.3)
[9.63]
logf$_0$t
[logf$_1$t]
$^{121}_{51}Sb_{70}$

Meyer - Fig. 3

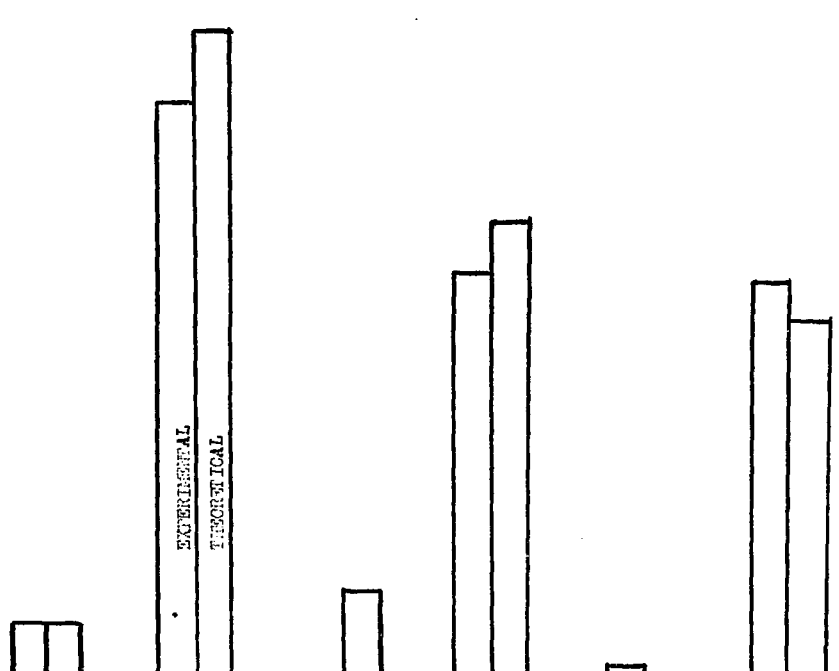
EXPERIMENTAL
THEORETICAL
3/2+
507
1/2+
573
9/2+
946
7/2+
1024
9/2+
1035
9/2+
1144

Meyer - Fig. 4

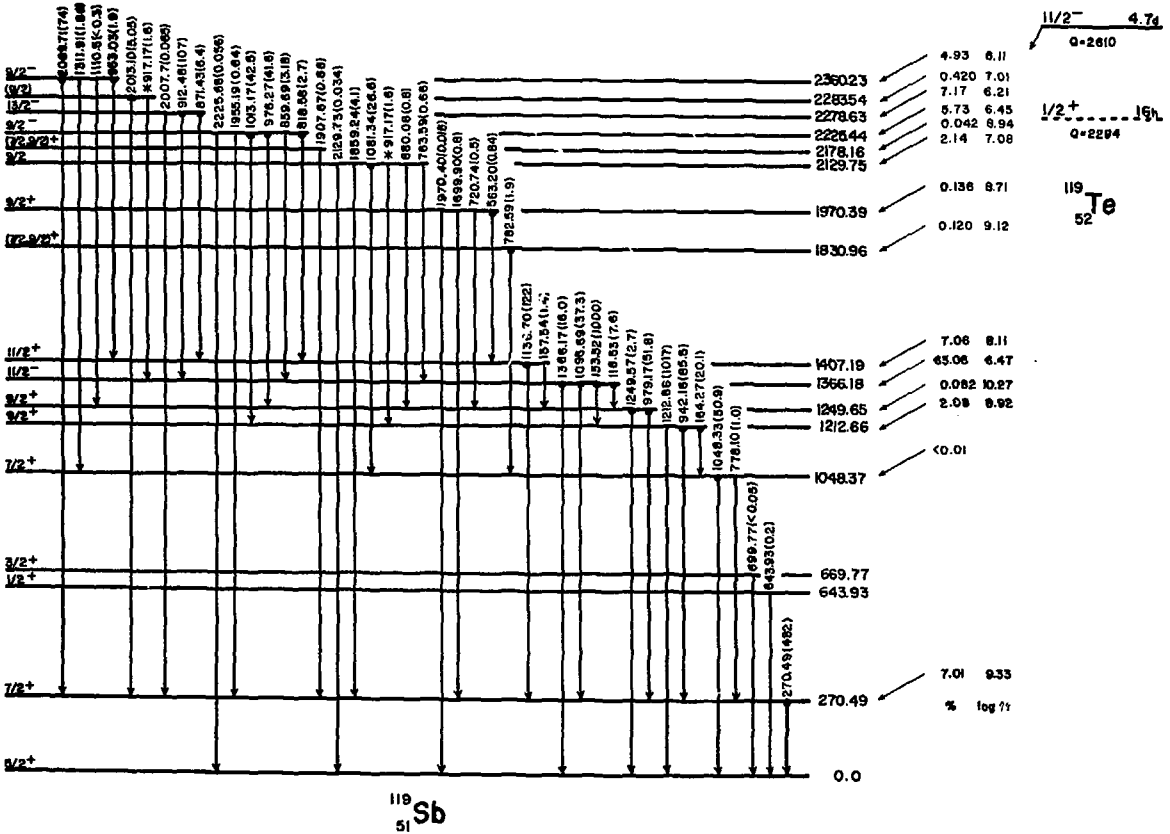
11/2⁻ 4.7d
Q=2610
1/2+ 16h
Q=2294
119 52 Te
119 51 Sb
2360.23
2283.54
2278.63
2226.44
2178.16
2129.75
1970.39
1830.96
1407.19
1366.18
1249.65
1212.66
1048.37
669.77
643.93
270.49
0.0
4.93 6.11
0.420 7.01
7.17 6.21
5.73 6.45
0.042 8.94
2.14 7.08
0.136 8.71
0.120 9.12
7.06 8.11
65.06 6.47
0.082 10.27
2.09 9.92
<0.01
7.01 9.33
% log ft

Meyer - Fig. 5

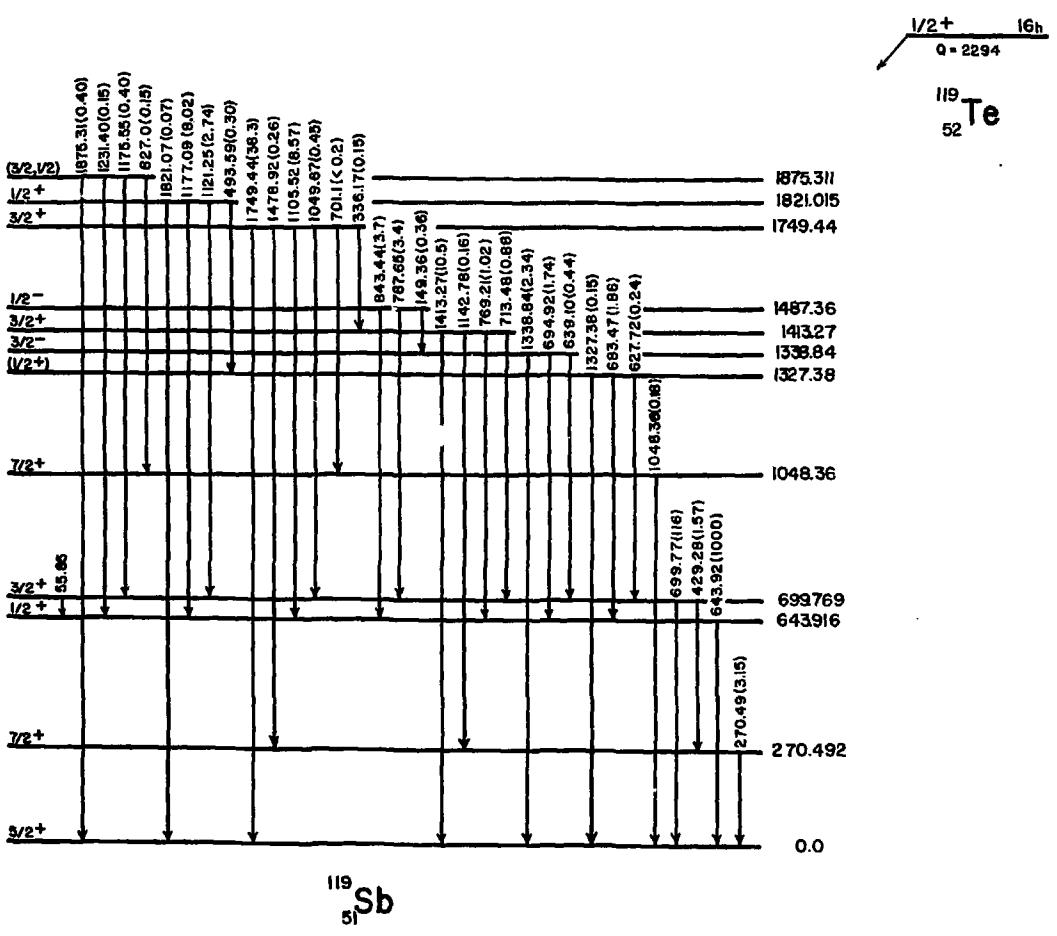
1/2+ 16h
Q = 2294
119 52 Te
(3/2,1/2)
1/2+
3/2+
1/2−
3/2+
3/2−
(1/2+)
7/2+
3/2+
1/2+
7/2+
5/2+
1875.31(0.40)
1231.40(0.15)
1175.55(0.40)
627.0(0.15)
1821.07(0.07)
1177.09(8.02)
1121.25(2.74)
493.59(0.30)
1749.44(38.3)
1478.92(0.26)
1105.52(8.57)
1049.87(0.45)
701.1(<0.2)
336.17(0.15)
843.44(3.7)
787.65(3.4)
749.36(0.36)
1413.27(0.5)
1142.78(0.16)
769.21(1.02)
713.48(0.88)
1338.84(2.34)
694.92(1.74)
639.10(0.44)
1327.38(0.15)
693.47(1.86)
627.72(0.24)
1048.36(0.16)
699.77(116)
429.28(1.57)
643.92(1000)
270.49(3.15)
55.85
1875.311
1821.015
1749.44
1487.36
1413.27
1338.84
1327.38
1048.36
699.769
643.916
270.492
0.0
119 51 Sb

Meyer - Fig. 6

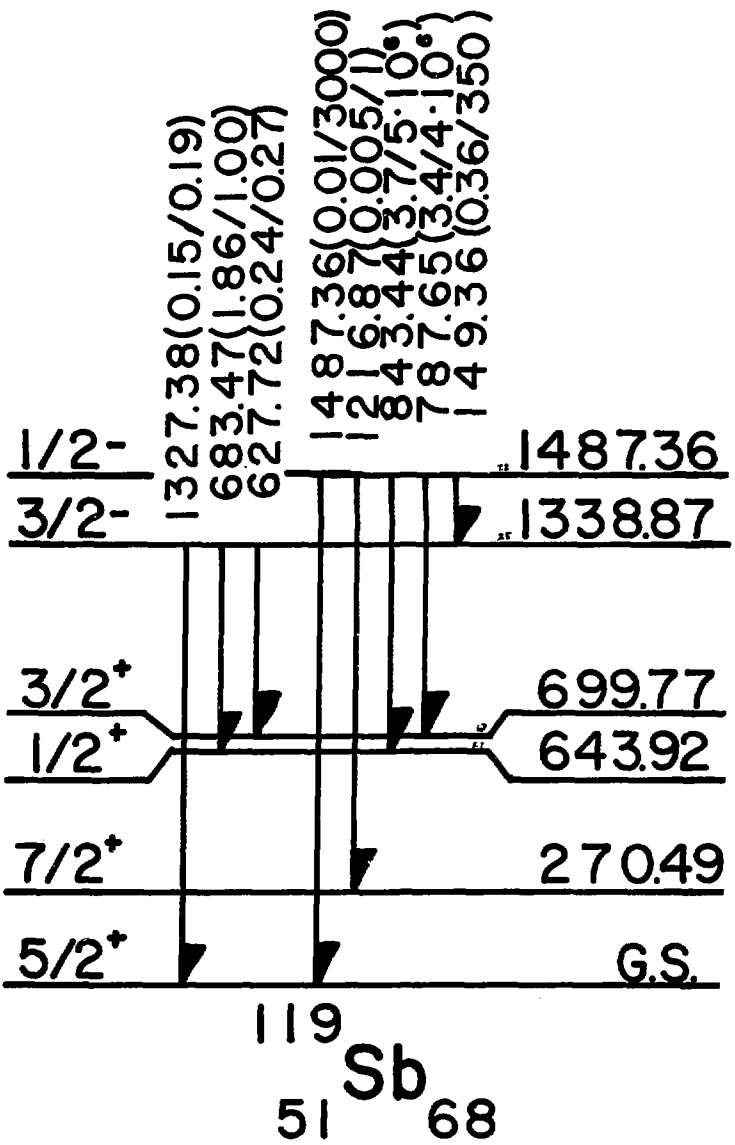
1/2-
3/2-
3/2+
1/2+
7/2+
5/2+
1487.36
1338.87
699.77
643.92
270.49
G.S.
1327.38(0.15/0.19)
683.47(1.86/1.00)
627.72(0.24/0.27)
1487.36(0.01/3000)
1216.87(0.005/1)
843.44(3.7/5·10⁻³)
787.65(3.4/4·10⁻³)
149.36(0.36/350)
119
51 Sb 68

Meyer - Fig. 7

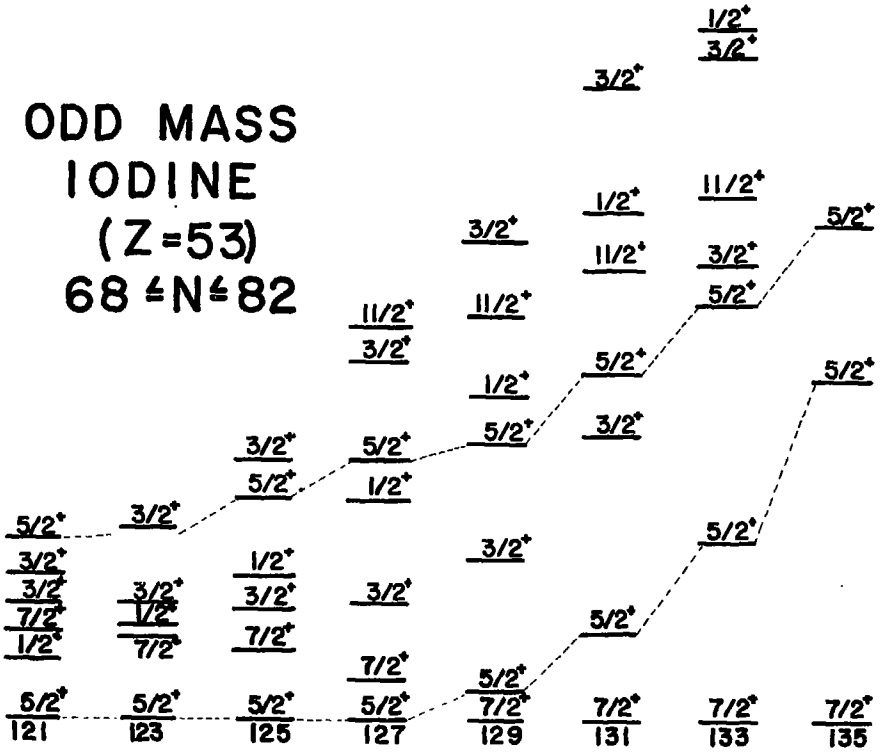
ODD MASS
IODINE
(Z=53)
68 ≤ N ≤ 82
5/2+ 3/2+ 3/2+ 7/2+ 1/2+
5/2+ 3/2+ 3/2+ 1/2+ 7/2+
3/2+ 5/2+ 1/2+ 3/2+ 7/2+
11/2+ 3/2+ 5/2+ 1/2+ 3/2+ 7/2+
3/2+ 11/2+ 1/2+ 5/2+ 3/2+ 5/2+ 7/2+
1/2+ 11/2+ 3/2+ 5/2+ 5/2+ 7/2+
1/2+ 3/2+ 5/2+ 7/2+
5/2+ 5/2+ 5/2+ 5/2+ 7/2+ 7/2+ 7/2+ 7/2+
121 123 125 127 129 131 133 135

Meyer - Fig. 8

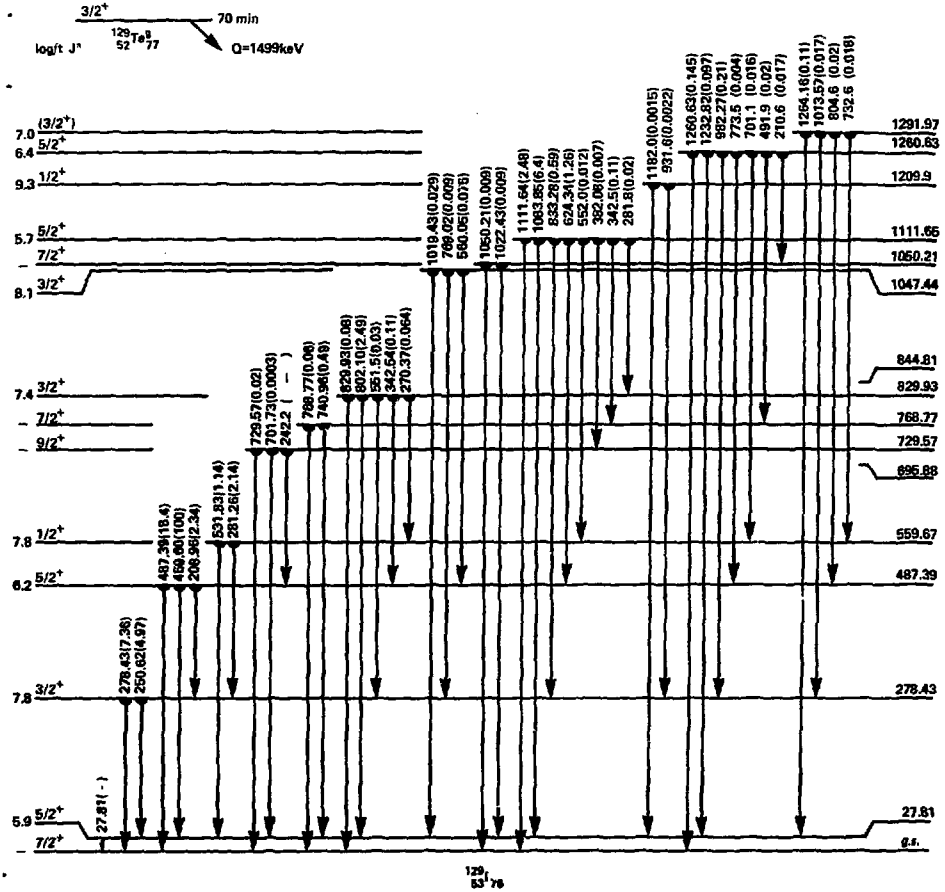
3/2+
70 min
129 52Te8 77
log/t J+
Q=1499keV
(3/2+)
5/2+
1/2+
5/2+
7/2+
3/2+
3/2+
7/2+
9/2+
1/2+
5/2+
3/2+
5/2+
7/2+
7.0
6.4
9.3
5.7
8.1
7.4
7.8
6.2
5.9
1291.97
1260.63
1209.9
1111.66
1050.21
1047.44
844.81
829.93
768.77
729.57
695.88
559.67
487.39
278.43
27.81
g.s.
1019.43(0.029)
769.02(0.009)
560.05(0.076)
1050.21(0.009)
1022.43(0.009)
1111.64(2.48)
1083.85(6.4)
833.28(0.59)
624.34(1.26)
552.0(0.012)
392.06(0.007)
342.5(0.11)
281.3(0.02)
1182.0(0.0015)
931.6(0.0022)
1260.63(0.145)
1232.82(0.097)
982.27(0.21)
773.5 (0.004)
701.1 (0.016)
491.9 (0.02)
210.6 (0.017)
1254.16(0.11)
1013.57(0.017)
804.6 (0.02)
732.5 (0.016)
829.93(0.08)
802.10(2.49)
351.5(0.03)
342.5(0.11)
270.37(0.064)
788.77(0.06)
740.96(0.48)
729.57(0.02)
701.73(0.0003)
242.2 (-)
531.83(1.14)
281.26(2.14)
487.39(18.4)
459.60(100)
208.95(2.34)
278.43(7.36)
250.62(4.97)
27.81(-)
129 53I76

Meyer - Fig. 9

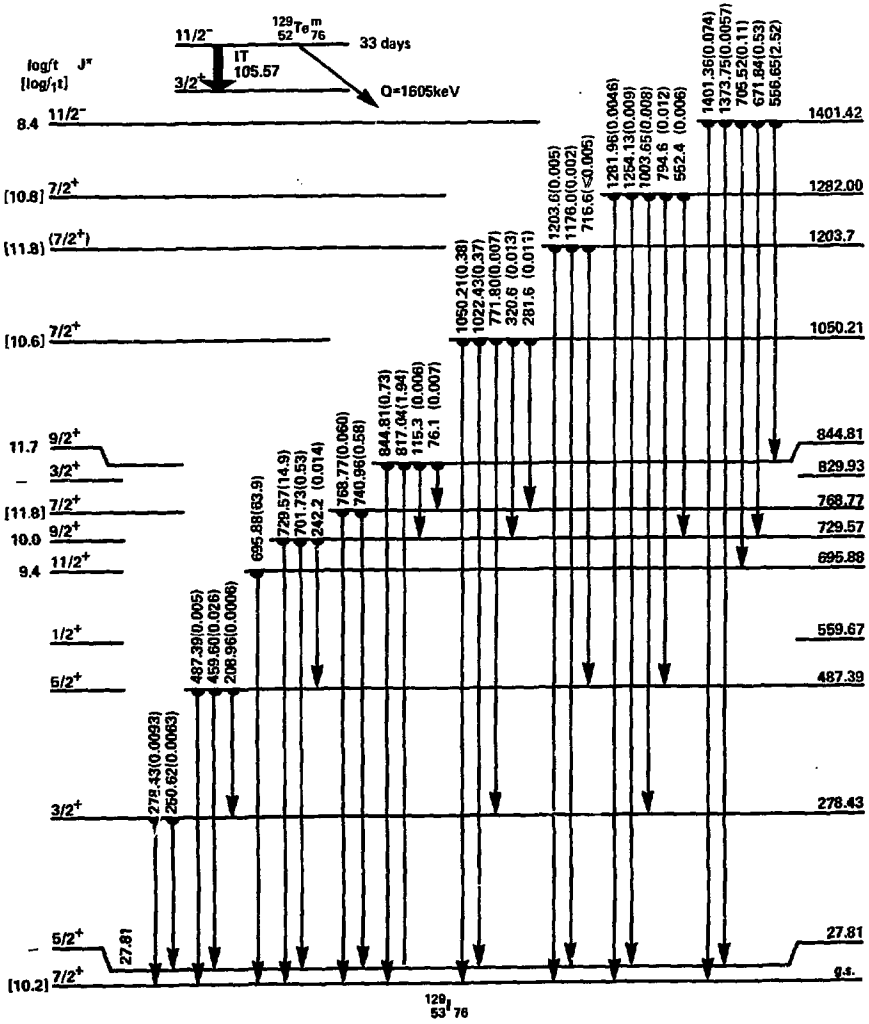
$^{129}_{52}Te^{m}_{76}$
11/2⁻
33 days
IT
105.57
3/2⁺
Q=1605keV
log/f
[log/ft]
J^π
8.4 11/2⁻
[10.8] 7/2⁺
[11.8] (7/2⁺)
[10.6] 7/2⁺
11.7 9/2⁺
3/2⁺
[11.8] 7/2⁺
10.0 9/2⁺
9.4 11/2⁺
1/2⁺
5/2⁺
3/2⁺
5/2⁺
[10.2] 7/2⁺
27.81
1401.42
1282.00
1203.7
1050.21
844.81
829.93
768.77
729.57
695.88
559.67
487.39
278.43
27.81
g.s.
1401.36(0.074)
1373.75(0.0057)
705.52(0.11)
671.84(0.53)
566.65(2.52)
1281.96(0.0046)
1254.13(0.009)
1003.65(0.008)
794.6 (0.012)
552.4 (0.006)
1203.6(0.005)
1176.0(0.002)
716.6(≤0.005)
1050.21(0.38)
1022.43(0.37)
771.80(0.007)
320.6 (0.013)
281.6 (0.011)
844.81(0.73)
817.04(1.94)
115.3 (0.006)
76.1 (0.007)
768.77(0.060)
740.96(0.58)
729.57(14.9)
701.73(0.53)
242.2 (0.014)
695.88(63.9)
487.39(0.005)
459.60(0.026)
208.96(0.0006)
278.43(0.0093)
250.62(0.0063)
$^{129}_{53}I_{76}$

Meyer - Fig. 10

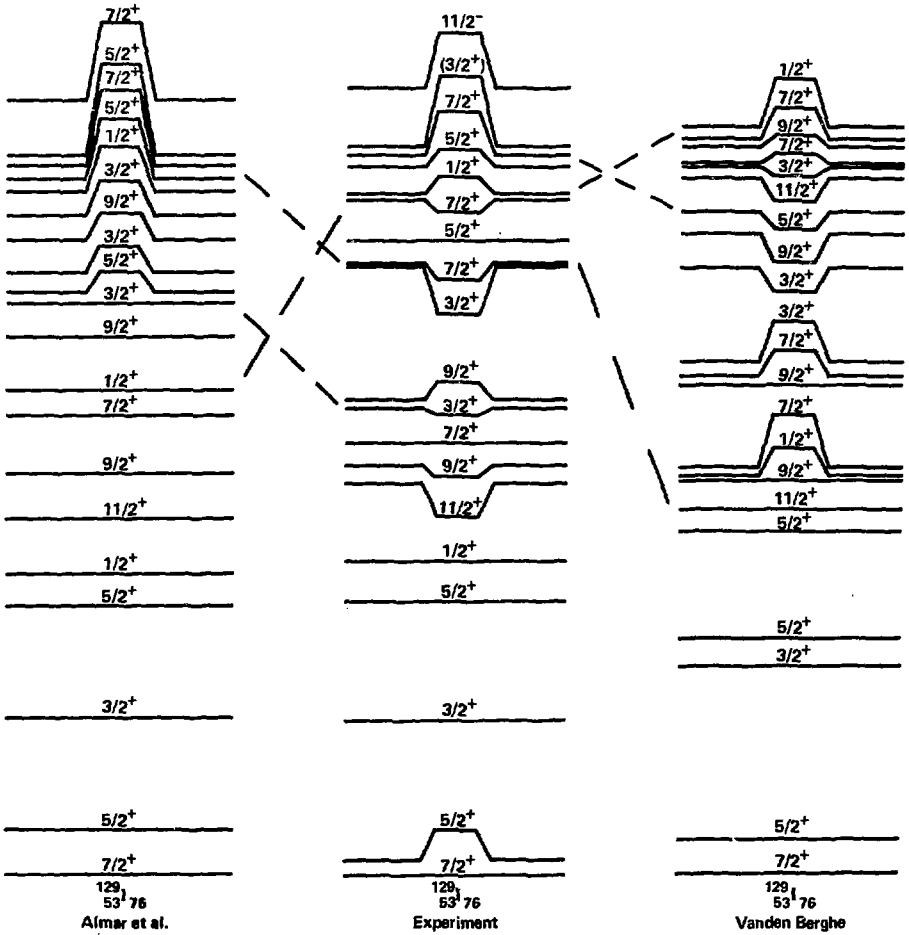
7/2+
5/2+
7/2+
5/2+
1/2+
3/2+
9/2+
3/2+
5/2+
3/2+
9/2+
1/2+
7/2+
9/2+
11/2+
1/2+
5/2+
3/2+
5/2+
7/2+
129 53 I 76
Almar et al.
11/2-
(3/2+)
7/2+
5/2+
1/2+
7/2+
5/2+
7/2+
3/2+
9/2+
3/2+
7/2+
9/2+
11/2+
1/2+
5/2+
3/2+
5/2+
7/2+
129 53 I 76
Experiment
1/2+
7/2+
9/2+
7/2+
3/2+
11/2+
5/2+
9/2+
3/2+
3/2+
7/2+
9/2+
7/2+
1/2+
9/2+
11/2+
5/2+
5/2+
3/2+
5/2+
7/2+
129 53 I 76
Vanden Berghe

Meyer - Fig. 11

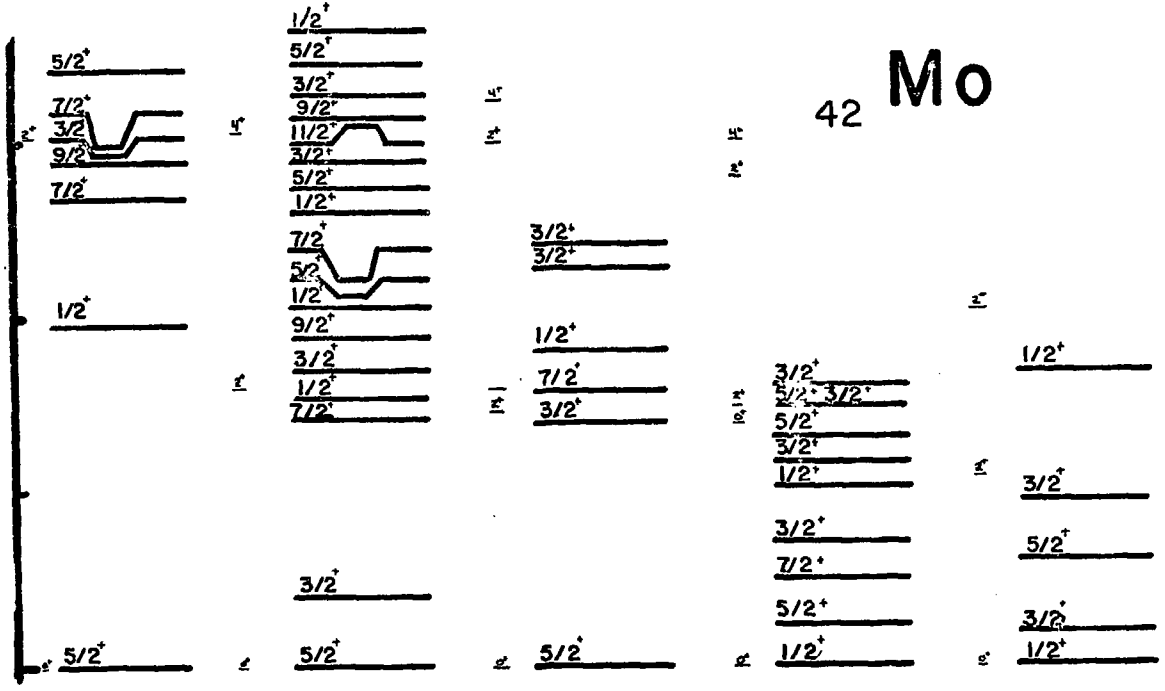
42 Mo
5/2+
7/2+
3/2+
9/2+
7/2+
1/2+
5/2+
93
51
1/2+
3/2+
11/2+
9/2+
7/2+
95
53
3/2+
3/2+
1/2+
7/2+
5/2+
97
55
3/2+
5/2+
3/2+
1/2+
7/2+
5/2+
1/2+
99
57
1/2+
3/2+
5/2+
3/2+
1/2+
101
59

Meyer - Fig. 12

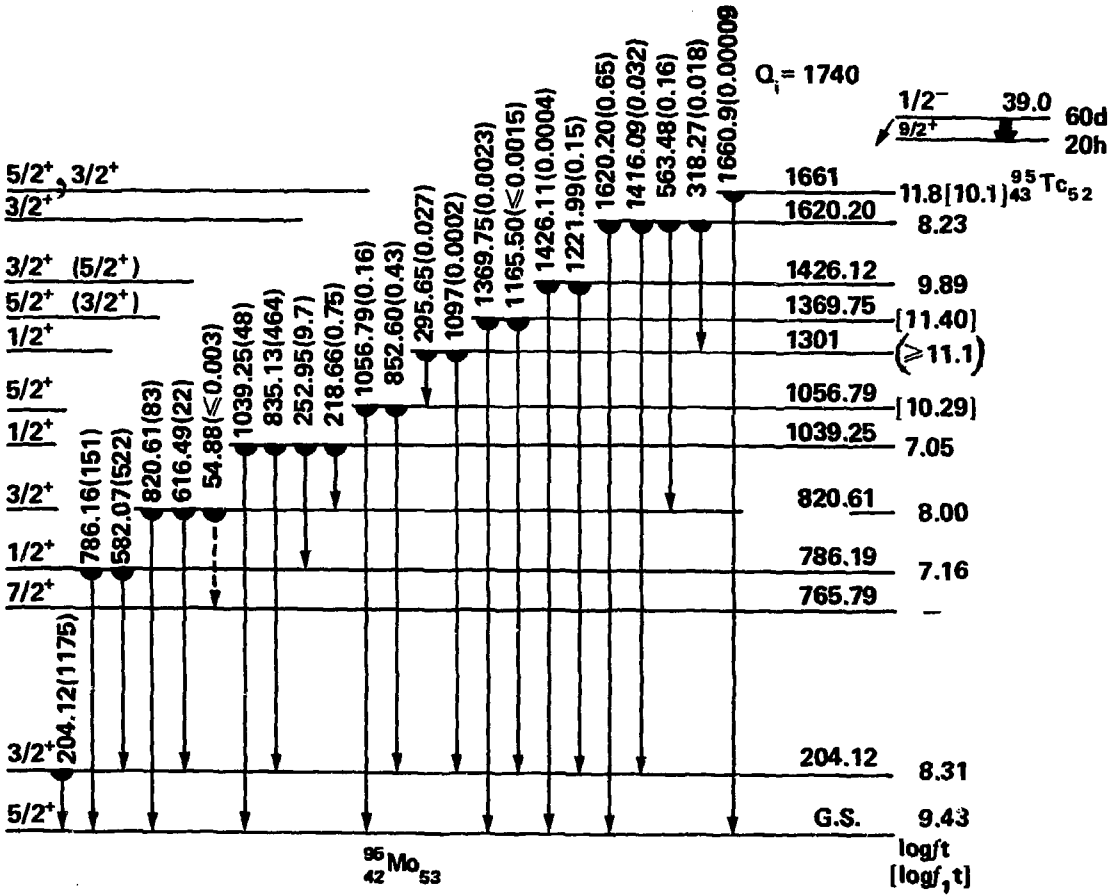
Q = 1740
1/2⁻ 39.0 60d
9/2⁺ 20h
5/2⁺, 3/2⁺
3/2⁺
3/2⁺ (5/2⁺)
5/2⁺ (3/2⁺)
1/2⁺
5/2⁺
1/2⁺
3/2⁺
1/2⁺
7/2⁺
3/2⁺
5/2⁺
786.16(151)
582.07(522)
820.61(83)
616.49(22)
54.88(≤0.003)
1039.25(48)
835.13(464)
252.95(9.7)
218.66(0.75)
1056.79(0.16)
852.60(0.43)
295.65(0.027)
1097(0.0002)
1369.75(0.0023)
1165.50(≤0.0015)
1426.11(0.0004)
1221.99(0.15)
1620.20(0.65)
1416.09(0.032)
563.48(0.16)
318.27(0.018)
1660.9(0.00009)
204.12(1175)
1661
11.8[10.1]
1620.20
8.23
1426.12
9.89
1369.75
[11.40]
1301
(≥11.1)
1056.79
[10.29]
1039.25
7.05
820.61
8.00
786.19
7.16
765.79
–
204.12
8.31
G.S.
9.43
log ft
[log f₁t]
95 42 Mo 53
95 43 Tc 52

Meyer - Fig. 13

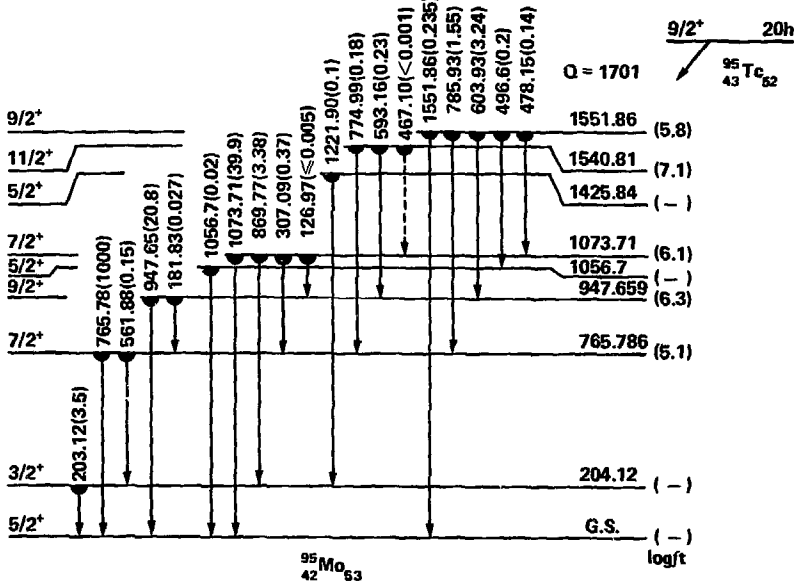
9/2+ 20h
95 43 Tc 52
Q = 1701
9/2+
11/2+
5/2+
7/2+
5/2+
9/2+
7/2+
3/2+
5/2+
765.78(1000)
561.88(0.15)
947.65(20.8)
181.83(0.027)
1056.7(0.02)
1073.71(39.9)
869.77(3.38)
307.09(0.37)
126.97(≤0.005)
1221.90(0.1)
774.99(0.18)
593.16(0.23)
467.10(<0.001)
1551.86(0.235)
785.93(1.55)
603.93(3.24)
496.6(0.2)
478.15(0.14)
203.12(3.5)
1551.86 (5.8)
1540.81 (7.1)
1425.84 (–)
1073.71 (6.1)
1056.7 (–)
947.659 (6.3)
765.786 (5.1)
204.12 (–)
G.S. (–)
95 42 Mo 53
log ft

Meyer - Fig. 14

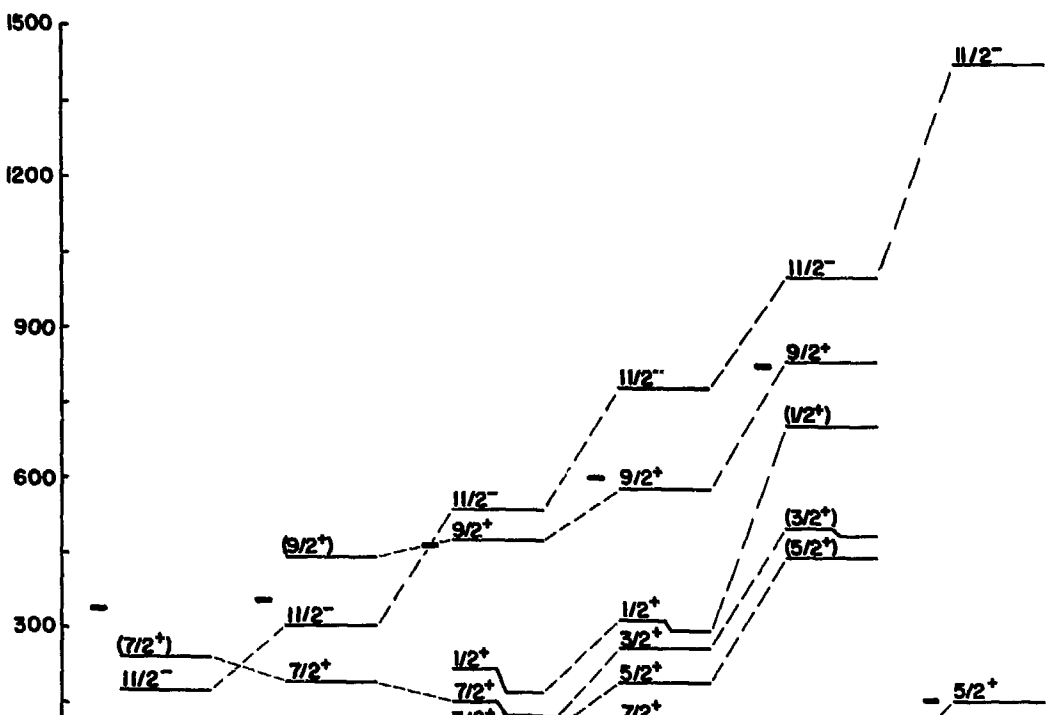
1500
1200
900
600
300
0
(7/2⁺)
11/2⁻
5/2⁺
3/2⁺
129 57La72
(9/2⁺)
11/2⁻
7/2⁺
5/2⁺
3/2⁺
131 57La74
11/2⁻
9/2⁺
1/2⁺
7/2⁺
3/2⁺
5/2⁺
5/2⁺
133 57La76
11/2⁻
9/2⁺
1/2⁺
3/2⁺
5/2⁺
7/2⁺
5/2⁺
135 57La78
11/2⁻
9/2⁺
(1/2⁺)
(3/2⁺)
(5/2⁺)
5/2⁺
7/2⁺
137 57La80
11/2⁻
5/2⁺
7/2⁺
139 57La82

Meyer - Fig. 15

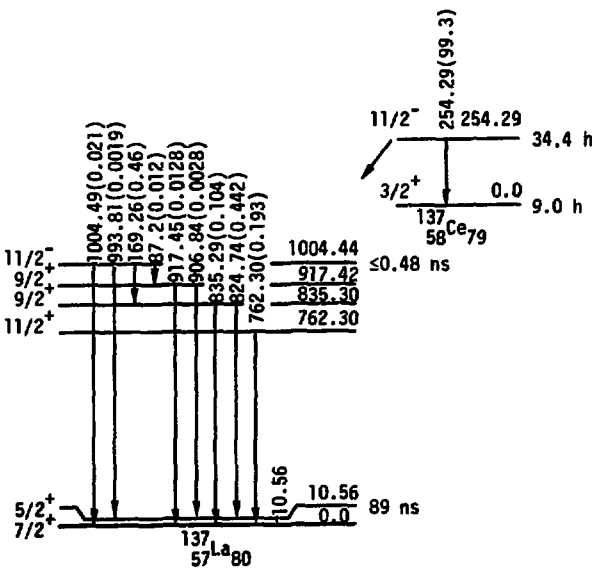
254.29(99.3)
11/2⁻
254.29
34.4 h
3/2⁺
0.0
9.0 h
137
58Ce79
1004.49(0.021)
993.81(0.0019)
169.26(0.46)
87.2(0.012)
917.45(0.0128)
906.84(0.0028)
835.29(0.104)
824.74(0.442)
762.30(0.193)
10.56
11/2⁻
9/2⁺
9/2⁺
11/2⁺
1004.44
917.42
835.30
762.30
≤0.48 ns
5/2⁺
7/2⁺
10.56
0.0
89 ns
137
57La80

Meyer - Fig. 16

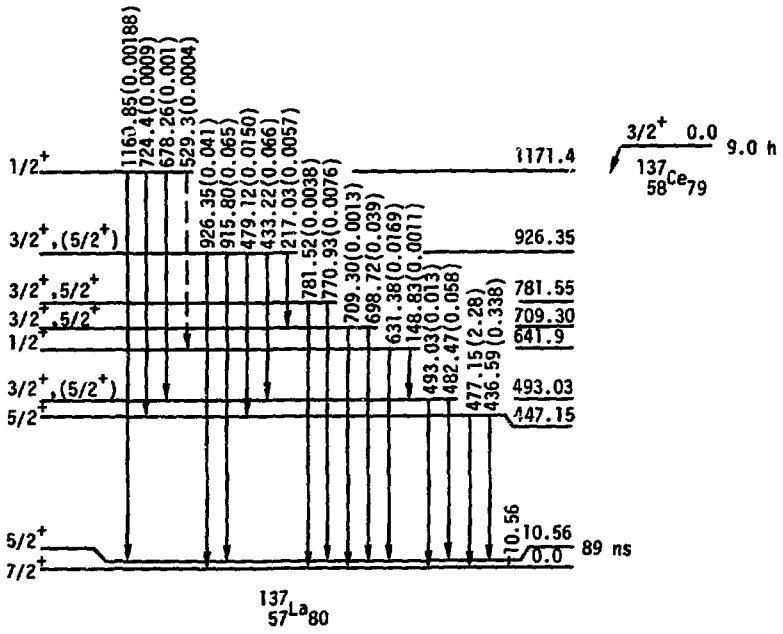
1160.85(0.00188)
724.4(0.0009)
678.26(0.001)
529.3(0.0004)
926.35(0.041)
915.80(0.065)
479.12(0.0150)
433.22(0.066)
217.03(0.0057)
781.52(0.0038)
770.93(0.0076)
709.30(0.0013)
698.72(0.039)
631.38(0.0169)
148.83(0.0011)
493.03(0.013)
482.47(0.058)
477.15(2.28)
436.59(0.338)
10.56
1/2+
3/2+,(5/2+)
3/2+,5/2+
3/2+,5/2+
1/2+
3/2+,(5/2+)
5/2+
5/2+
7/2+
1171.4
926.35
781.55
709.30
641.9
493.03
447.15
10.56
0.0
89 ns
3/2+ 0.0
9.0 h
137 58Ce79
137 57La80

Meyer - Fig. 17

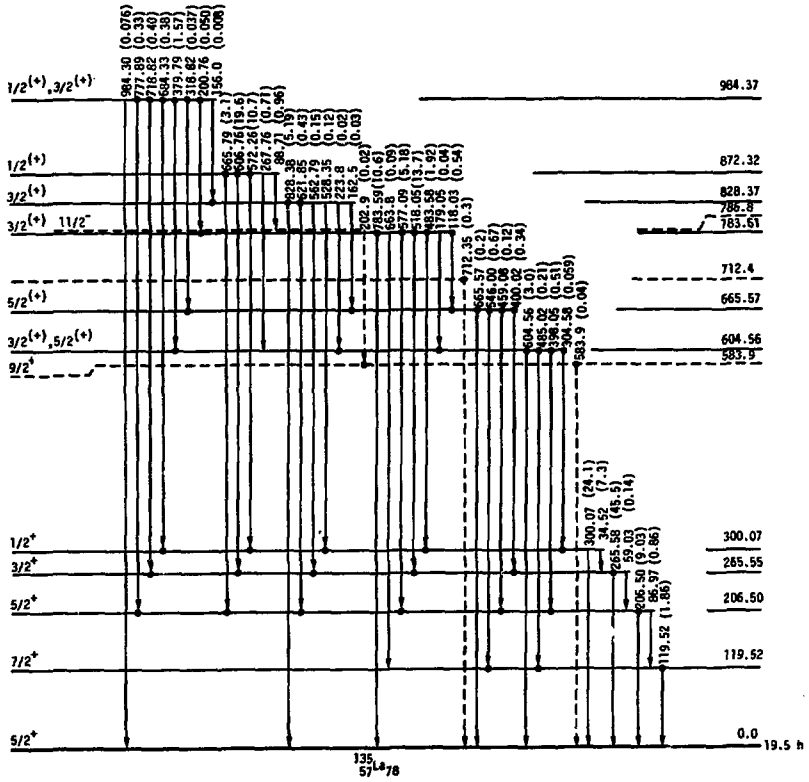
984.30 (0.076)
777.89 (0.33)
718.82 (0.40)
594.33 (0.38)
513.62 (1.57)
200.76 (0.050)
156.0 (0.008)
665.79 (3.1)
606.76 (19.6)
572.26 (10.7)
267.76 (0.71)
98.71 (0.96)
828.35 (0.43)
621.85 (0.15)
562.79 (0.12)
528.35 (0.12)
223.8 (0.02)
162.5 (0.03)
202.9 (0.02)
783.59 (10.6)
693.8 (0.09)
577.09 (5.18)
538.05 (13.7)
483.58 (1.92)
179.05 (0.04)
118.03 (0.54)
712.35 (0.3)
665.57 (0.2)
646.00 (0.67)
559.08 (0.12)
400.02 (0.34)
604.56 (3.01)
585.02 (0.21)
198.05 (0.059)
304.58 (0.04)
583.9 (0.04)
300.07 (24.1)
34.52 (7.3)
265.58 (46.5)
59.03 (0.14)
206.50 (5.03)
96.57 (0.86)
119.52 (1.86)
1/2(+),3/2(+)
984.37
1/2(+)
872.32
3/2(+)
828.37
3/2(+) 11/2-
788.8
783.61
712.4
5/2(+)
665.57
3/2(+),5/2(+)
604.56
9/2+
583.9
1/2+
300.07
3/2+
265.55
5/2+
206.50
7/2+
119.52
5/2+
0.0
19.5 h
135
57La78

Meyer - Fig. 18

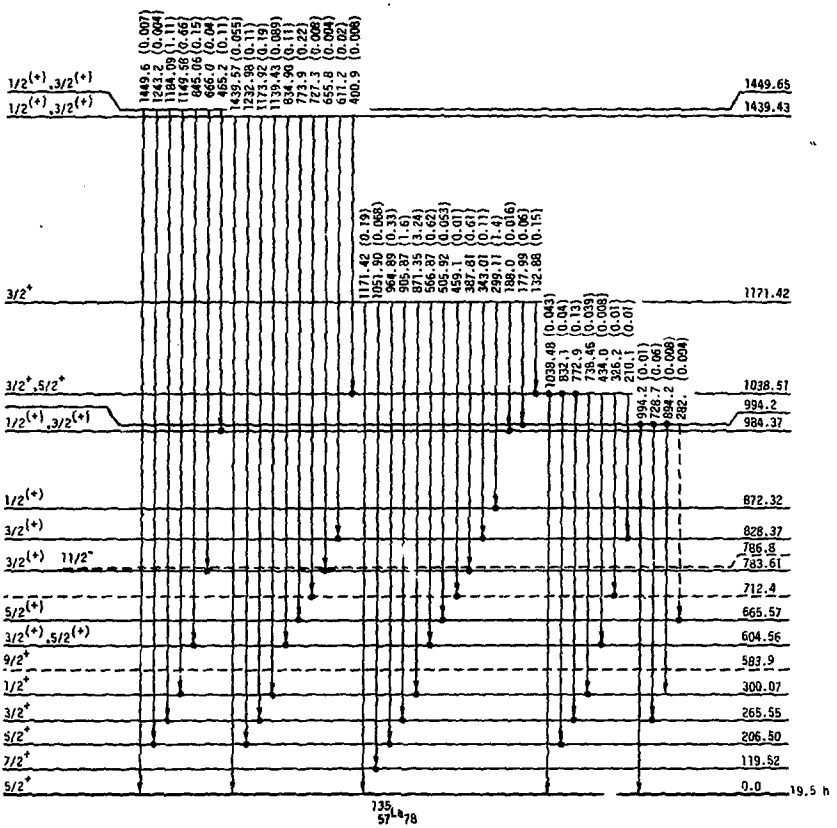
1/2(+),3/2(+)
1/2(+),3/2(+)
3/2+
3/2+,5/2+
1/2(+),3/2(+)
1/2(+)
3/2(+)
3/2(+) 11/2-
5/2(+)
3/2(+),5/2(+)
9/2+
1/2+
3/2+
5/2+
7/2+
5/2+
1449.65
1439.43
1171.42
1038.51
994.2
984.37
872.32
828.37
786.8
783.61
712.4
665.57
604.56
583.9
309.07
265.55
206.50
119.52
0.0
19.5 h
1449.6 (0.007)
1243.2 (0.004)
1184.09 (1.11)
1145.58 (0.15)
666.06 (0.04)
465.2 (0.11)
1439.57 (0.055)
1232.98 (0.11)
1173.92 (0.19)
1139.43 (0.089)
834.90 (0.11)
773.9 (0.22)
727.3 (0.008)
655.8 (0.004)
611.2 (0.02)
400.9 (0.006)
1171.42 (0.19)
1051.90 (0.068)
964.89 (0.33)
905.87 (1.6)
871.35 (3.24)
566.87 (0.62)
505.92 (0.053)
459.1 (0.01)
387.81 (0.61)
343.01 (0.11)
299.11 (1.4)
188.0 (0.016)
177.99 (0.06)
132.88 (0.15)
1038.48 (0.043)
832.1 (0.04)
772.9 (0.13)
738.46 (0.093)
724.10 (0.008)
334.2 (0.01)
210.1 (0.01)
994.2 (0.01)
728.7 (0.06)
894.2 (0.008)
282. (0.004)
135 57La 78

Meyer - Fig. 19

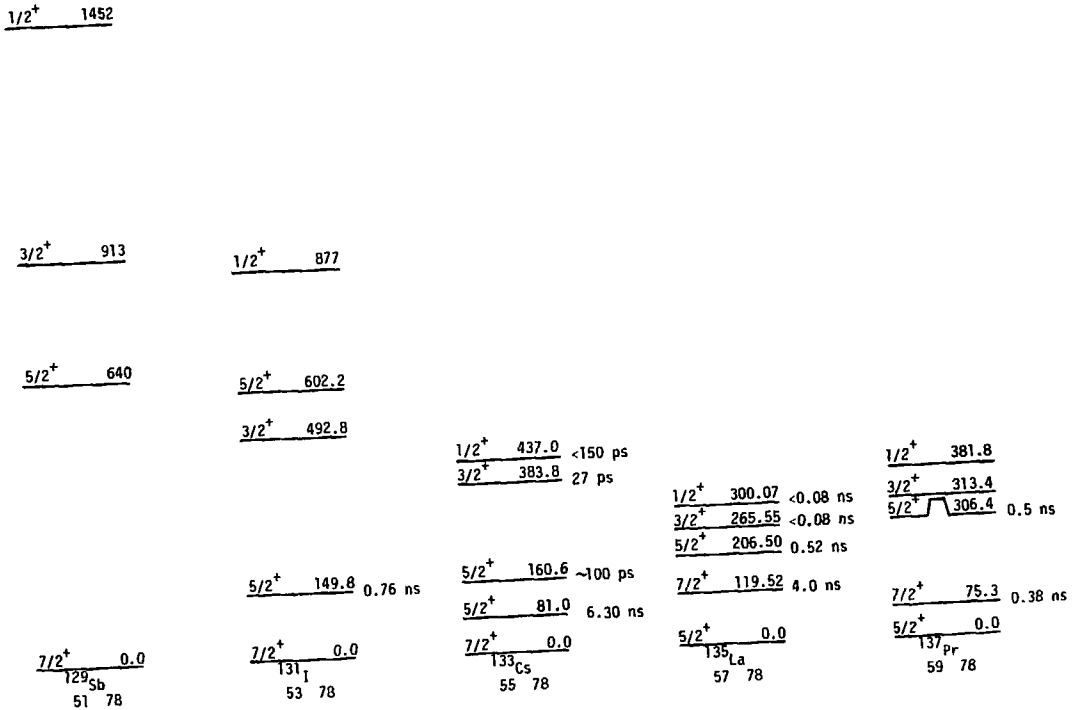
1/2+ 1452
3/2+ 913
1/2+ 877
5/2+ 640
5/2+ 602.2
3/2+ 492.8
1/2+ 437.0 <150 ps
3/2+ 383.8 27 ps
1/2+ 381.8
3/2+ 313.4
5/2+ 306.4 0.5 ns
1/2+ 300.07 <0.08 ns
3/2+ 265.55 <0.08 ns
5/2+ 206.50 0.52 ns
5/2+ 149.8 0.76 ns
5/2+ 160.6 ~100 ps
7/2+ 119.52 4.0 ns
7/2+ 75.3 0.38 ns
5/2+ 81.0 6.30 ns
7/2+ 0.0
129Sb
51 78
7/2+ 0.0
131I
53 78
7/2+ 0.0
133Cs
55 78
5/2+ 0.0
135La
57 78
5/2+ 0.0
137Pr
59 78

Meyer - Fig. 20

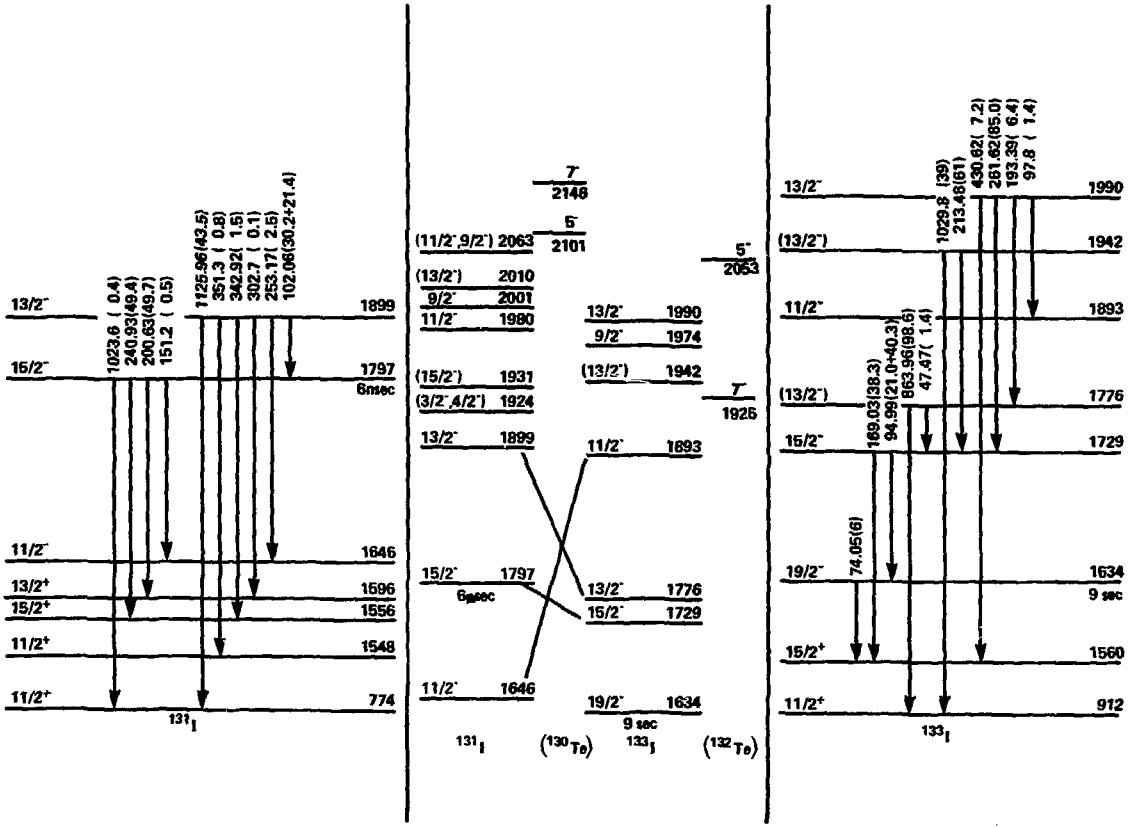
13/2⁻ 1899
15/2⁻ 1797
6nsec
11/2⁻ 1646
13/2⁺ 1596
15/2⁺ 1556
11/2⁺ 1548
11/2⁺ 774
131I
1023.6 (0.4)
240.93(49.4)
200.63(49.7)
151.2 (0.5)
1125.96(43.5)
351.3 (0.8)
342.92(1.5)
302.7 (0.1)
253.17(2.5)
102.06(30.2+21.4)
7⁻ 2146
5⁻ 2101
(11/2⁻,9/2⁻) 2063
(13/2⁻) 2010
9/2⁻ 2001
11/2⁻ 1980
(15/2⁻) 1931
(3/2⁻,4/2⁻) 1924
13/2⁻ 1899
15/2⁻ 1797
6μsec
11/2⁻ 1646
131I
(130Te)
13/2⁻ 1990
9/2⁻ 1974
(13/2⁻) 1942
11/2⁻ 1893
13/2⁻ 1776
15/2⁻ 1729
19/2⁻ 1634
9 sec
133I
(132Te)
5⁻ 2053
7⁻ 1926
13/2⁻ 1990
(13/2⁻) 1942
11/2⁻ 1893
(13/2⁻) 1776
15/2⁻ 1729
19/2⁻ 1634
9 sec
15/2⁺ 1560
11/2⁺ 912
133I
1029.8 (39)
213.46(61)
430.62(7.2)
261.62(65.0)
193.39(6.4)
97.8 (1.4)
169.03(38.3)
94.99(21.0+40.3)
863.96(98.6)
47.47(1.4)
74.05(6)

Meyer - Fig. 21

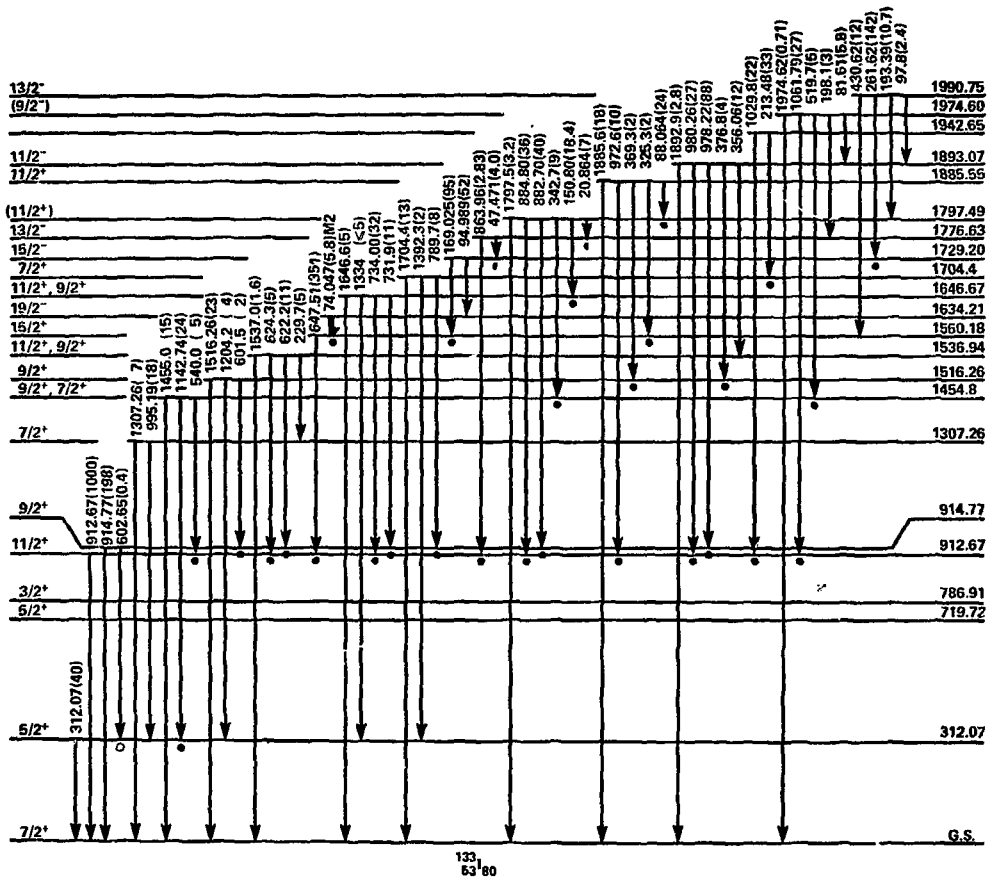
13/2⁻
(9/2⁻)
11/2⁻
11/2⁺
(11/2⁺)
13/2⁻
15/2⁻
7/2⁺
11/2⁺, 9/2⁺
19/2⁻
16/2⁺
11/2⁺, 9/2⁺
9/2⁺
9/2⁺, 7/2⁺
7/2⁺
9/2⁺
11/2⁺
3/2⁺
5/2⁺
5/2⁺
7/2⁺
1990.75
1974.60
1942.65
1893.07
1885.55
1797.49
1776.63
1729.20
1704.4
1646.67
1634.21
1560.18
1536.94
1516.26
1454.8
1307.26
914.77
912.67
786.91
719.72
312.07
G.S.
1307.26(7)
995.19(18)
1455.0 (15)
1142.74(24)
540.0 (5)
1516.26(23)
1204.2 (4)
601.5 (2)
1537.01(1.6)
824.3(5)
622.2(11)
229.7(5)
(647.51(351)
74.047(5.8)M2
1646.6(5)
1334 (<5)
734.00(32)
731.9(11)
1704.4(13)
1392.3(2)
789.7(8)
169.025(95)
94.999(52)
863.39(12.83)
47.471(4.0)
1797.5(3.2)
884.80(36)
882.70(40)
342.7(9)
150.80(18.4)
20.864(7)
1885.6(18)
972.6(10)
369.3(2)
325.3(2)
88.064(24)
1892.9(2.8)
980.26(27)
978.22(88)
376.8(4)
356.06(12)
1029.8(22)
213.48(33)
1974.62(0.71)
1061.79(27)
519.7(6)
198.1(3)
81.61(5.8)
430.62(12)
261.52(142)
193.39(10.7)
97.8(2.4)
912.67(1000)
914.77(198)
602.65(0.4)
312.07(40)
133
63 80

Meyer - Fig. 22

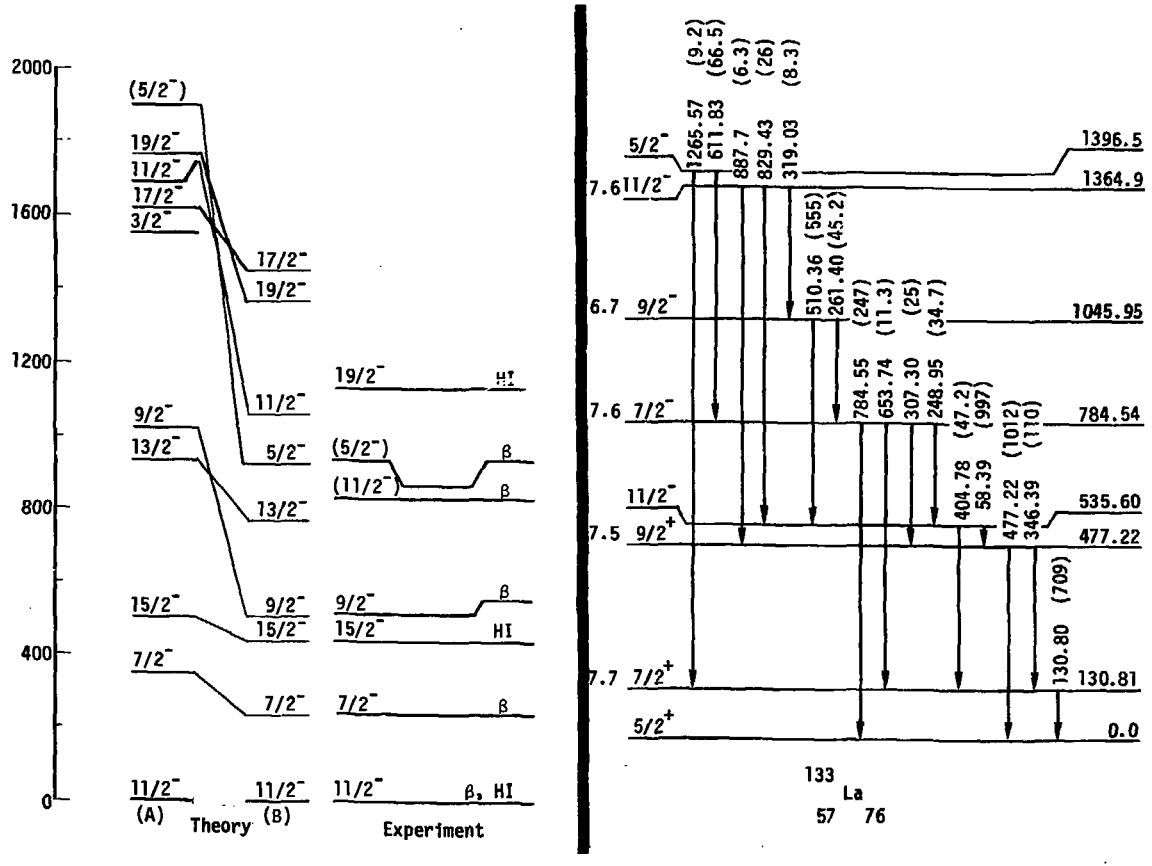
2000
1600
1200
800
400
0
(5/2⁻)
19/2⁻
11/2⁻
17/2⁻
3/2⁻
17/2⁻
19/2⁻
11/2⁻
5/2⁻
9/2⁻
13/2⁻
13/2⁻
15/2⁻
9/2⁻
15/2⁻
7/2⁻
7/2⁻
11/2⁻ (A)
11/2⁻ (B)
Theory
19/2⁻ HI
(5/2⁻) β
(11/2⁻) β
9/2⁻ β
15/2⁻ HI
7/2⁻ β
11/2⁻ β, HI
Experiment
(9.2)
(66.5)
(6.3)
(26)
(8.3)
1265.57
611.83
887.7
829.43
319.03
5/2⁻ 1396.5
7.6 11/2⁻ 1364.9
510.36 (555)
261.40 (45.2)
(247)
(11.3)
(25)
(34.7)
6.7 9/2⁻ 1045.95
784.55
653.74
307.30
248.95
(47.2)
(997)
(1012)
(110)
7.6 7/2⁻ 784.54
11/2⁻ 535.60
404.78
58.39
477.22
346.39
7.5 9/2⁺ 477.22
(709)
130.80
7.7 7/2⁺ 130.81
5/2⁺ 0.0
133 La
57 76

Meyer - Fig. 23

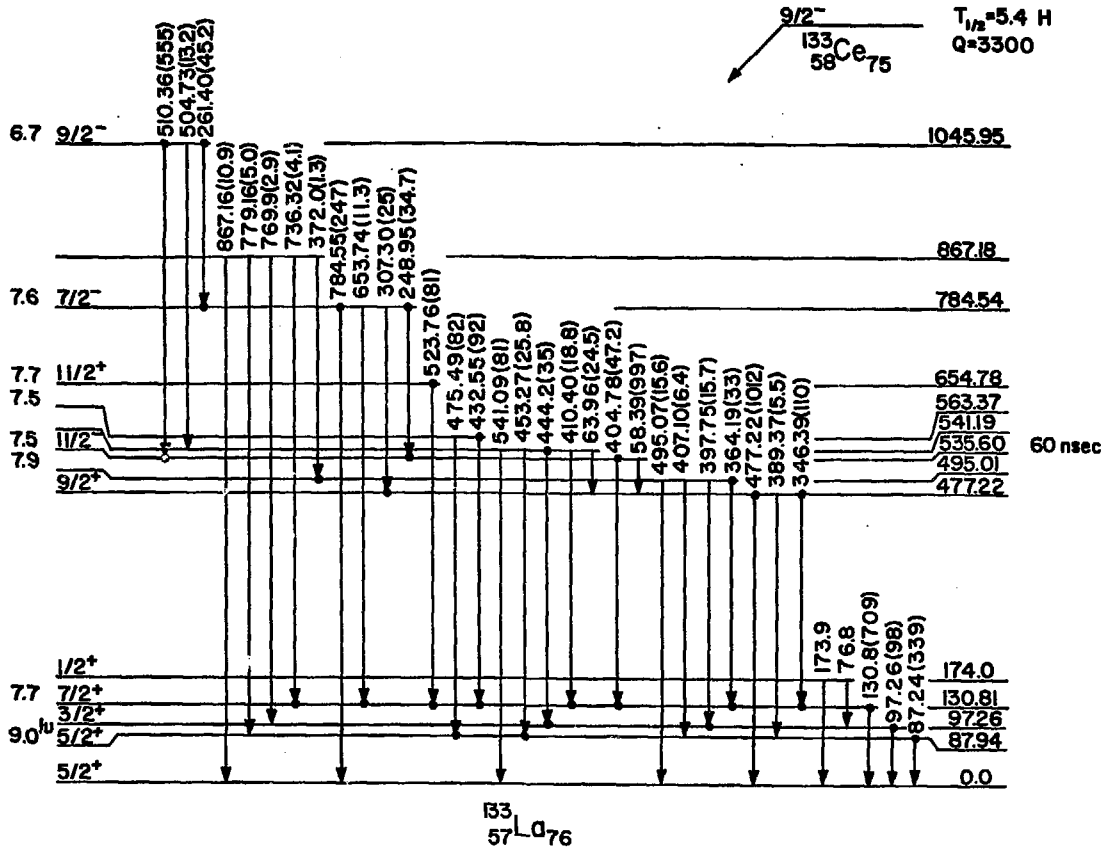
9/2⁻
133 58Ce75
T1/2=5.4 H
Q=3300
6.7 9/2⁻
1045.95
867.18
7.6 7/2⁻
784.54
7.7 11/2⁺
654.78
7.5
563.37
7.5 11/2⁻
541.19
535.60
60 nsec
7.9
495.01
9/2⁺
477.22
1/2⁺
7.7 7/2⁺
174.0
130.81
3/2⁺
97.26
9.0fu 5/2⁺
87.94
5/2⁺
0.0
510.36(555)
504.73(13.2)
261.40(452)
867.16(10.9)
779.16(5.0)
769.9(2.9)
736.32(4.1)
372.0(1.3)
784.55(247)
653.74(11.3)
307.30(25)
248.95(34.7)
523.76(81)
475.49(82)
432.55(92)
541.09(81)
453.27(25.8)
444.2(35)
410.40(18.8)
63.96(24.5)
404.78(47.2)
58.39(997)
495.07(15.6)
407.10(6.4)
397.75(15.7)
364.19(33)
477.22(1012)
389.37(5.5)
346.39(110)
173.9
76.8
130.8(709)
97.26(98)
87.24(339)
133 57La76

Meyer - Fig. 24

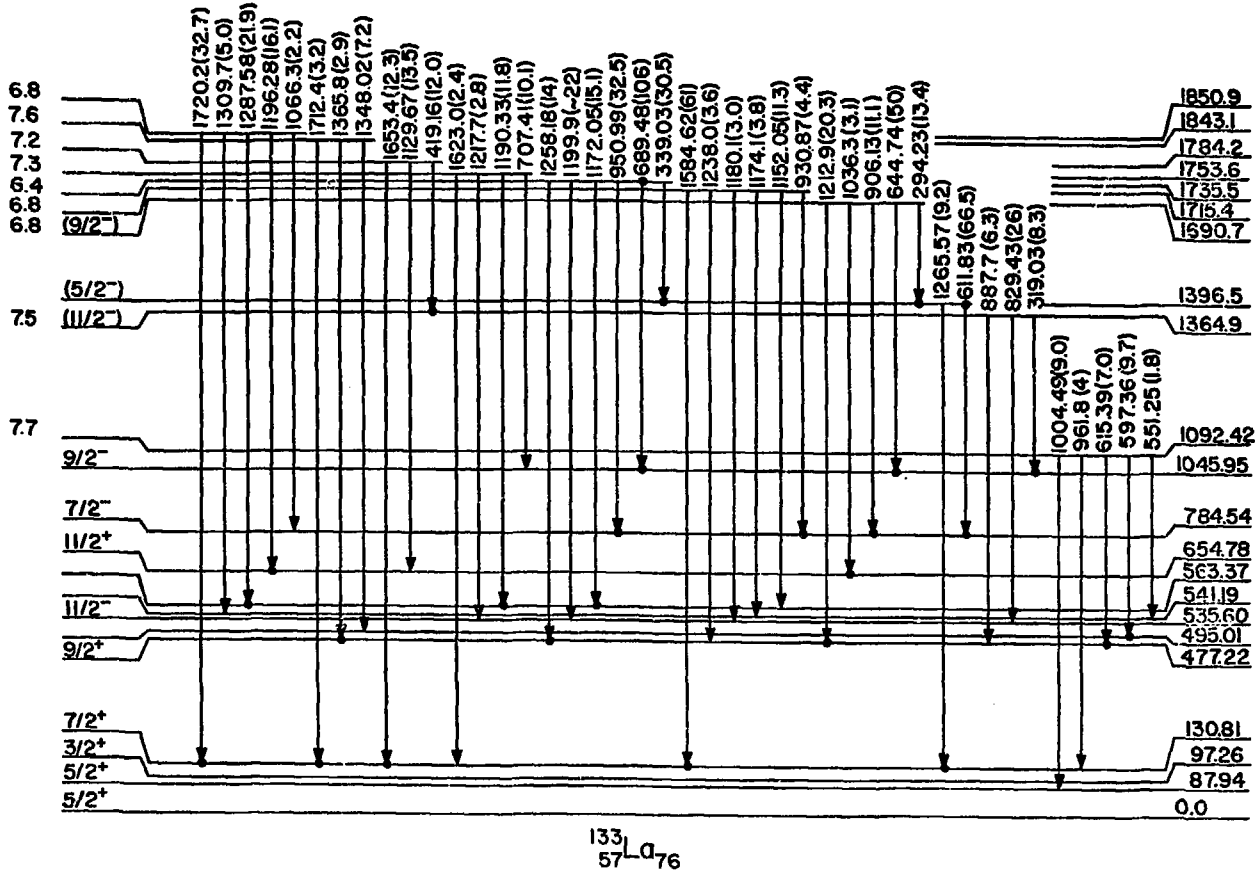

$^{133}_{57}La_{76}$

Meyer - Fig. 25

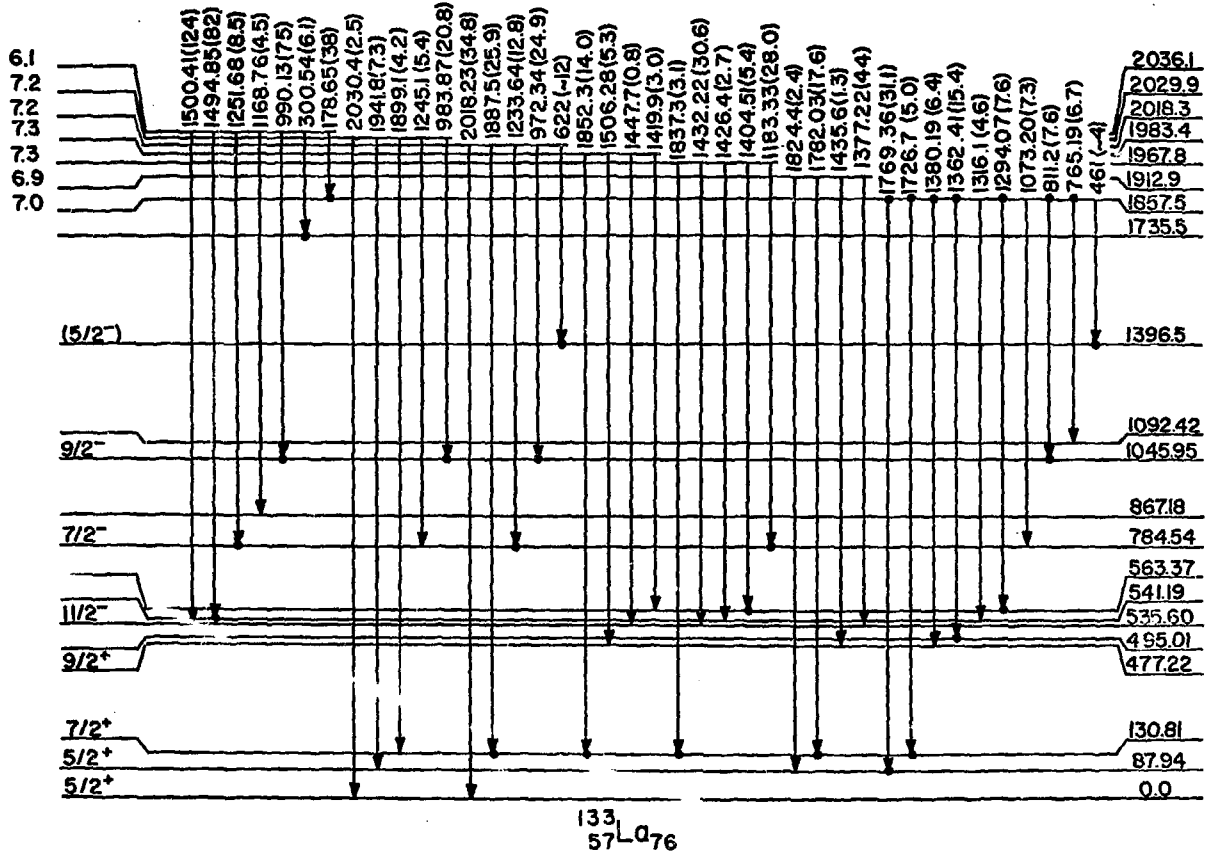
6.1
7.2
7.2
7.3
7.3
6.9
7.0
1500.41(124)
1494.85(82)
1251.68 (8.5)
1168.76(4.5)
990.13(75)
300.54(6.1)
178.65(38)
2030.4(2.5)
1941.8(7.3)
1899.1(4.2)
1245.1(5.4)
983.87(20.8)
2018.23(34.8)
1887.5(25.9)
1233.64(12.8)
972.34(24.9)
622 (~12)
1852.3(14.0)
1506.28(5.3)
1447.7(0.8)
1419.9(3.0)
1837.3(3.1)
1432.22(30.6)
1426.4(2.7)
1404.5(5.4)
1183.33(28.0)
1824.4(2.4)
1782.03(17.6)
1435.6(1.3)
1377.22(44)
1769.36(31.1)
1726.7 (5.0)
1380.19 (6.4)
1362.41(15.4)
1316.1 (4.6)
1294.07(7.6)
1073.20(7.3)
811.2(7.6)
765.19(6.7)
461 (~4)
2036.1
2029.9
2018.3
1983.4
1967.8
1912.9
1857.5
1735.5
(5/2⁻)
1396.5
9/2⁻
1092.42
1045.95
867.18
7/2⁻
784.54
563.37
541.19
11/2⁻
535.60
495.01
9/2⁺
477.22
7/2⁺
130.81
5/2⁺
87.94
5/2⁺
0.0
133
57La76

Meyer - Fig. 26

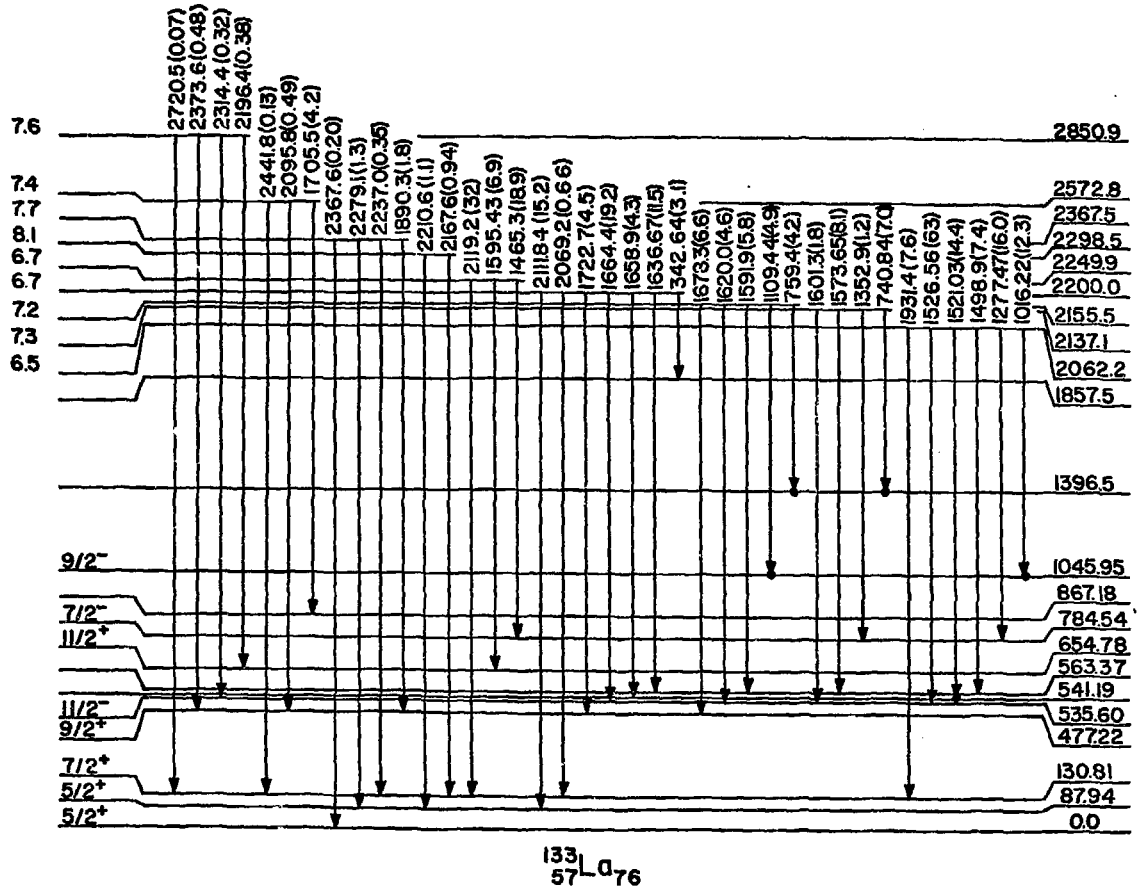
2720.5(0.07)
2373.6(0.48)
2314.4(0.32)
2196.4(0.38)
2441.8(0.13)
2095.8(0.49)
1705.5(4.2)
2367.6(0.20)
2279.1(1.3)
2237.0(0.35)
1890.3(1.8)
2210.6(1.1)
2167.6(0.94)
2119.2(32)
1595.43(6.9)
1465.3(18.9)
2111.84(15.2)
2069.2(0.66)
1722.7(4.5)
1664.4(19.2)
1658.9(4.3)
1636.67(11.5)
342.64(3.1)
1673.36(6.6)
1620.0(4.6)
1591.9(5.8)
1109.44(4.9)
759.4(4.2)
1601.3(1.8)
1573.65(8.1)
1352.91(1.2)
740.84(7.0)
931.4(7.6)
1526.56(63)
1521.03(14.4)
1498.91(7.4)
1277.47(16.0)
1016.22(12.3)
7.6
7.4
7.7
8.1
6.7
6.7
7.2
7.3
6.5
2850.9
2572.8
2367.5
2298.5
2249.9
2200.0
2155.5
2137.1
2062.2
1857.5
1396.5
9/2⁻
1045.95
7/2⁻
867.18
11/2⁺
784.54
654.78
563.37
11/2⁻
541.19
9/2⁺
535.60
477.22
7/2⁺
130.81
5/2⁺
87.94
5/2⁺
0.0
133 57 La 76

Meyer - Fig. 27

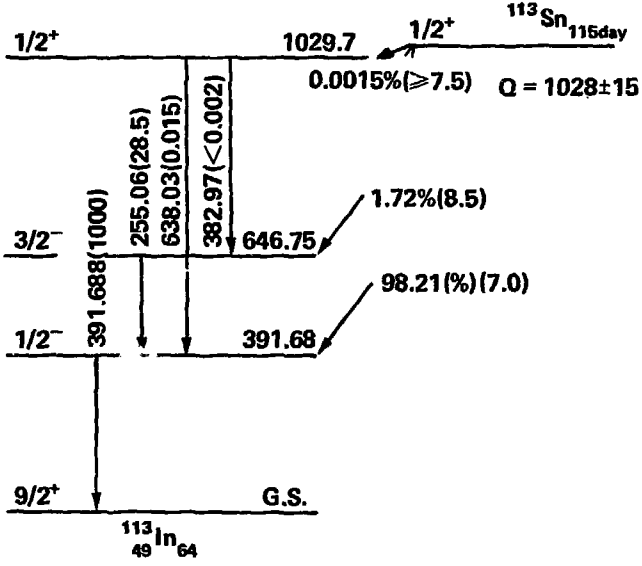
1/2+
1029.7
1/2+
113Sn115day
0.0015%(≥7.5)
Q = 1028±15
382.97(<0.002)
638.03(0.015)
255.06(28.5)
391.688(1000)
1.72%(8.5)
3/2−
646.75
98.21(%)(7.0)
1/2−
391.68
9/2+
G.S.
113In64
49

Meyer - Fig. 28

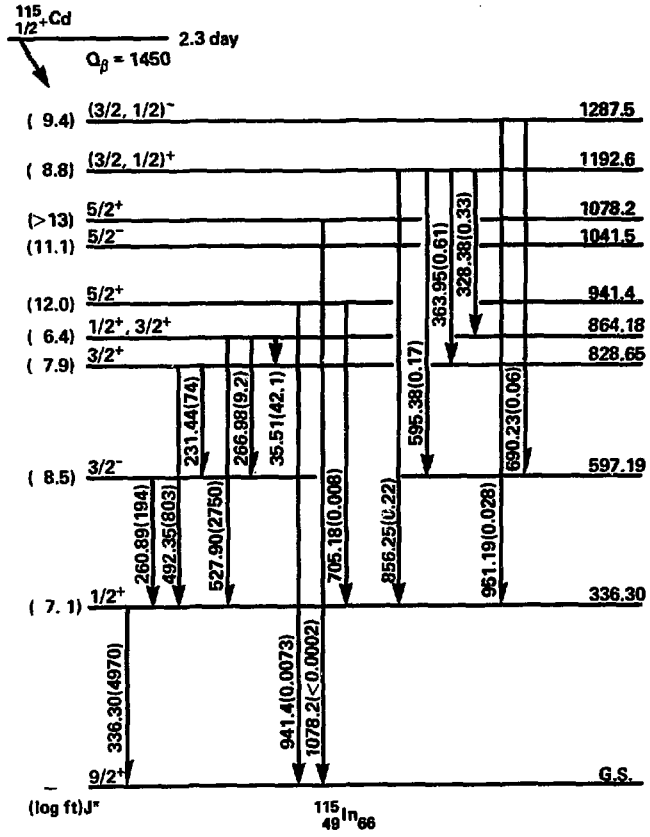
115 1/2+Cd
2.3 day
Qβ = 1450
(9.4) (3/2, 1/2)⁻ 1287.5
(8.8) (3/2, 1/2)+ 1192.6
(>13) 5/2+ 1078.2
(11.1) 5/2⁻ 1041.5
(12.0) 5/2+ 941.4
(6.4) 1/2+, 3/2+ 864.18
(7.9) 3/2+ 828.65
(8.5) 3/2⁻ 597.19
(7. 1) 1/2+ 336.30
9/2+ G.S.
(log ft)Jπ
231.44(74)
266.98(9.2)
35.51(42.1)
595.38(0.17)
363.95(0.61)
328.38(0.33)
690.23(0.06)
260.89(194)
492.35(803)
527.90(2750)
705.18(0.008)
856.25(0.22)
961.19(0.028)
336.30(4970)
941.4(0.0073)
1078.2(<0.0002)
115 49In66

Meyer - Fig. 29

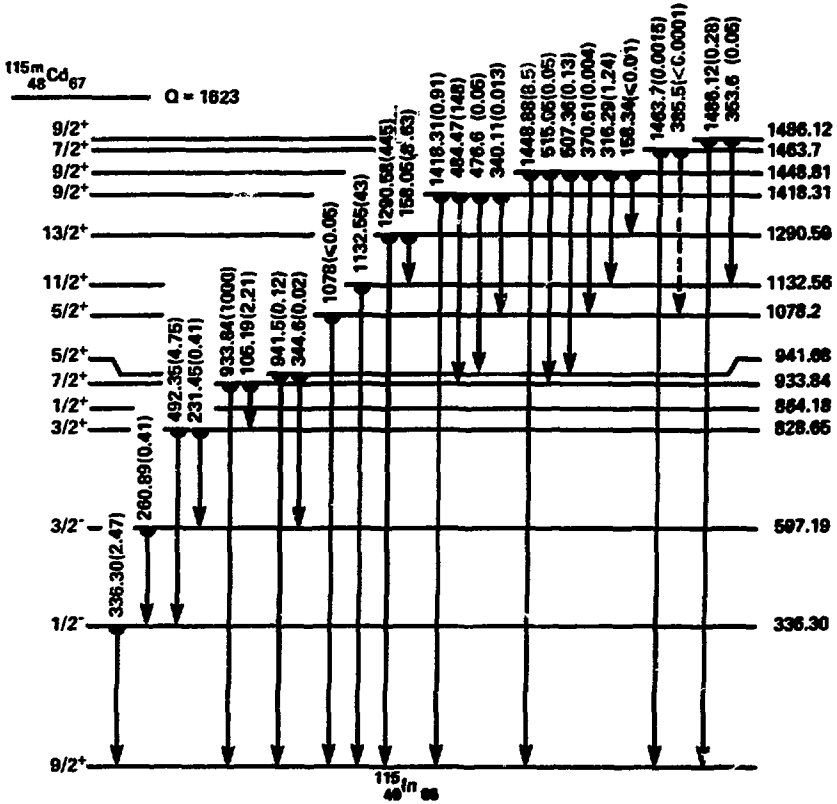
115m 48Cd67
Q = 1623
9/2+
7/2+
9/2+
9/2+
13/2+
11/2+
5/2+
5/2+
7/2+
1/2+
3/2+
3/2-
1/2-
9/2+
1486.12
1463.7
1448.81
1418.31
1290.59
1132.56
1078.2
941.66
933.84
864.18
828.65
597.19
336.30
1078(<0.06)
1132.56(43)
1290.58(445)
158.05(≥.63)
1418.31(0.91)
484.47(148)
476.6 (0.05)
340.11(0.013)
1448.88(8.5)
515.06(0.05)
507.36(0.13)
370.61(0.004)
316.29(1.24)
158.34(<0.01)
1463.7(0.0015)
385.5(<0.0001)
1486.12(0.28)
353.6 (0.05)
933.84(1000)
105.19(2.21)
941.5(0.12)
344.6(0.02)
492.35(4.75)
231.45(0.41)
260.89(0.41)
336.30(2.47)
115 49In 66

Meyer - Fig. 30

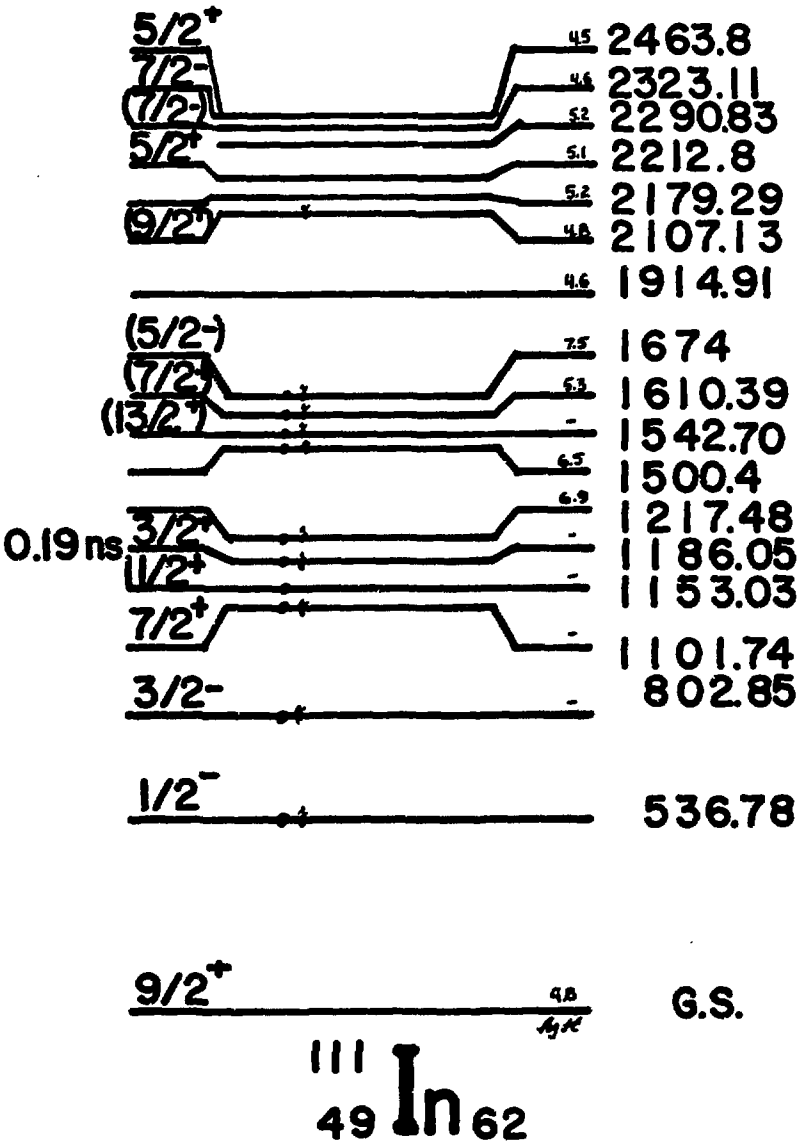
5/2+
7/2-
(7/2-)
5/2+
(9/2+)
(5/2-)
(7/2+)
(13/2+)
0.19 ns
3/2+
1/2+
7/2+
3/2-
1/2-
9/2+
4.5
4.6
5.2
5.1
5.2
4.8
4.6
7.5
5.3
-
6.5
6.9
-
-
-
-
4.8
2463.8
2323.11
2290.83
2212.8
2179.29
2107.13
1914.91
1674
1610.39
1542.70
1500.4
1217.48
1186.05
1153.03
1101.74
802.85
536.78
G.S.
111
49 In 62

Meyer - Fig. 31

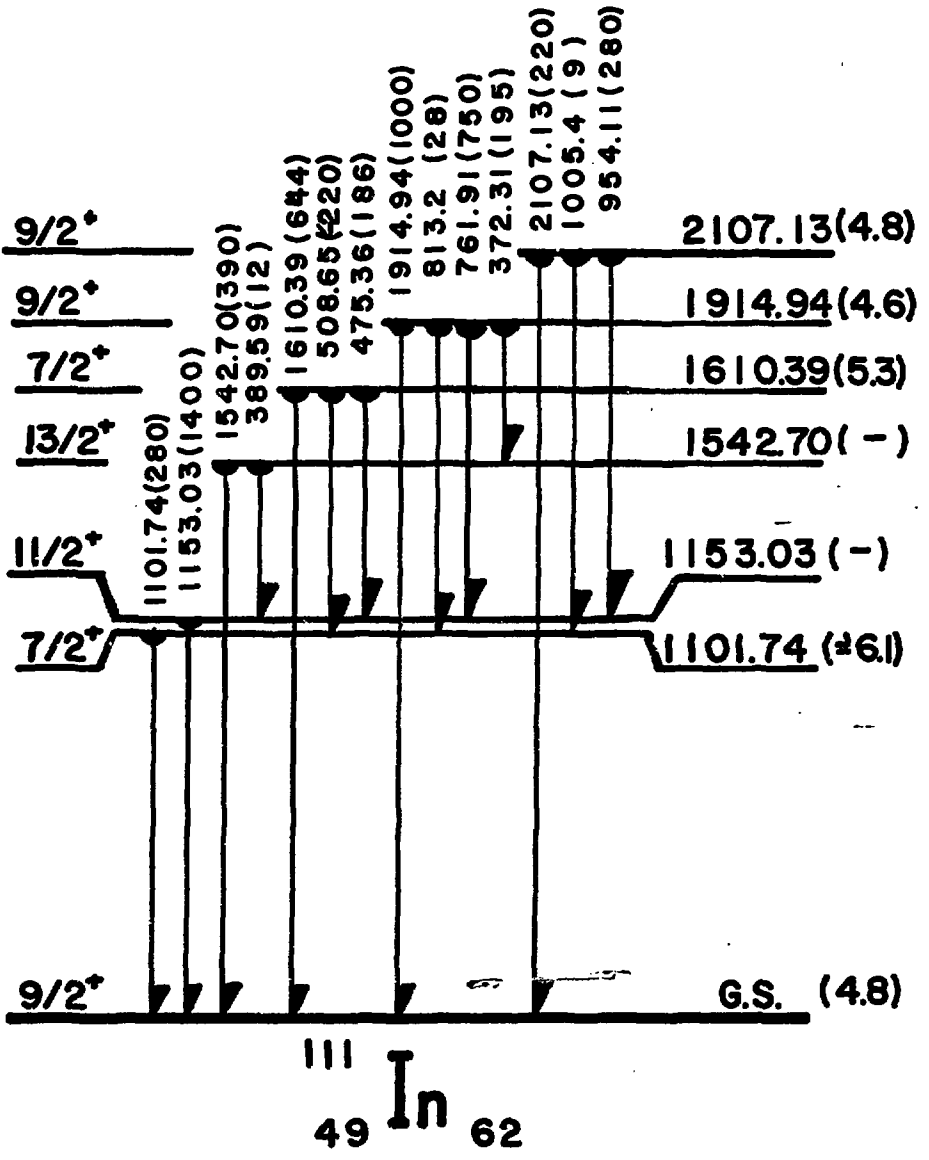
9/2+
9/2+
7/2+
13/2+
11/2+
7/2+
9/2+
2107.13(4.8)
1914.94(4.6)
1610.39(5.3)
1542.70(-)
1153.03 (-)
1101.74 (±6.1)
G.S. (4.8)
1542.70(390)
389.59(12)
1610.39 (644)
508.65(220)
475.36(186)
1914.94(1000)
813.2 (28)
761.91(750)
372.31(195)
2107.13(220)
1005.4 (9)
954.11(280)
1101.74(280)
1153.03(1400)
111 In 62
49

Meyer - Fig. 32

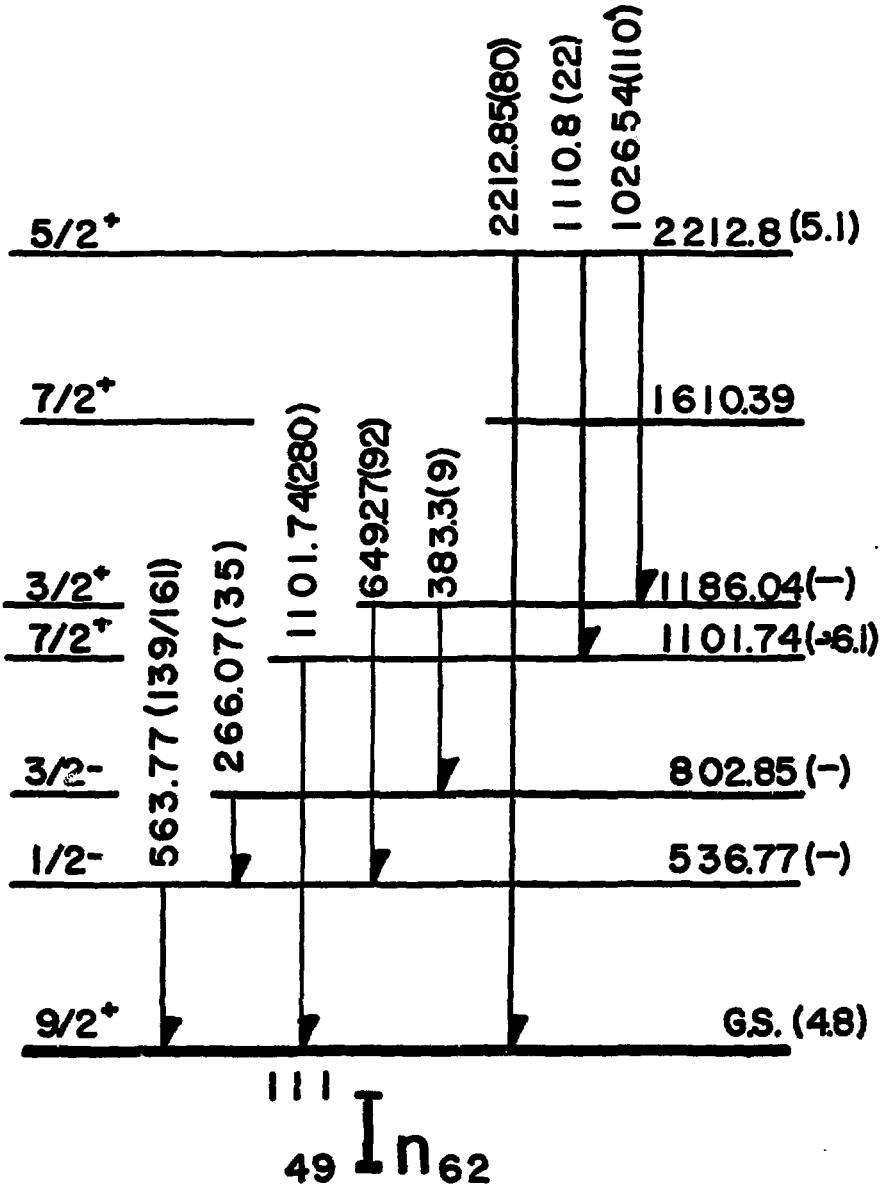
2212.85(80)
1110.8 (22)
1026.54(110)
5/2+
2212.8 (5.1)
7/2+
1610.39
1101.74(280)
649.27(92)
383.3(9)
3/2+
1186.04(−)
7/2+
1101.74(+6.1)
563.77 (139/161)
266.07(35)
3/2-
802.85 (−)
1/2-
536.77 (−)
9/2+
G.S. (4.8)
111
49 In 62

Meyer - Fig. 33

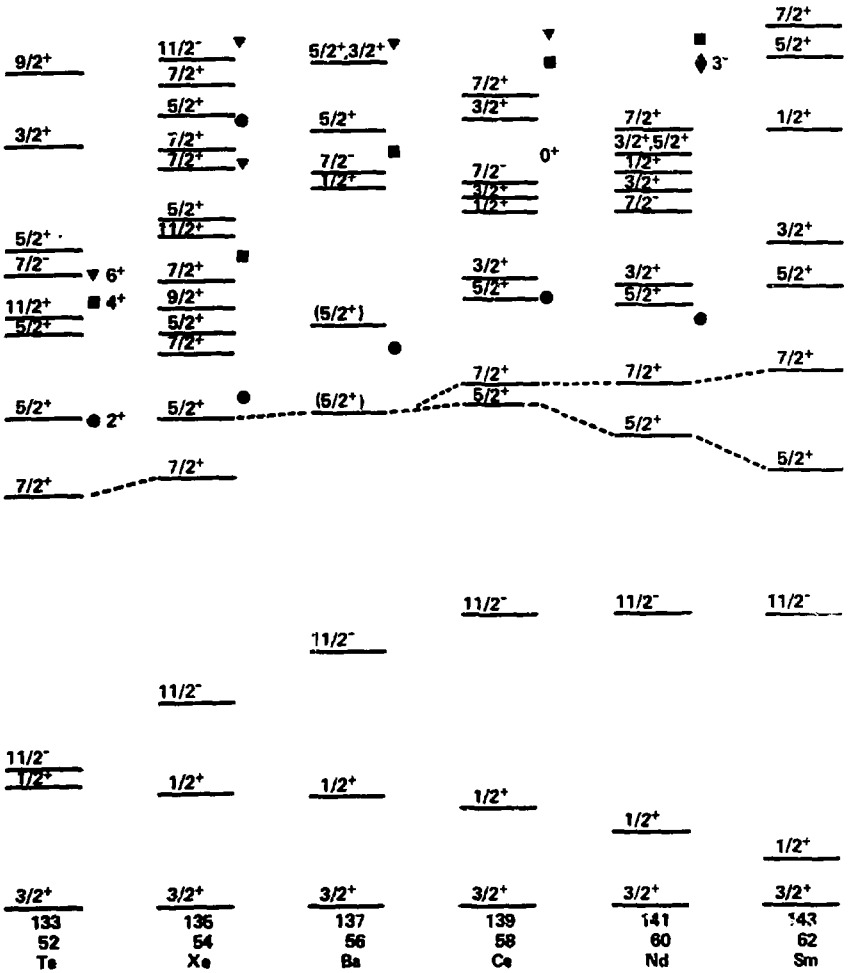
9/2+
3/2+
5/2+
7/2-
6+
11/2+
4+
5/2+
5/2+
2+
7/2+
11/2-
7/2+
5/2+
7/2+
7/2+
5/2+
11/2+
7/2+
9/2+
5/2+
7/2+
5/2+
7/2+
5/2+,3/2+
5/2+
7/2-
1/2+
(5/2+)
(5/2+)
7/2+
3/2+
0+
7/2-
3/2+
1/2+
3/2+
5/2+
7/2+
5/2+
3-
7/2+
3/2+,5/2+
1/2+
3/2+
7/2-
3/2+
5/2+
7/2+
5/2+
7/2+
1/2+
3/2+
5/2+
7/2+
5/2+
11/2-
11/2-
11/2-
11/2-
1/2+
1/2+
1/2+
1/2+
1/2+
3/2+
3/2+
3/2+
3/2+
3/2+
3/2+
133
52
Te
136
54
Xe
137
56
Ba
139
58
Ce
141
60
Nd
143
62
Sm

Meyer - Fig. 34

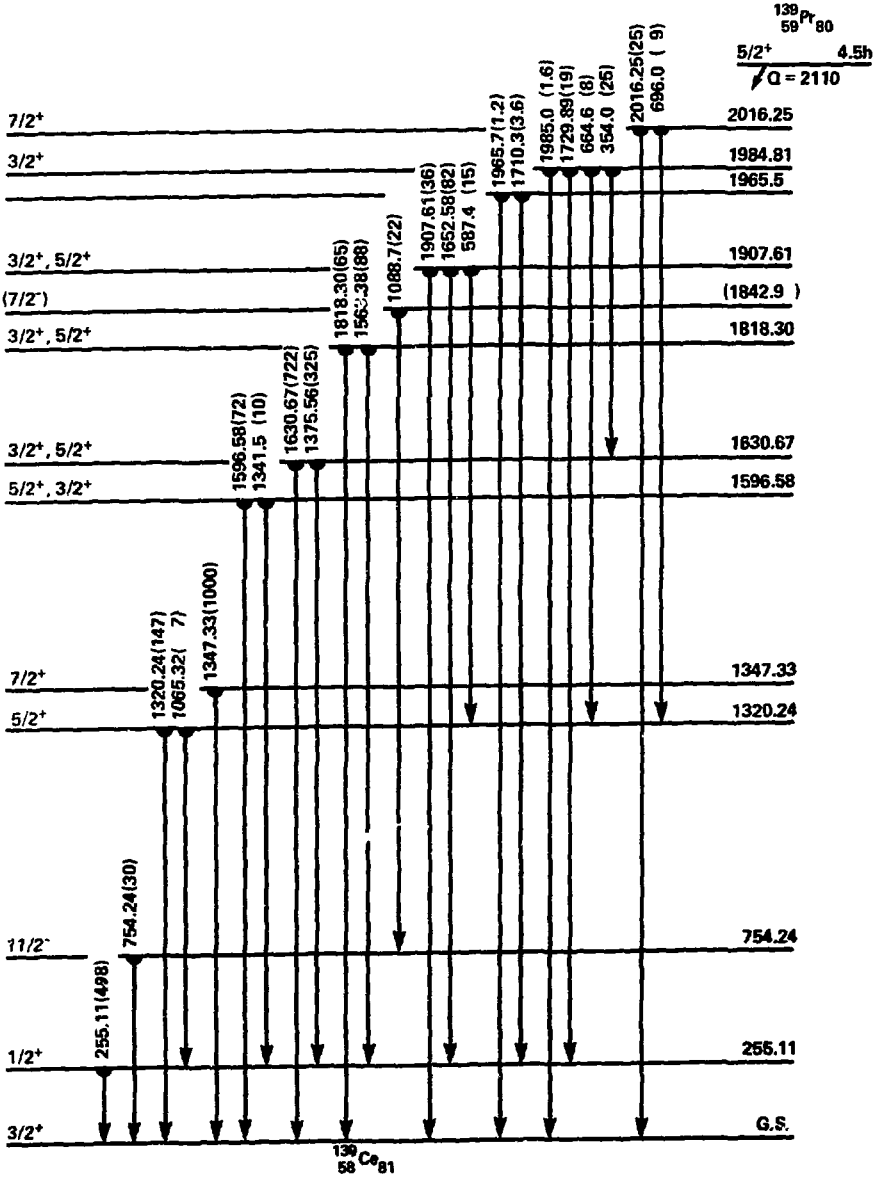
$^{139}_{59}Pr_{80}$
5/2+ 4.5h
Q = 2110
7/2+
3/2+
3/2+, 5/2+
(7/2-)
3/2+, 5/2+
3/2+, 5/2+
5/2+, 3/2+
7/2+
5/2+
11/2-
1/2+
3/2+
2016.25
1984.81
1965.5
1907.61
(1842.9)
1818.30
1630.67
1596.58
1347.33
1320.24
754.24
255.11
G.S.
2016.25(25) 696.0 (9)
1985.0 (1.6) 1729.89(19) 664.6 (8) 354.0 (26)
1965.7(1.2) 1710.3(3.6)
1907.61(36) 1652.58(82) 587.4 (15)
1088.7(22)
1818.30(65) 1562.38(88)
1630.67(722) 1375.56(325)
1596.58(72) 1341.5 (10)
1347.33(1000)
1320.24(147) 1065.32(7)
754.24(30)
255.11(498)
$^{139}_{58}Ce_{81}$

Meyer - Fig. 35

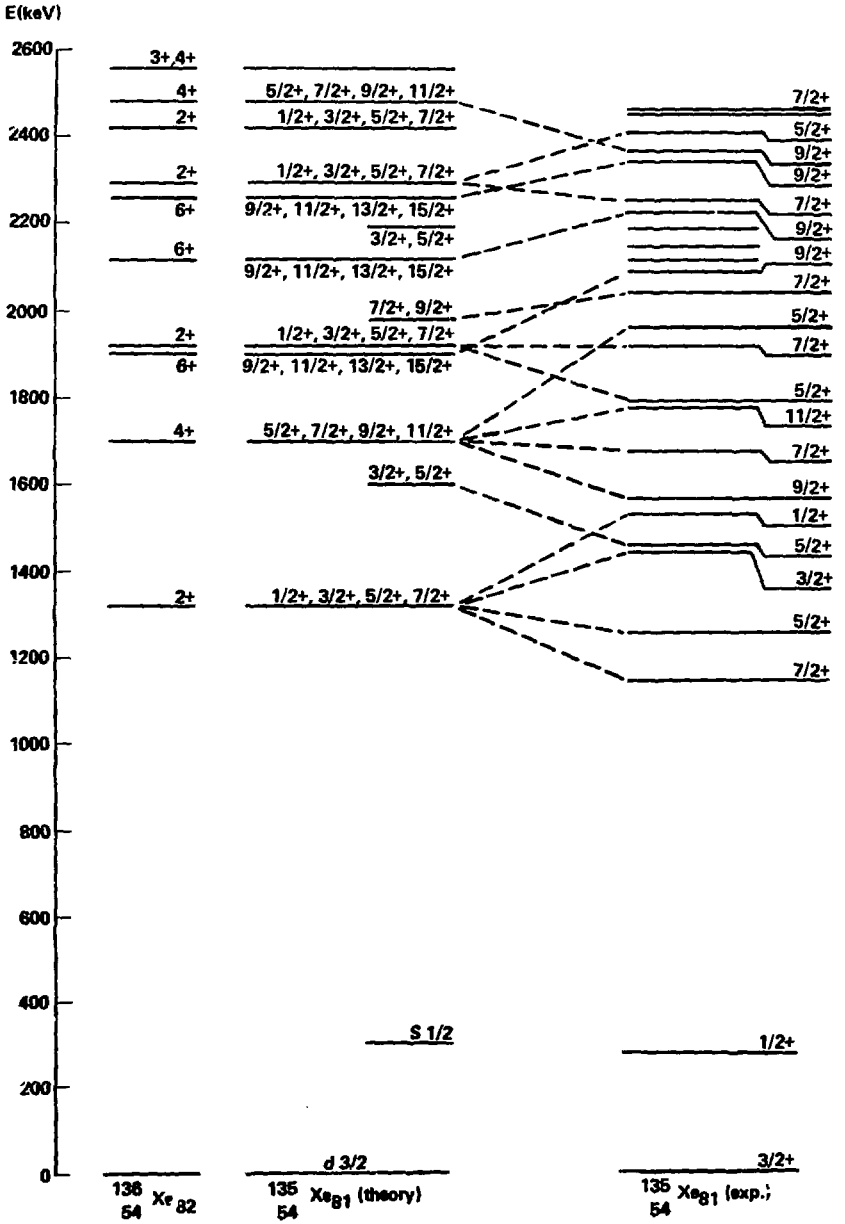
E(keV)
2600
2400
2200
2000
1800
1600
1400
1200
1000
800
600
400
200
0
3+,4+
4+
2+
2+
6+
6+
2+
6+
4+
2+
5/2+, 7/2+, 9/2+, 11/2+
1/2+, 3/2+, 5/2+, 7/2+
1/2+, 3/2+, 5/2+, 7/2+
9/2+, 11/2+, 13/2+, 15/2+
3/2+, 5/2+
9/2+, 11/2+, 13/2+, 15/2+
7/2+, 9/2+
1/2+, 3/2+, 5/2+, 7/2+
9/2+, 11/2+, 13/2+, 15/2+
5/2+, 7/2+, 9/2+, 11/2+
3/2+, 5/2+
1/2+, 3/2+, 5/2+, 7/2+
S 1/2
d 3/2
7/2+
5/2+
9/2+
9/2+
7/2+
9/2+
9/2+
7/2+
5/2+
7/2+
5/2+
11/2+
7/2+
9/2+
1/2+
5/2+
3/2+
5/2+
7/2+
1/2+
3/2+
136 54 Xe82
135 54 Xe81 (theory)
135 54 Xe81 (exp.)

Meyer - Fig. 36

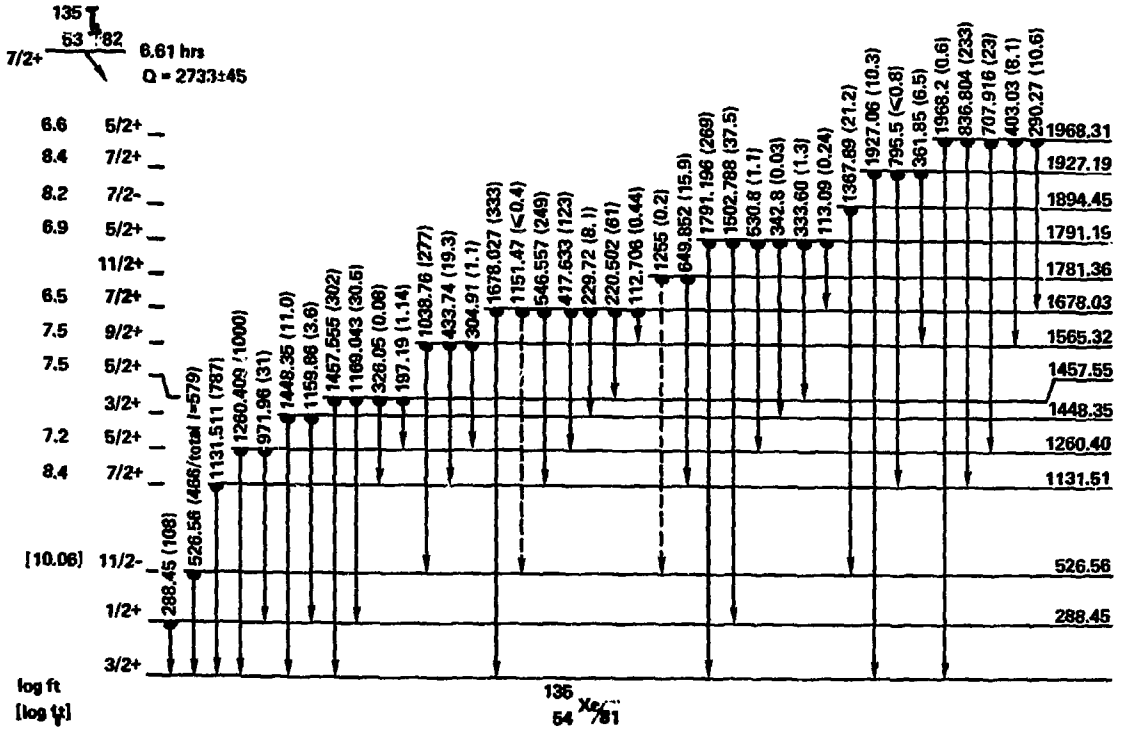
135 53 82
6.61 hrs
Q = 2733±45
7/2+
6.6 5/2+
8.4 7/2+
8.2 7/2-
6.9 5/2+
11/2+
6.5 7/2+
7.5 9/2+
7.5 5/2+
3/2+
7.2 5/2+
8.4 7/2+
[10.06] 11/2-
1/2+
3/2+
log ft
[log tt]
288.45 (108)
526.56 (486/total I=579)
1131.511 (787)
1260.409 (1000)
971.96 (31)
1448.35 (11.0)
1159.86 (3.6)
1457.555 (302)
1169.043 (30.5)
328.05 (0.08)
197.19 (1.14)
1038.76 (277)
433.74 (19.3)
304.91 (1.1)
1678.027 (333)
1151.47 (<0.4)
546.557 (249)
417.633 (123)
229.72 (8.1)
220.502 (61)
112.706 (0.44)
1255 (0.2)
649.852 (15.9)
1791.196 (269)
1502.788 (37.5)
530.8 (1.1)
342.8 (0.03)
333.60 (1.3)
113.09 (0.24)
1387.89 (21.2)
1927.06 (10.3)
795.5 (<0.8)
361.85 (6.5)
1968.2 (0.6)
836.804 (233)
707.916 (23)
403.03 (8.1)
290.27 (10.6)
1968.31
1927.19
1894.45
1791.19
1781.36
1678.03
1565.32
1457.55
1448.35
1260.40
1131.51
526.56
288.45
135 Xe 81
54

Meyer - Fig. 37

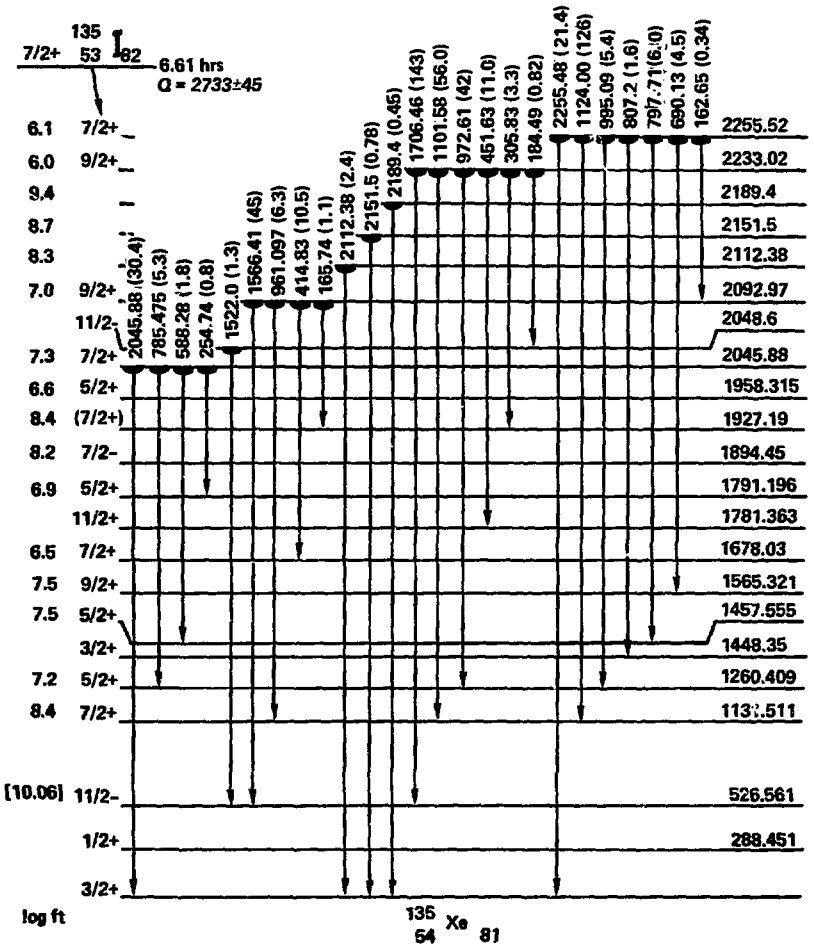
135 53 I 82
7/2+
6.61 hrs
Q = 2733±45
6.1 7/2+
6.0 9/2+
9.4
8.7
8.3
7.0 9/2+
11/2-
7.3 7/2+
6.6 5/2+
8.4 (7/2+)
8.2 7/2-
6.9 5/2+
11/2+
6.5 7/2+
7.5 9/2+
7.5 5/2+
3/2+
7.2 5/2+
8.4 7/2+
[10.06] 11/2-
1/2+
3/2+
log ft
2045.88 (30.4)
785.475 (5.3)
588.28 (1.8)
254.74 (0.8)
1522.0 (1.3)
1566.41 (45)
961.097 (6.3)
414.83 (10.5)
165.74 (1.1)
2112.38 (2.4)
2151.5 (0.78)
2189.4 (0.45)
1706.46 (143)
1101.58 (56.0)
972.61 (42)
451.63 (11.0)
305.83 (3.3)
184.49 (0.82)
2255.48 (21.4)
1124.00 (126)
995.09 (5.4)
807.2 (1.6)
797.71(6.0)
690.13 (4.5)
162.65 (0.34)
2255.52
2233.02
2189.4
2151.5
2112.38
2092.97
2048.6
2045.88
1958.315
1927.19
1894.45
1791.196
1781.363
1678.03
1565.321
1457.555
1448.35
1260.409
1131.511
526.561
288.451
135 Xe 81
54

Meyer - Fig. 38

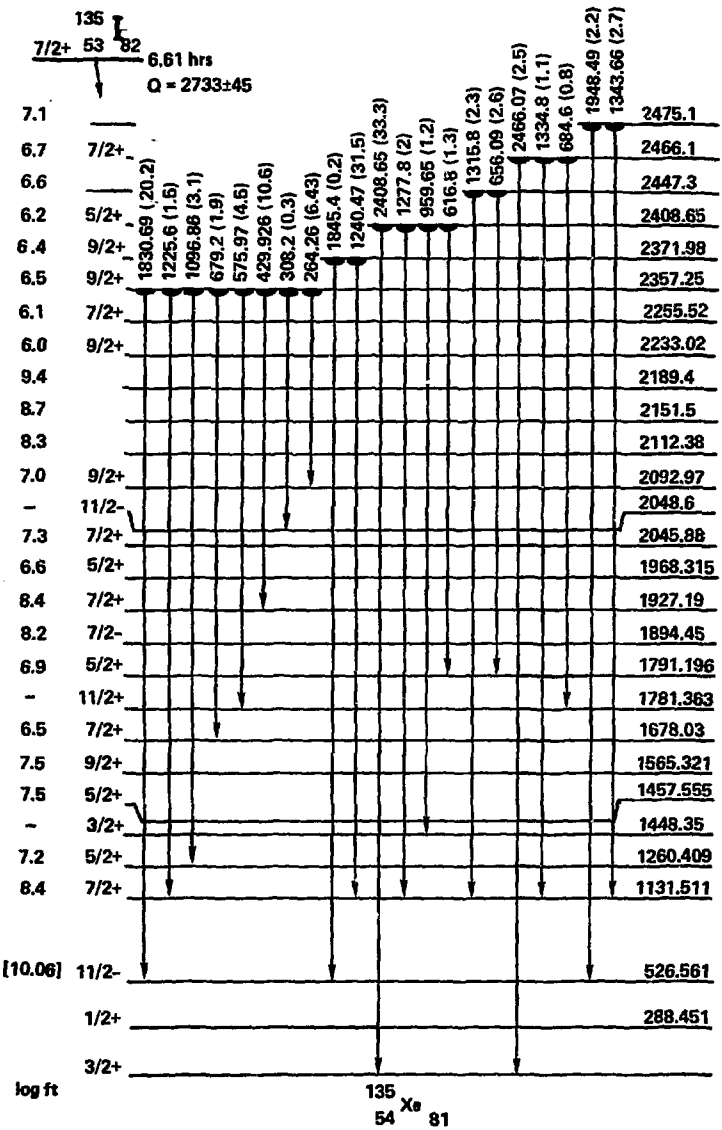
135 I
7/2+ 53 82
6.61 hrs
Q = 2733±45
7.1
6.7 7/2+
6.6
6.2 5/2+
6.4 9/2+
6.5 9/2+
6.1 7/2+
6.0 9/2+
9.4
8.7
8.3
7.0 9/2+
– 11/2-
7.3 7/2+
6.6 5/2+
6.4 7/2+
8.2 7/2-
6.9 5/2+
– 11/2+
6.5 7/2+
7.5 9/2+
7.5 5/2+
– 3/2+
7.2 5/2+
8.4 7/2+
[10.06] 11/2-
1/2+
3/2+
log ft
1830.69 (.20.2)
1225.6 (1.5)
1096.86 (3.1)
679.2 (1.9)
575.97 (4.5)
429.926 (10.6)
308.2 (0.3)
264.26 (6.43)
1845.4 (0.2)
1240.47 (31.5)
2408.65 (33.3)
1277.8 (2)
959.65 (1.2)
616.8 (1.3)
1315.8 (2.3)
656.09 (2.6)
2466.07 (2.5)
1334.8 (1.1)
684.6 (0.8)
1948.49 (2.2)
1343.66 (2.7)
2475.1
2466.1
2447.3
2408.65
2371.98
2357.25
2255.52
2233.02
2189.4
2151.5
2112.38
2092.97
2048.6
2045.88
1968.315
1927.19
1894.45
1791.196
1781.363
1678.03
1565.321
1457.555
1448.35
1260.409
1131.511
526.561
288.451
135 Xe 81
54

Meyer - Fig. 39

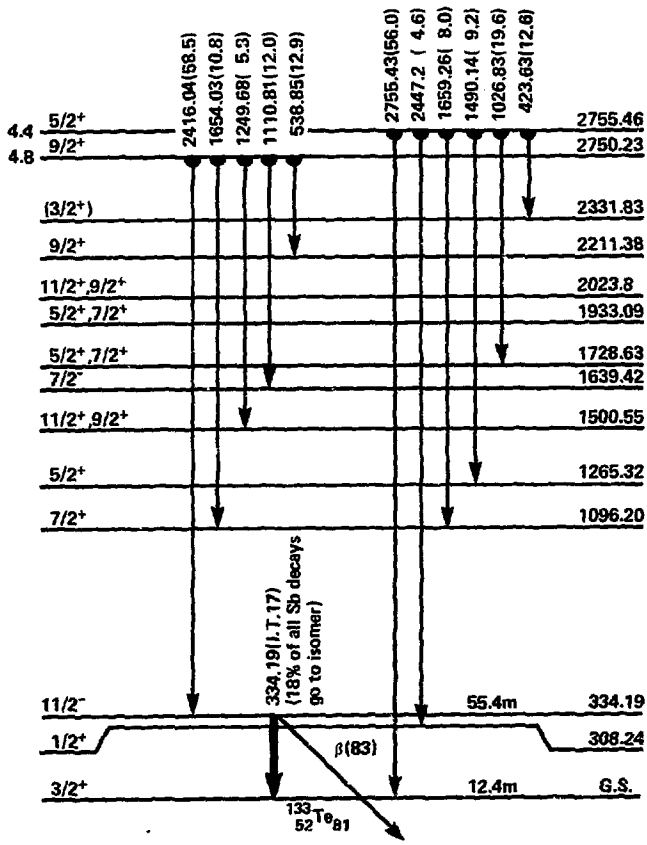
2416.04(58.5)
1654.03(10.8)
1249.68(5.3)
1110.81(12.0)
538.85(12.9)
2755.43(56.0)
2447.2 (4.6)
1659.26(8.0)
1490.14(9.2)
1026.83(19.6)
423.63(12.6)
4.4 5/2+ 2755.46
4.8 9/2+ 2750.23
(3/2+) 2331.83
9/2+ 2211.38
11/2+,9/2+ 2023.8
5/2+,7/2+ 1933.09
5/2+,7/2+ 1728.63
7/2- 1639.42
11/2+,9/2+ 1500.55
5/2+ 1265.32
7/2+ 1096.20
334.19(I.T.17)
(18% of all Sb decays
go to isomer)
11/2- 55.4m 334.19
1/2+ 308.24
β(83)
3/2+ 12.4m G.S.
133 52Te81

Meyer - Fig. 40

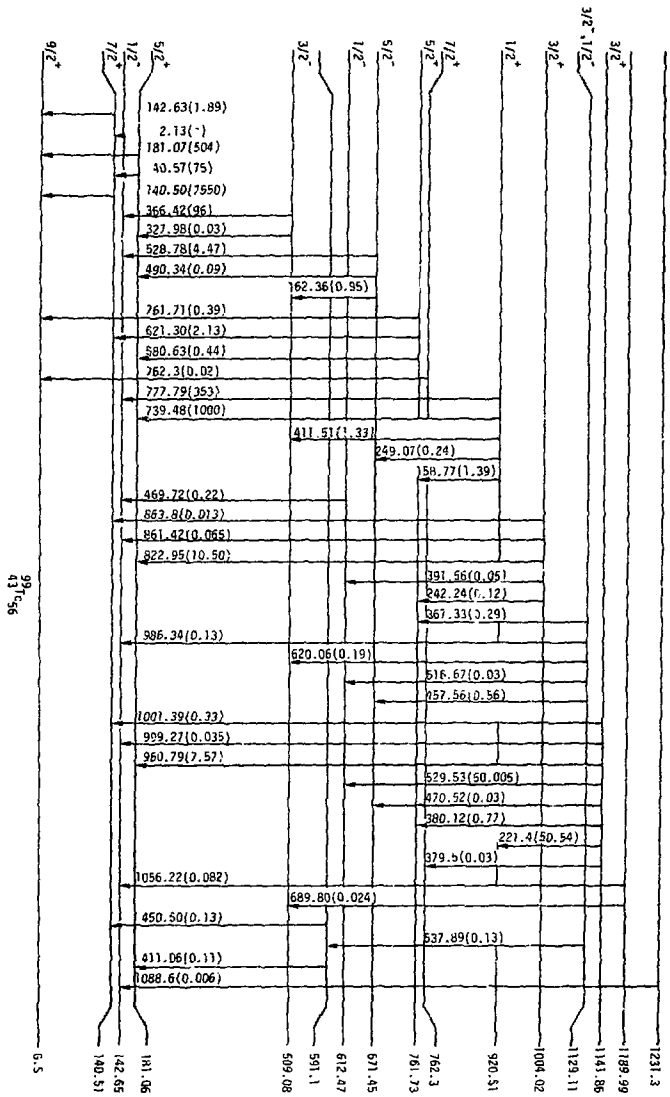
$^{99}_{43}Tc_{56}$
9/2+
7/2+
1/2-
5/2+
3/2-
1/2-
5/2-
5/2-
7/2+
1/2+
3/2+
3/2-,1/2-
3/2+
142.63(1.89)
2.13(-)
181.07(504)
40.57(75)
140.50(7550)
366.42(96)
327.98(0.03)
528.78(4.47)
490.34(0.09)
162.36(0.95)
761.71(0.39)
621.30(2.13)
580.63(0.44)
762.3(0.02)
777.79(353)
739.48(1000)
411.51(1.33)
249.07(0.24)
158.77(1.39)
469.72(0.22)
863.8(0.013)
861.42(0.065)
822.95(10.50)
391.56(0.05)
242.24(0.12)
367.33(0.29)
986.34(0.13)
620.06(0.19)
516.67(0.03)
757.56(0.56)
1001.39(0.33)
909.27(0.035)
960.79(7.57)
529.53(50.005)
470.52(0.03)
380.12(0.77)
221.4(50.54)
379.5(0.03)
1056.22(0.082)
689.80(0.024)
450.50(0.13)
537.89(0.13)
411.06(0.11)
1088.6(0.006)
G.S
140.51
142.65
181.06
509.08
591.1
612.47
671.45
761.73
762.3
920.51
1004.02
1129.11
1141.86
1189.99
1231.3

Meyer - Fig. 41

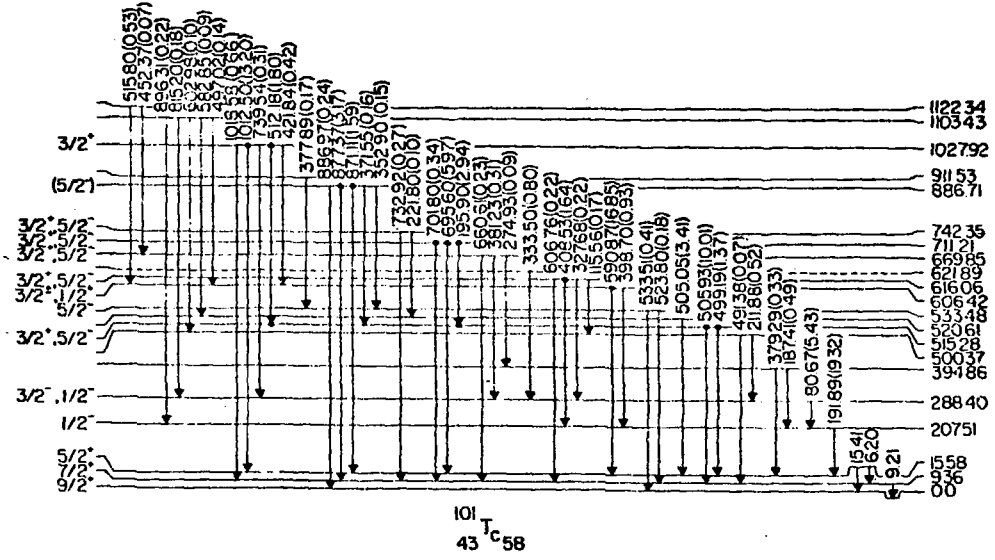

Figure 8. The ^{101}Tc level scheme

Meyer - Fig. 42

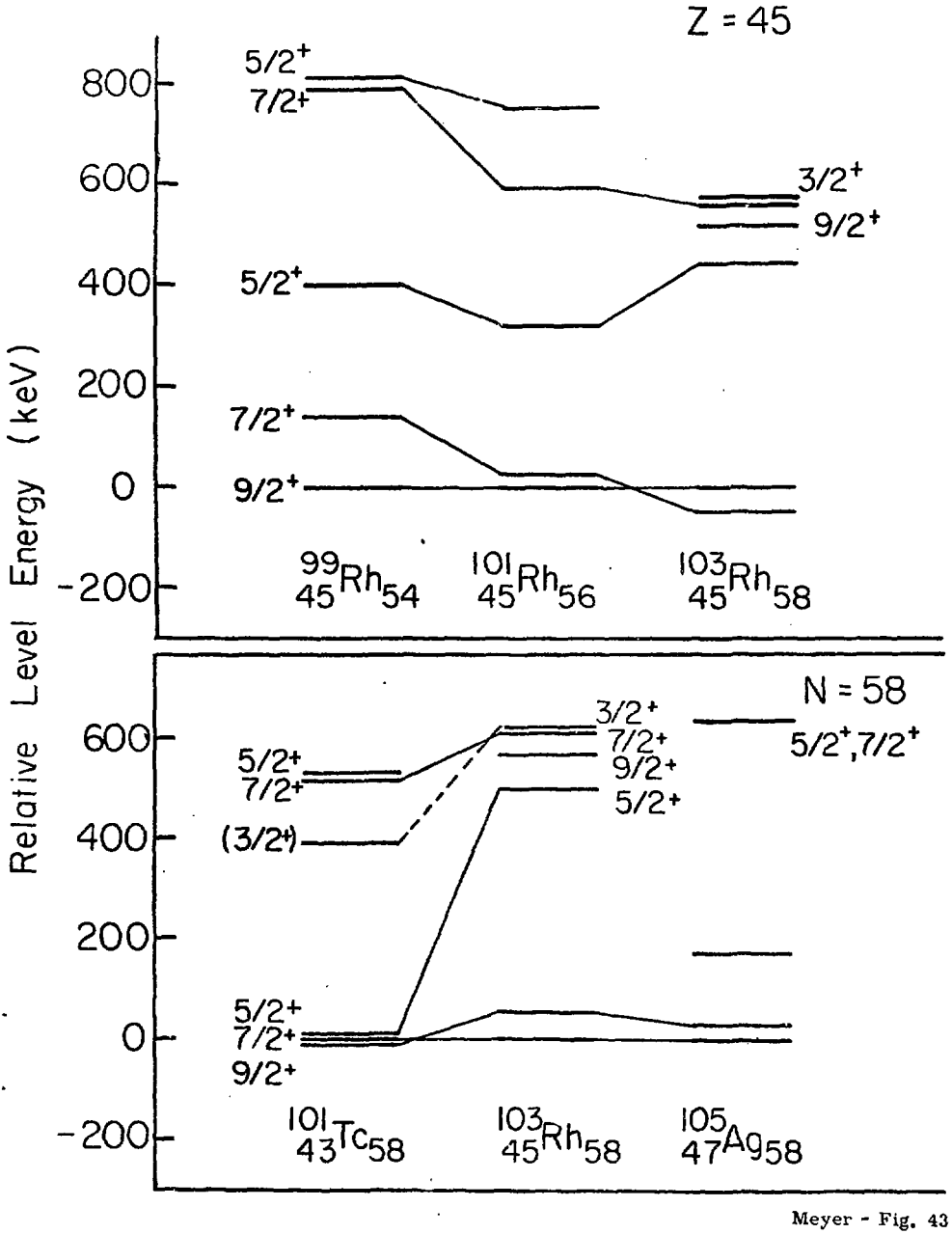
Z = 45
Relative Level Energy (keV)
800
600
400
200
0
-200
5/2+
7/2+
3/2+
9/2+
5/2+
7/2+
9/2+
99 45Rh54
101 45Rh56
103 45Rh58
N = 58
600
400
200
0
-200
3/2+
7/2+
9/2+
5/2+
5/2+,7/2+
5/2+
7/2+
(3/2+)
5/2+
7/2+
9/2+
101 43Tc58
103 45Rh58
105 47Ag58

Meyer - Fig. 43

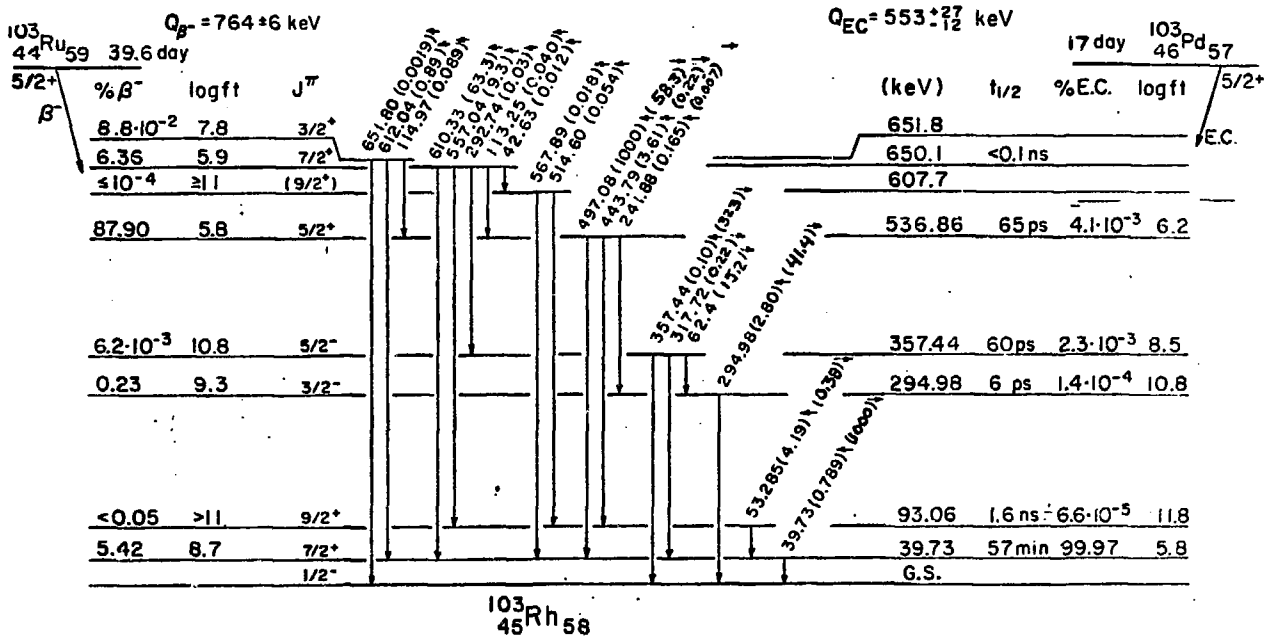
$^{103}_{44}Ru_{59}$ 39.6 day
Q_{β^-} = 764 ± 6 keV
5/2+
β⁻
%β⁻ logft J^π
8.8·10⁻² 7.8 3/2⁺
6.36 5.9 7/2⁺
≤10⁻⁴ ≥11 (9/2⁺)
87.90 5.8 5/2⁺
6.2·10⁻³ 10.8 5/2⁻
0.23 9.3 3/2⁻
<0.05 >11 9/2⁺
5.42 8.7 7/2⁺
1/2⁻
651.80 (0.0019)
612.04 (0.89)
114.97 (0.089)
610.33 (63.3)
557.04 (9.3)
292.74 (0.03)
113.25 (<0.040)
42.63 (<0.012)
567.89 (0.018)
514.60 (0.054)
497.08 (1000)
443.79 (3.61)
241.88 (0.16)
357.44 (0.10)
317.72 (0.22)
62.4 (13.2)
294.98 (41.4)
53.285 (4.19)
39.73 (0.789)
Q_{EC} = 553 +27 −12 keV
17 day $^{103}_{46}Pd_{57}$
5/2+
E.C.
(keV) t1/2 %E.C. logft
651.8
650.1 <0.1 ns
607.7
536.86 65 ps 4.1·10⁻³ 6.2
357.44 60 ps 2.3·10⁻³ 8.5
294.98 6 ps 1.4·10⁻⁴ 10.8
93.06 1.6 ns 6.6·10⁻⁵ 11.8
39.73 57 min 99.97 5.8
G.S.
$^{103}_{45}Rh_{58}$

Meyer - Fig. 44

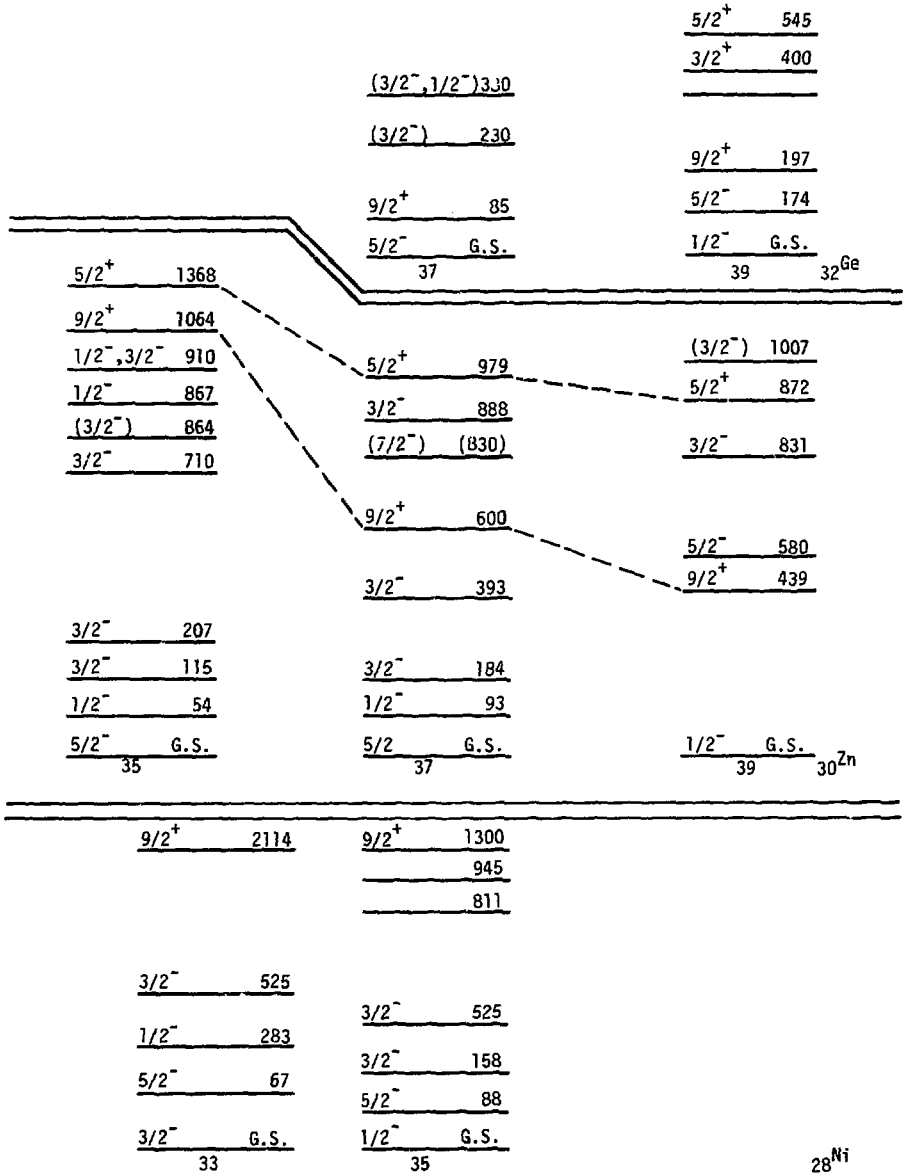
5/2+ 545
3/2+ 400
(3/2-,1/2-)330
(3/2-) 230
9/2+ 197
9/2+ 85
5/2- 174
5/2- G.S.
1/2- G.S.
37
39
32Ge
5/2+ 1368
9/2+ 1064
1/2-,3/2- 910
1/2- 867
(3/2-) 864
3/2- 710
5/2+ 979
3/2- 888
(7/2-) (830)
(3/2-) 1007
5/2+ 872
3/2- 831
9/2+ 600
3/2- 393
5/2- 580
9/2+ 439
3/2- 207
3/2- 115
1/2- 54
5/2- G.S.
3/2- 184
1/2- 93
5/2 G.S.
1/2- G.S.
35
37
39
30Zn
9/2+ 2114
9/2+ 1300
945
811
3/2- 525
1/2- 283
5/2- 67
3/2- G.S.
3/2- 525
3/2- 158
5/2- 88
1/2- G.S.
33
35
28Ni

Meyer - Fig. 45

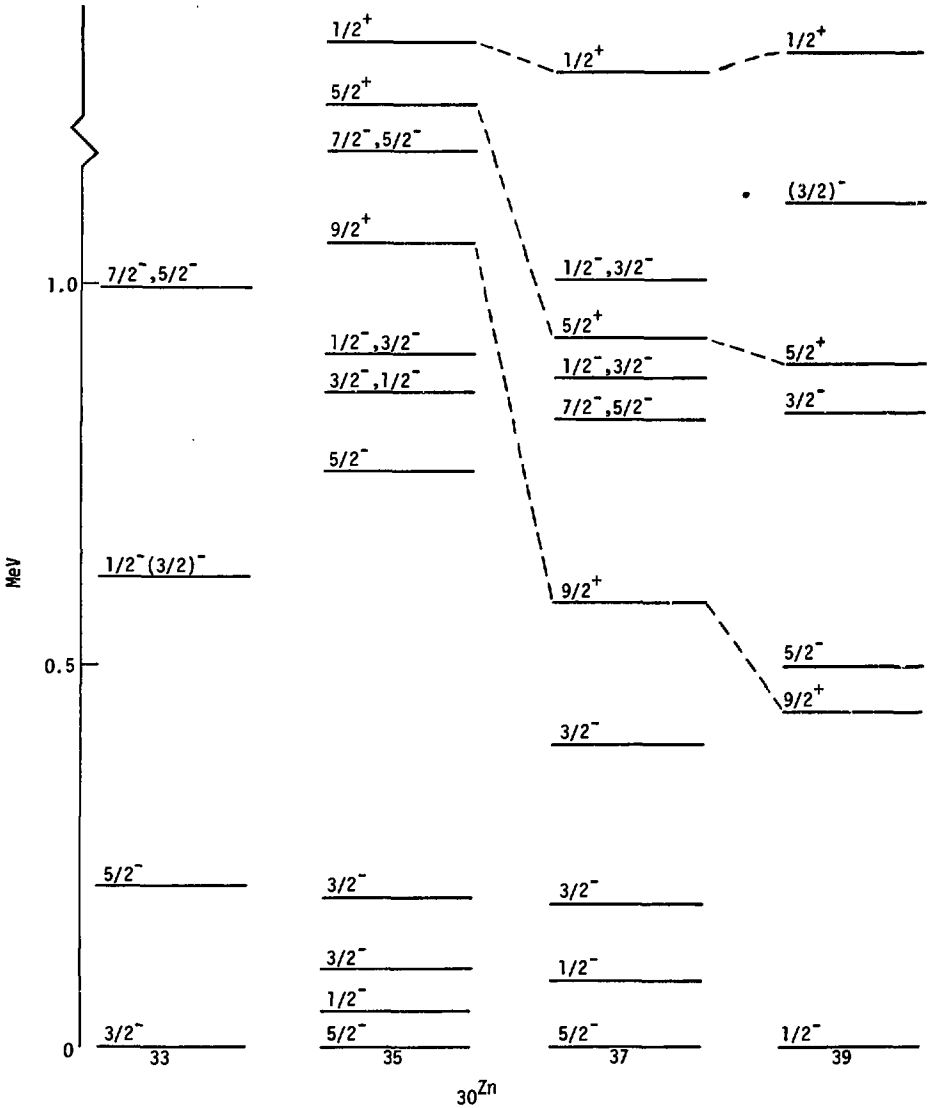
MeV
1.0
0.5
0
7/2⁻,5/2⁻
1/2⁻(3/2)⁻
5/2⁻
3/2⁻
33
1/2⁺
5/2⁺
7/2⁻,5/2⁻
9/2⁺
1/2⁻,3/2⁻
3/2⁻,1/2⁻
5/2⁻
3/2⁻
3/2⁻
1/2⁻
5/2⁻
35
1/2⁺
1/2⁻,3/2⁻
5/2⁺
1/2⁻,3/2⁻
7/2⁻,5/2⁻
9/2⁺
3/2⁻
3/2⁻
1/2⁻
5/2⁻
37
1/2⁺
(3/2)⁻
5/2⁺
3/2⁻
5/2⁻
9/2⁺
1/2⁻
39
30Zn

Meyer - Fig. 46

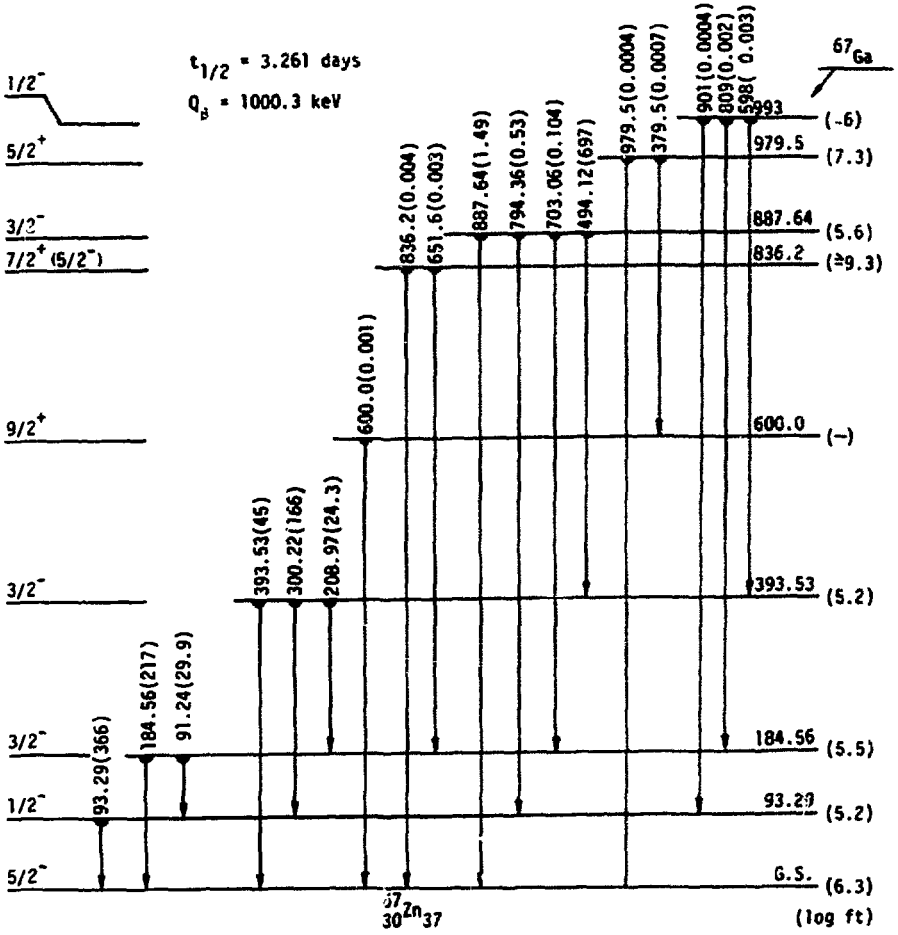
$t_{1/2}$ = 3.261 days
Q_β = 1000.3 keV
^{67}Ga
1/2⁻
5/2⁺
3/2⁻
7/2⁺(5/2⁻)
9/2⁺
3/2⁻
3/2⁻
1/2⁻
5/2⁻
993 (-.6)
979.5 (7.3)
887.64 (5.6)
836.2 (≥9.3)
600.0 (-)
393.53 (5.2)
184.56 (5.5)
93.29 (5.2)
G.S. (6.3)
(log ft)
901(0.0004)
809(0.002)
598(0.003)
979.5(0.0004)
379.5(0.0007)
887.64(1.49)
836.2(0.004)
794.36(0.53)
703.06(0.104)
651.6(0.003)
494.12(697)
600.0(0.001)
393.53(45)
300.22(166)
208.97(24.3)
184.56(217)
91.24(29.9)
93.29(366)
$^{67}_{30}Zn_{37}$

Meyer - Fig. 47

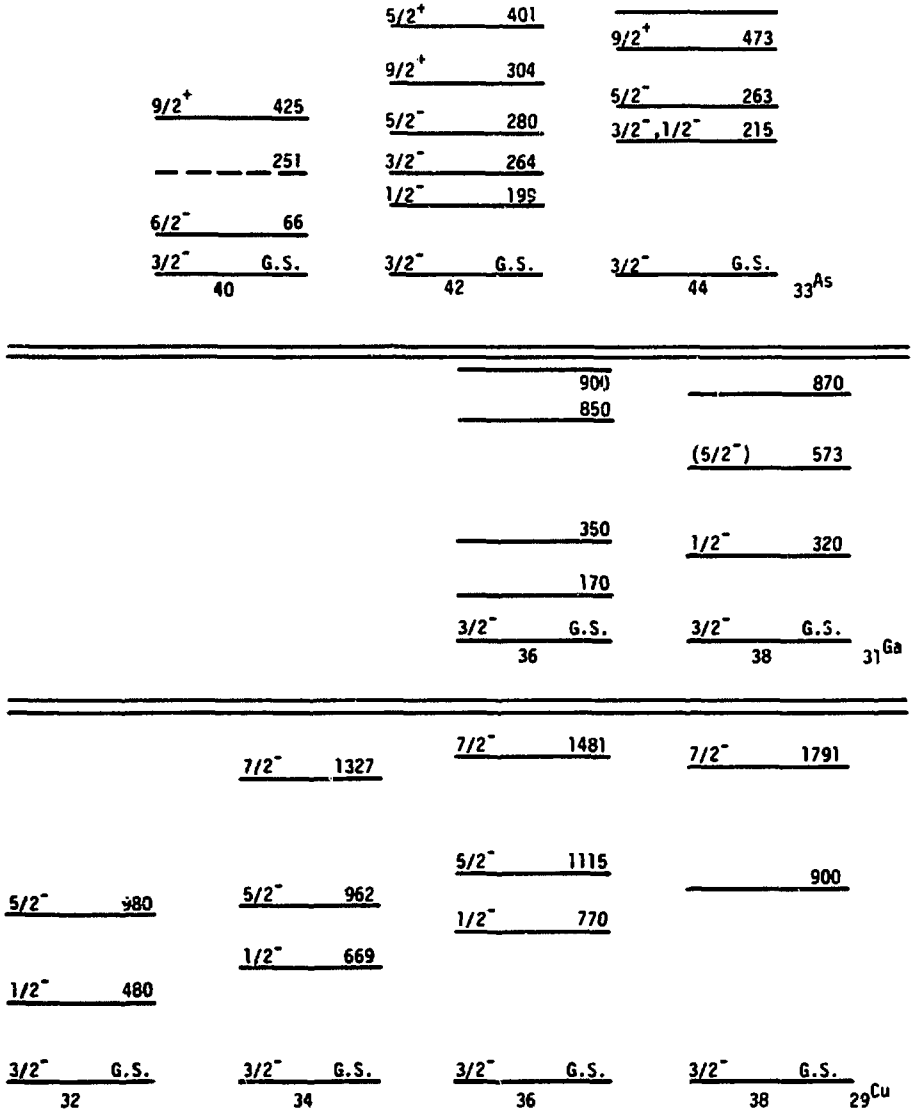
5/2+ 401
9/2+ 304
5/2- 280
3/2- 264
1/2- 199
3/2- G.S.
42
9/2+ 473
5/2- 263
3/2-,1/2- 215
3/2- G.S.
44
33As
9/2+ 425
251
6/2- 66
3/2- G.S.
40
901
850
350
170
3/2- G.S.
36
870
(5/2-) 573
1/2- 320
3/2- G.S.
38
31Ga
7/2- 1481
5/2- 1115
1/2- 770
3/2- G.S.
36
7/2- 1791
900
3/2- G.S.
38
7/2- 1327
5/2- 962
1/2- 669
3/2- G.S.
34
5/2- 980
1/2- 480
3/2- G.S.
32
29Cu

Meyer - Fig. 48

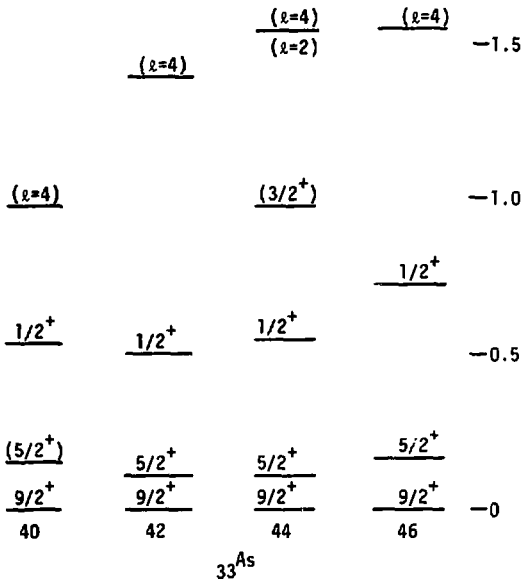
(ℓ=4)
(ℓ=4)
(ℓ=2)
(ℓ=4)
−1.5
(ℓ=4)
(3/2+)
−1.0
1/2+
1/2+
1/2+
1/2+
−0.5
(5/2+)
5/2+
5/2+
5/2+
9/2+
9/2+
9/2+
9/2+
−0
40
42
44
46
33As

Meyer - Fig. 49

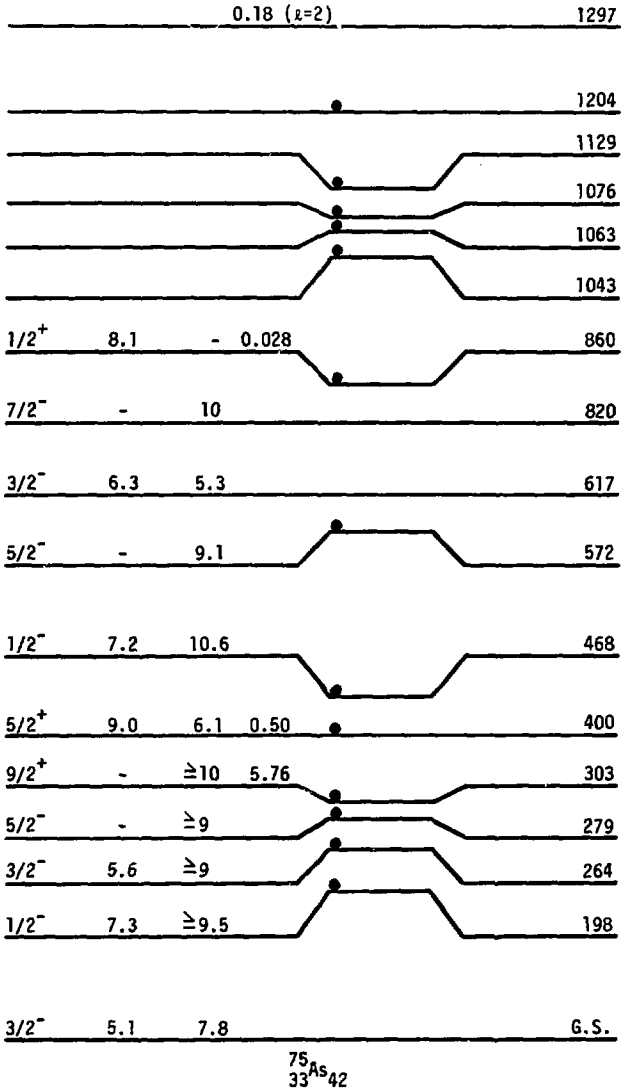
0.18 (ℓ=2) 1297
1204
1129
1076
1063
1043
1/2+ 8.1 - 0.028 860
7/2- - 10 820
3/2- 6.3 5.3 617
5/2- - 9.1 572
1/2- 7.2 10.6 468
5/2+ 9.0 6.1 0.50 400
9/2+ - ≥10 5.76 303
5/2- - ≥9 279
3/2- 5.6 ≥9 264
1/2- 7.3 ≥9.5 198
3/2- 5.1 7.8 G.S.
75 33As42

Meyer - Fig. 50

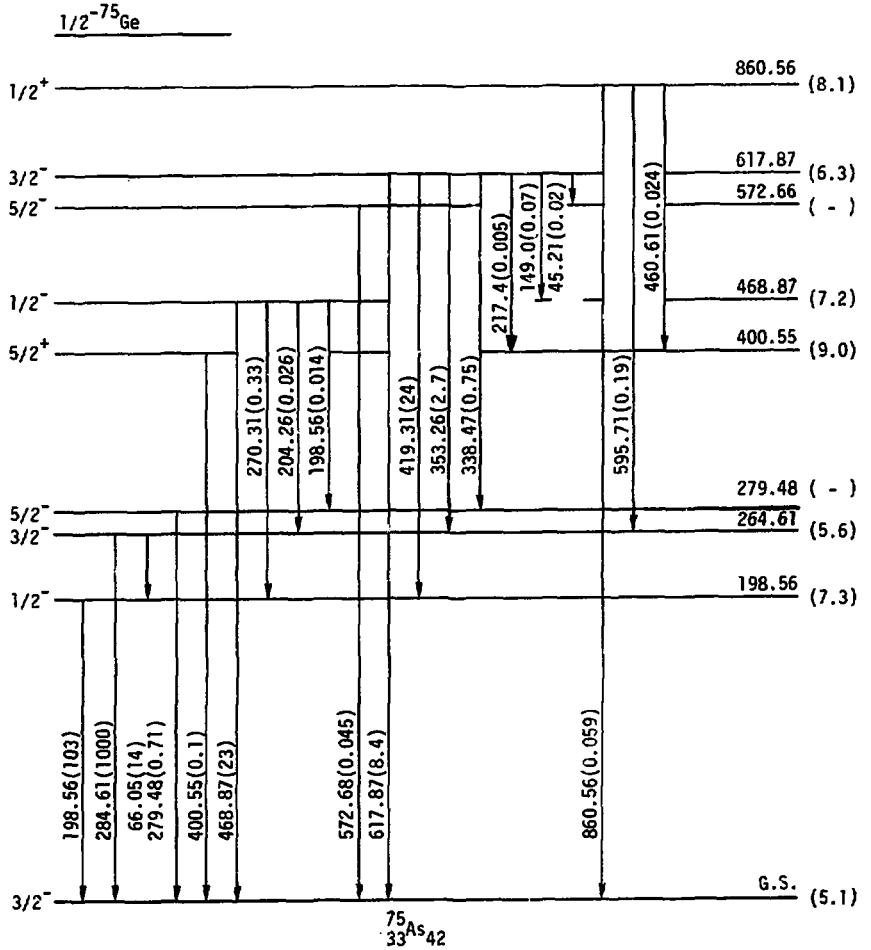
1/2 -75Ge
860.56
(8.1)
1/2+
617.87
(6.3)
3/2-
572.66
(-)
5/2-
468.87
(7.2)
1/2-
400.55
(9.0)
5/2+
279.48
(-)
5/2-
264.61
(5.6)
3/2-
198.56
(7.3)
1/2-
G.S.
(5.1)
3/2-
198.56(103)
284.61(1000)
66.05(14)
279.48(0.71)
400.55(0.1)
468.87(23)
572.68(0.045)
617.87(8.4)
860.56(0.059)
270.31(0.33)
204.26(0.026)
198.56(0.014)
419.31(24)
353.26(2.7)
338.47(0.75)
217.4(0.005)
149.0(0.07)
45.21(0.02)
595.71(0.19)
460.61(0.024)
75 33As42

Meyer - Fig. 51

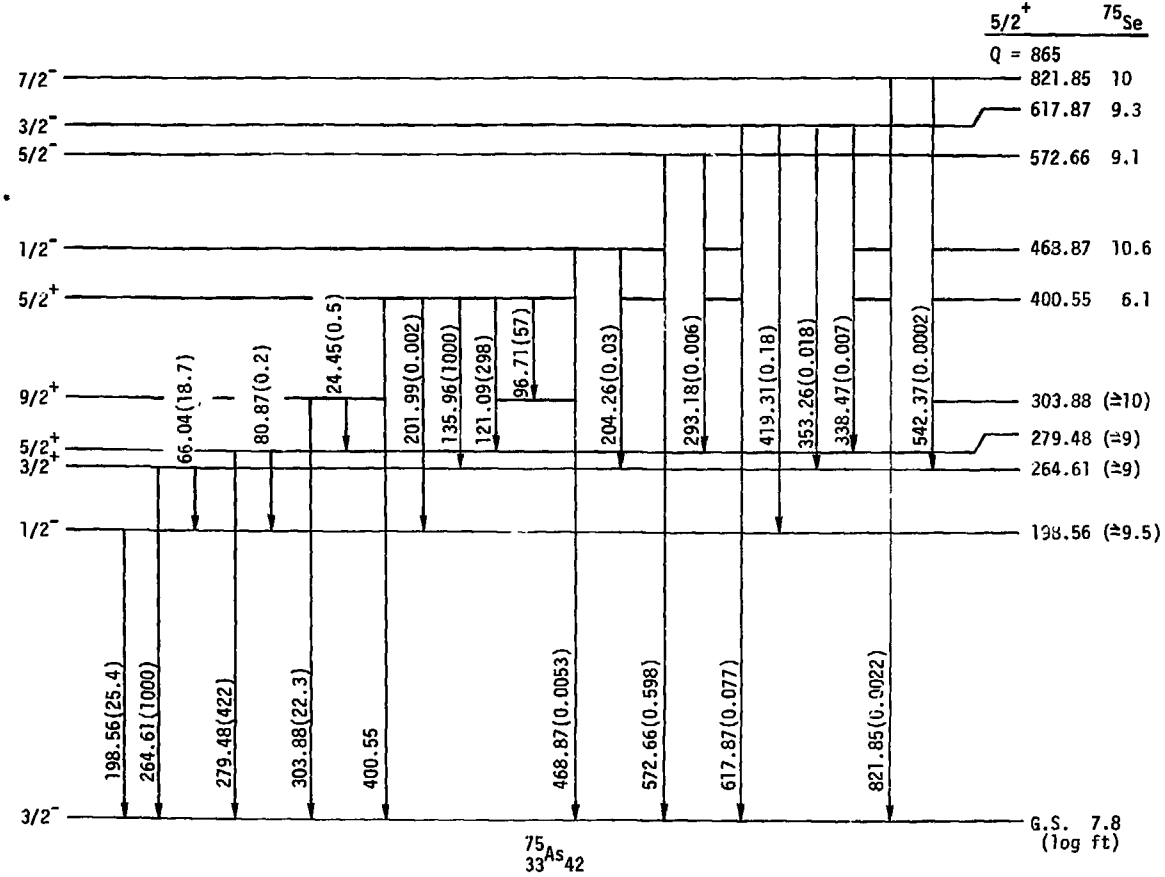
5/2+ 75Se
Q = 865
7/2−
3/2−
5/2−
1/2−
5/2+
9/2+
5/2+
3/2+
1/2−
3/2−
821.85 10
617.87 9.3
572.66 9.1
468.87 10.6
400.55 6.1
303.88 (≐10)
279.48 (≐9)
264.61 (≐9)
198.56 (≐9.5)
G.S. 7.8
(log ft)
24.45(0.5)
66.04(18.7)
80.87(0.2)
96.71(57)
121.09(298)
135.96(1000)
201.99(0.002)
204.26(0.03)
293.18(0.006)
338.47(0.007)
353.26(0.018)
419.31(0.18)
542.37(0.0002)
198.56(25.4)
264.61(1000)
279.48(422)
303.88(22.3)
400.55
468.87(0.0053)
572.66(0.598)
617.87(0.077)
821.85(0.0022)
75As42
33

Meyer - Fig. 52

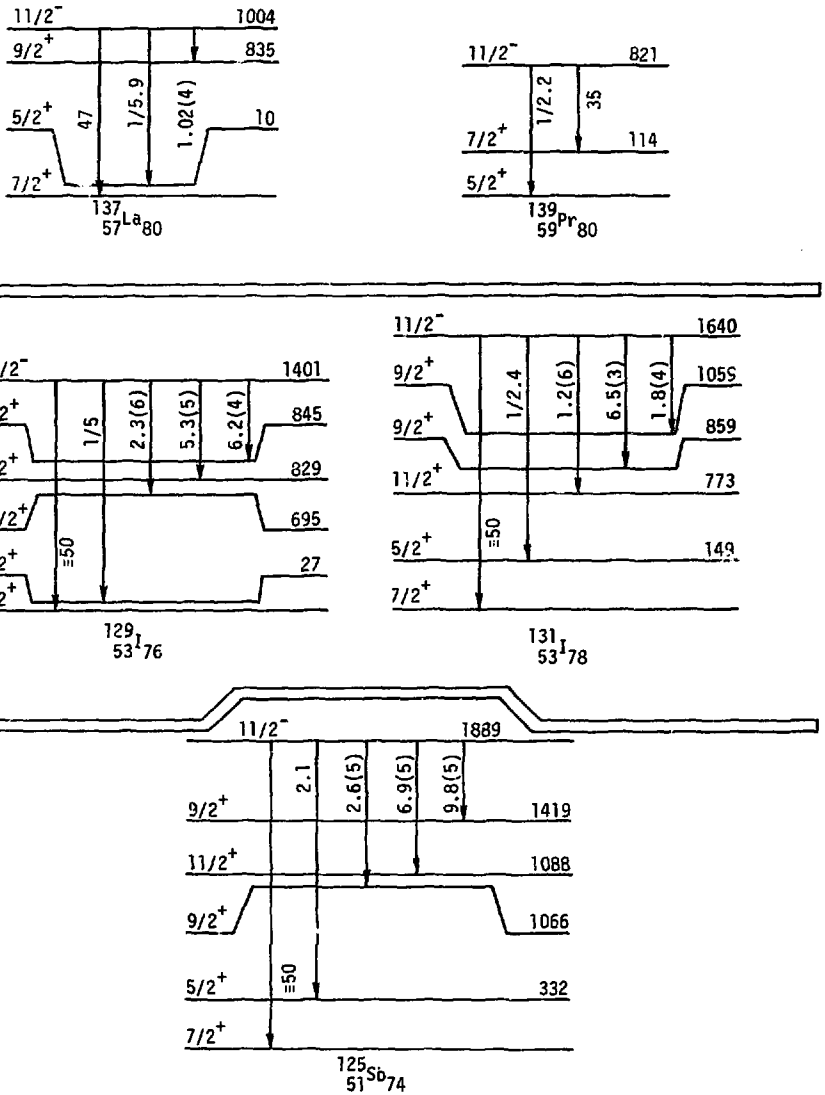
11/2⁻
1004
9/2⁺
835
5/2⁺
47
1/5.9
1.02(4)
10
7/2⁺
137 57La80
11/2⁻
821
1/2.2
35
7/2⁺
114
5/2⁺
139 59Pr80
11/2⁻
1401
9/2⁺
1/5
2.3(6)
5.3(5)
6.2(4)
845
9/2⁺
829
11/2⁺
695
5/2⁺
≡50
27
7/2⁺
129 53I76
11/2⁻
1640
9/2⁺
1/2.4
1.2(6)
6.5(3)
1.8(4)
1059
9/2⁺
859
11/2⁺
773
5/2⁺
≡50
149
7/2⁺
131 53I78
11/2⁻
1889
2.1
2.6(5)
6.9(5)
9.8(5)
9/2⁺
1419
11/2⁺
1088
9/2⁺
1066
5/2⁺
≡50
332
7/2⁺
125 51Sb74

Meyer - Fig. 53

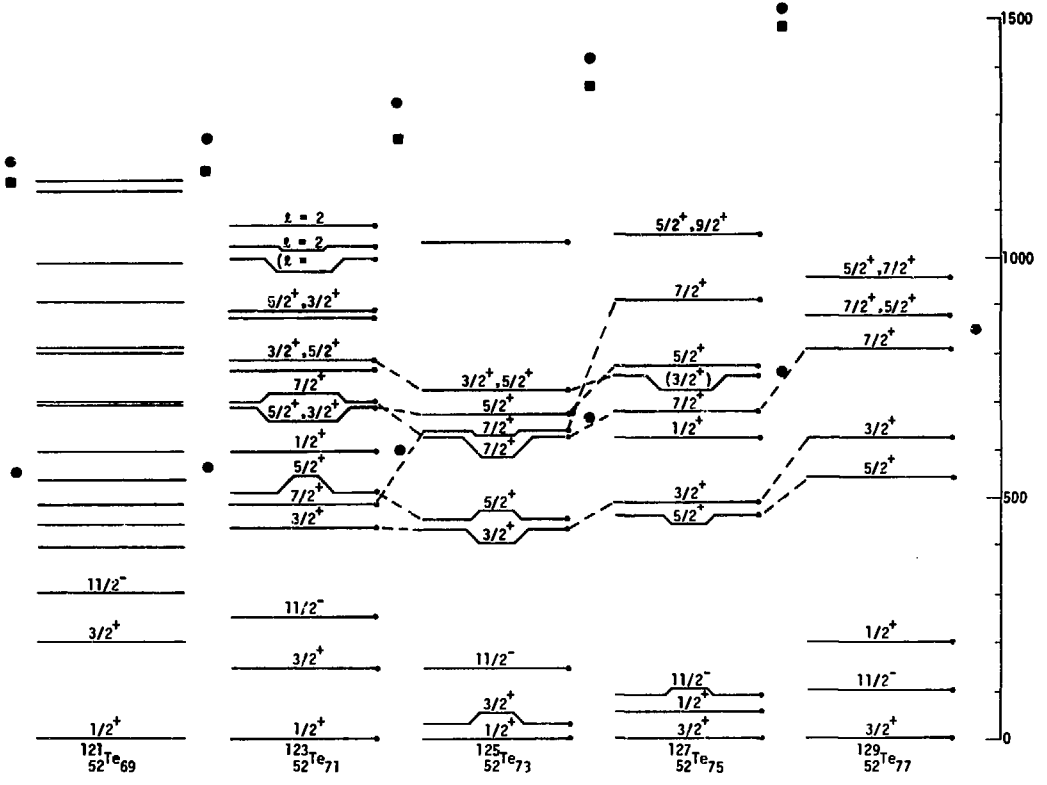
1500
1000
500
0
ℓ = 2
ℓ = 2
(ℓ =
5/2+,3/2+
3/2+,5/2+
7/2+
5/2+,3/2+
1/2+
5/2+
7/2+
3/2+
11/2−
3/2+
1/2+
121 52Te69
3/2+,5/2+
5/2+
7/2+
7/2+
5/2+
3/2+
11/2−
3/2+
1/2+
125 52Te73
5/2+,9/2+
7/2+
5/2+
(3/2+)
7/2+
1/2+
3/2+
5/2+
11/2−
1/2+
3/2+
127 52Te75
5/2+,7/2+
7/2+,5/2+
7/2+
3/2+
5/2+
1/2+
11/2−
3/2+
129 52Te77

Meyer - Fig. 54

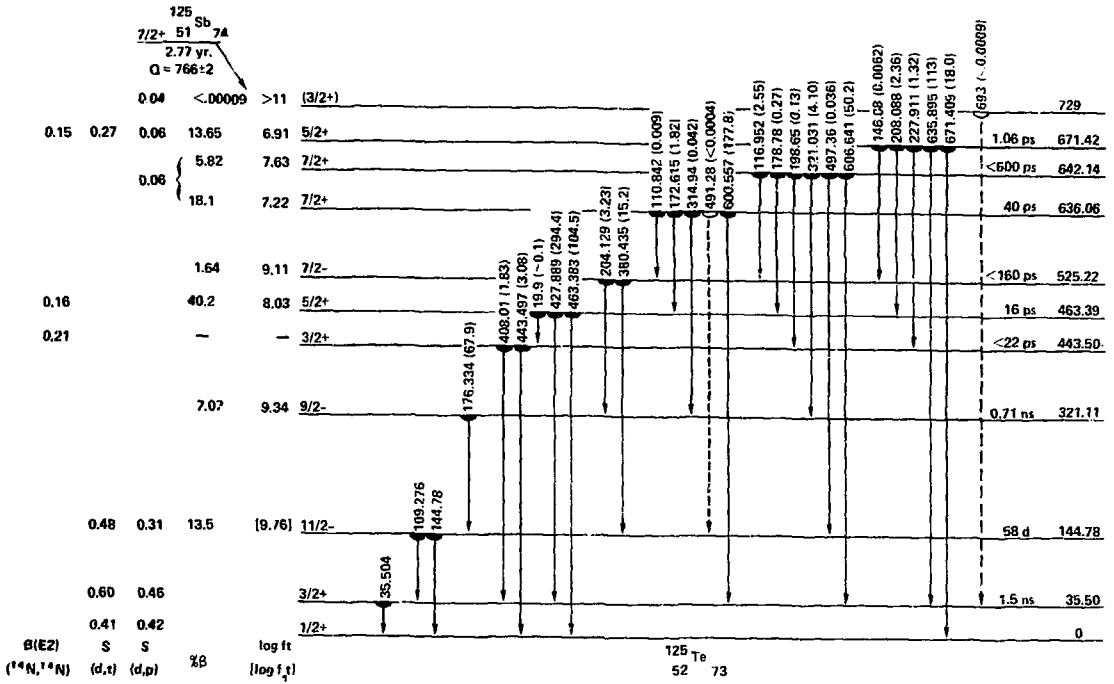
125 Sb 74
51
7/2+
2.77 yr.
Q = 766±2
125 Te
52 73
B(E2)
(14N,14N)
S (d,t)
S (d,p)
%β
log ft
[log f1t]
(3/2+)
5/2+
7/2+
7/2+
7/2-
5/2+
3/2+
9/2-
11/2-
3/2+
1/2+
729
671.42
642.14
636.06
525.22
463.39
443.50
321.11
144.78
35.50
0
1.06 ps
<600 ps
40 ps
<160 ps
16 ps
<22 ps
0.71 ns
58 d
1.5 ns
110.842 (0.009)
172.615 (1.82)
314.94 (0.042)
491.28 (<0.0004)
600.557 (177.8)
116.952 (2.55)
178.78 (0.27)
198.65 (0.13)
321.031 (4.10)
497.36 (0.036)
606.641 (50.2)
146.08 (0.0062)
208.088 (2.36)
227.911 (1.32)
635.895 (113)
671.405 (18.0)
204.129 (3.23)
380.435 (15.2)
427.889 (294.4)
463.383 (104.5)
176.334 (67.9)
408.01 (1.83)
443.497 (3.08)
19.9 (~0.1)
109.276
144.78
35.504

Meyer - Fig. 55

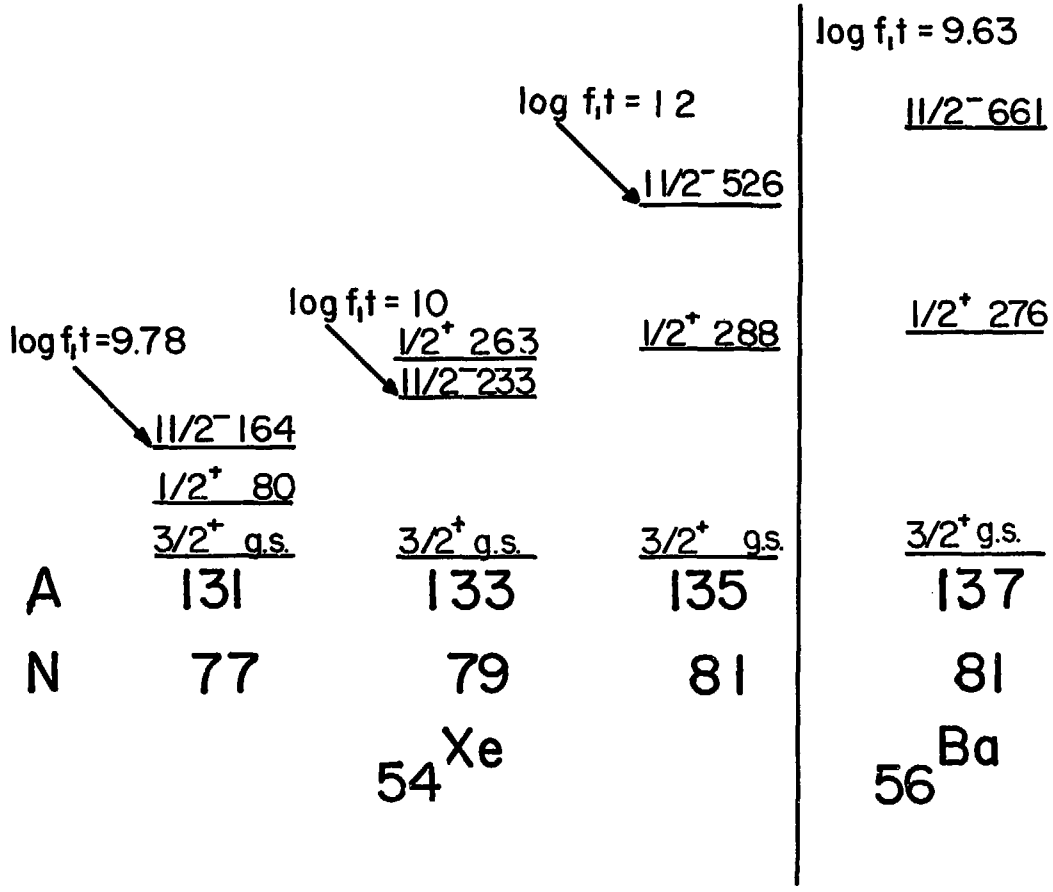
log f₁t = 9.63
log f₁t = 12
11/2⁻ 661
11/2⁻ 526
log f₁t = 10
log f₁t=9.78
1/2⁺ 263
1/2⁺ 288
1/2⁺ 276
11/2⁻ 233
11/2⁻ 164
1/2⁺ 80
3/2⁺ g.s.
3/2⁺ g.s.
3/2⁺ g.s.
3/2⁺ g.s.
A
131
133
135
137
N
77
79
81
81
54 Xe
56 Ba

Meyer - Fig. 56

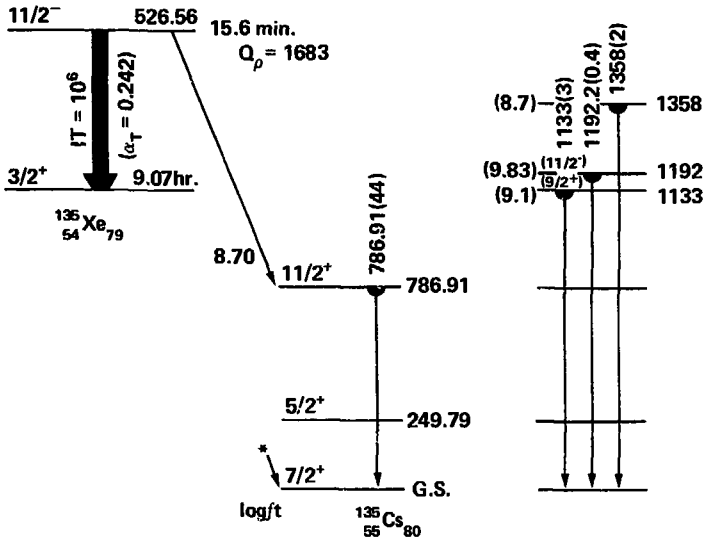

(*n.b. if $\log f_1 t = 10$ then $I_\beta^{g.s.} = 0.02\%$)

Meyer - Fig. 57

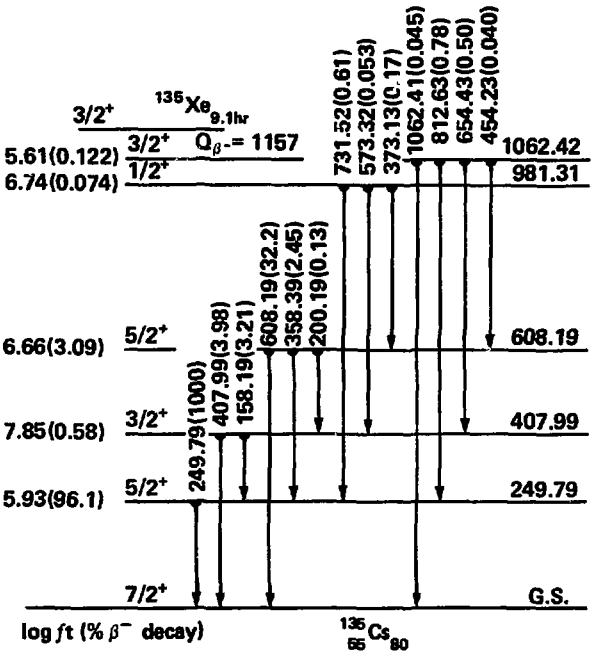
3/2+
135Xe9.1hr
Qβ-= 1157
5.61(0.122) 3/2+
6.74(0.074) 1/2+
6.66(3.09) 5/2+
7.85(0.58) 3/2+
5.93(96.1) 5/2+
7/2+
log ft (% β− decay)
135 55Cs80
731.52(0.61)
573.32(0.053)
373.13(C.17)
1062.41(0.045)
812.63(0.78)
654.43(0.50)
454.23(0.040)
608.19(32.2)
358.39(2.45)
200.19(0.13)
407.99(3.98)
158.19(3.21)
249.79(1000)
1062.42
981.31
608.19
407.99
249.79
G.S.

Meyer - Fig. 58

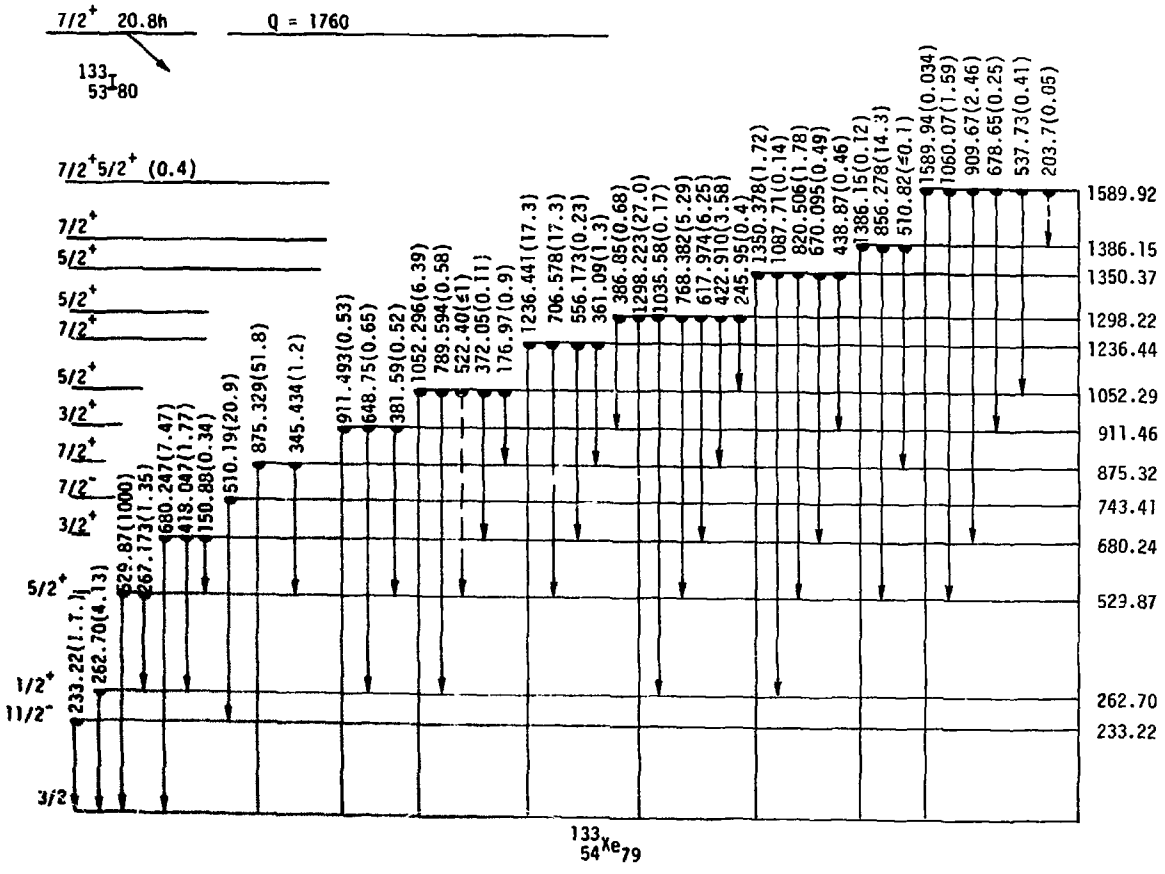
7/2+ 20.8h
Q = 1760
133 53 80
7/2+5/2+ (0.4)
7/2+
5/2+
5/2+
7/2+
5/2+
3/2+
7/2+
7/2-
3/2+
5/2+
1/2+
11/2-
3/2-
529.87(1000)
267.173(1.35)
680.247(7.47)
418.047(1.77)
150.88(0.34)
510.19(20.9)
875.329(51.8)
345.434(1.2)
911.493(0.53)
648.75(0.65)
381.59(0.52)
1052.296(6.39)
789.594(0.58)
522.40(≤1)
372.05(0.11)
176.97(0.9)
1236.441(17.3)
706.578(17.3)
556.173(0.23)
361.09(1.3)
386.85(0.68)
1298.223(27.0)
1035.58(0.17)
768.382(5.29)
617.974(6.25)
422.910(3.58)
245.95(0.4)
1350.378(1.72)
1087.71(0.14)
820.506(1.78)
670.095(0.49)
438.87(0.46)
1386.15(0.12)
856.278(14.3)
510.82(≤0.1)
1589.94(0.034)
1060.07(1.59)
909.67(2.46)
678.65(0.25)
537.73(0.41)
203.7(0.05)
233.22(I.T.)
262.70(4.13)
1589.92
1386.15
1350.37
1298.22
1236.44
1052.29
911.46
875.32
743.41
680.24
529.87
262.70
233.22
133 54 79

Meyer - Fig. 59

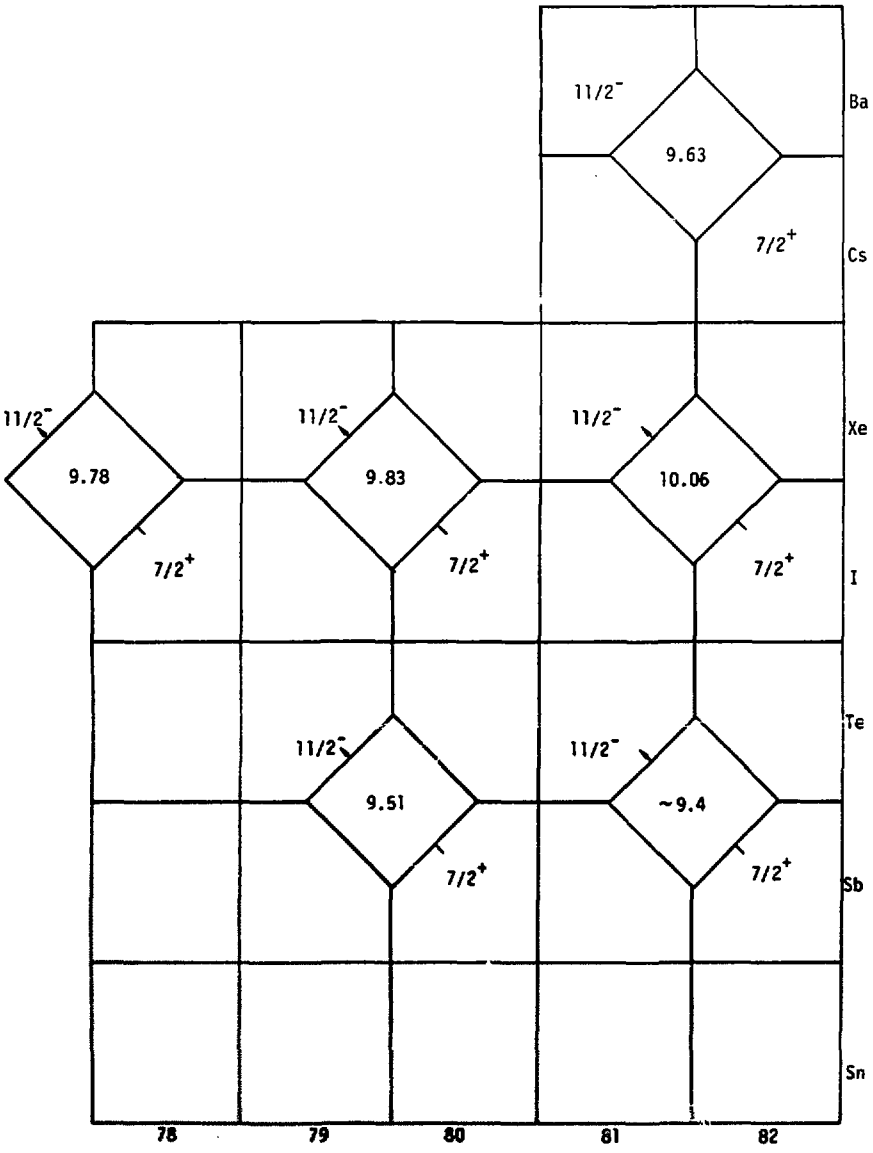
11/2⁻
9.63
7/2⁺
Ba
Cs
11/2⁻
9.78
7/2⁺
11/2⁻
9.83
7/2⁺
11/2⁻
10.06
7/2⁺
Xe
I
11/2⁻
9.51
7/2⁺
11/2⁻
~9.4
7/2⁺
Te
Sb
Sn
78
79
80
81
82

Meyer - Fig. 60

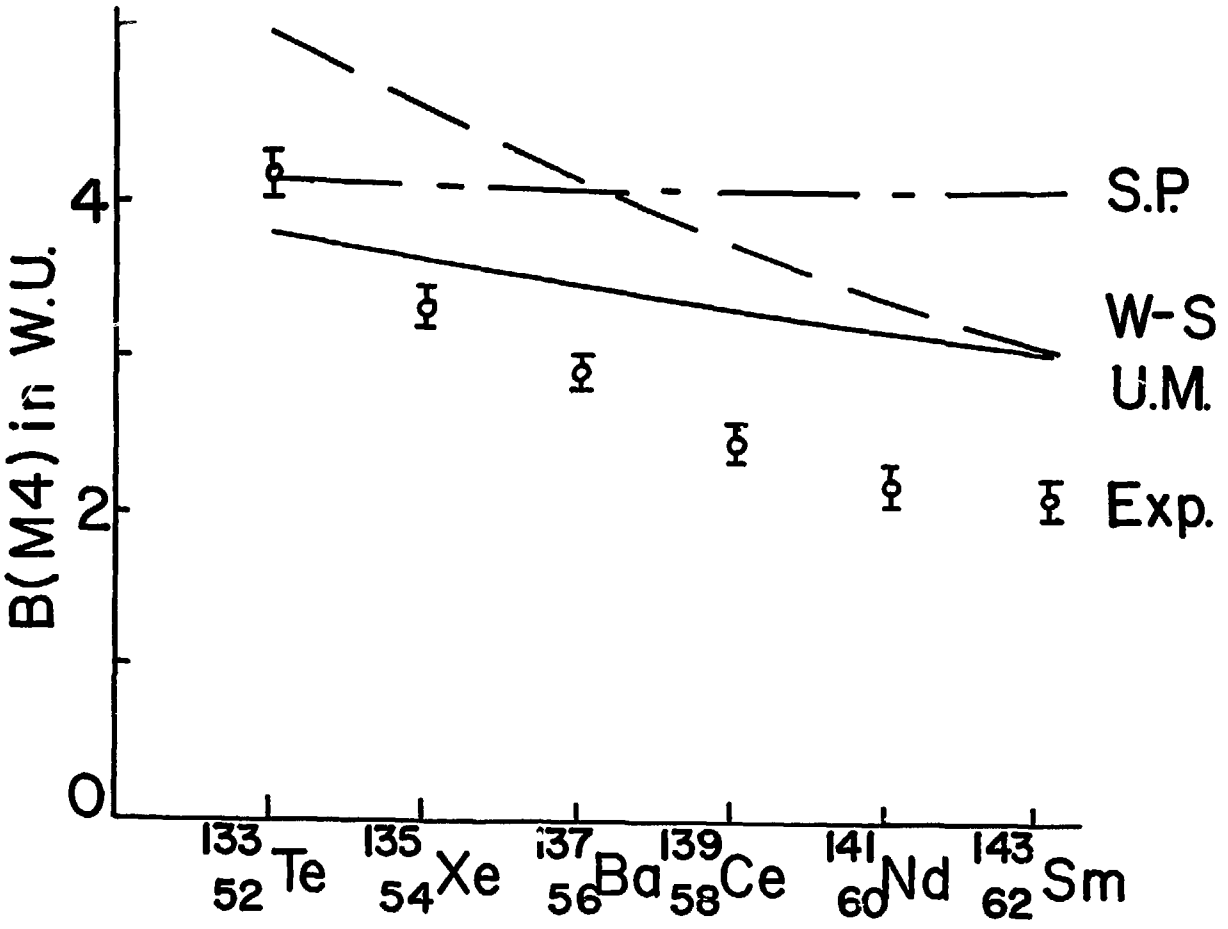
B(M4) in W.U.
4
2
0
S.P.
W-S
U.M.
Exp.
133 52 Te
135 54 Xe
137 56 Ba
139 58 Ce
141 60 Nd
143 62 Sm

Meyer - Fig. 61

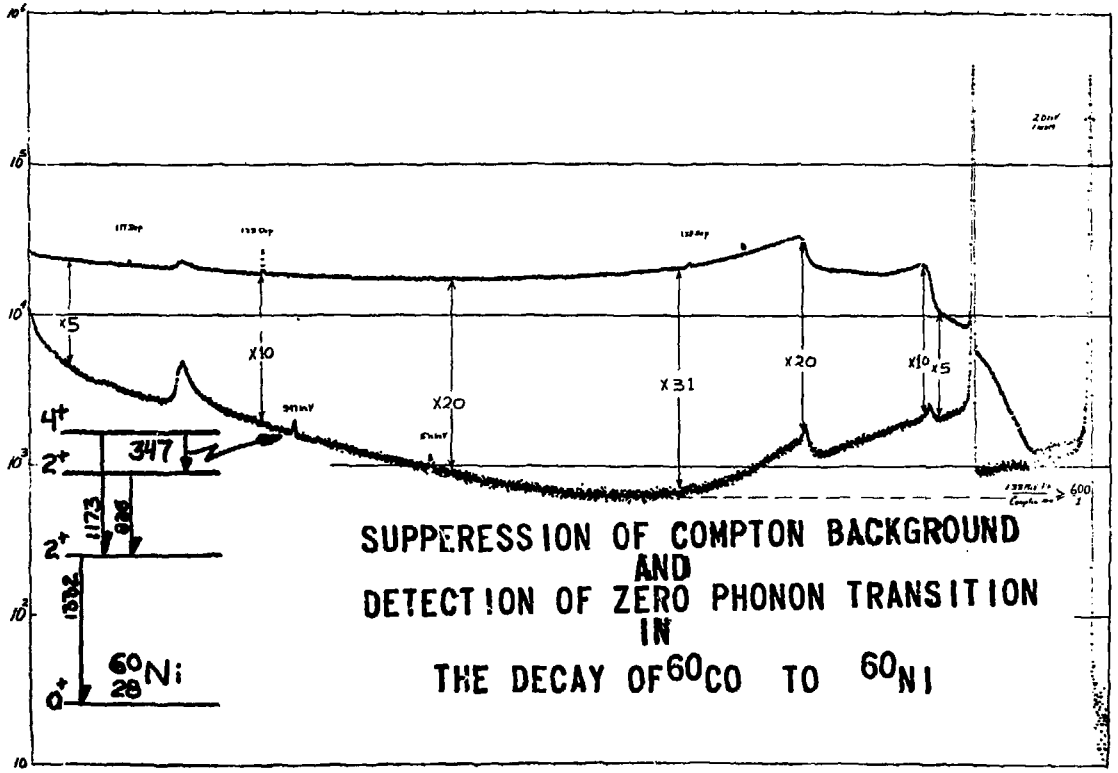
SUPPERESSION OF COMPTON BACKGROUND
AND
DETECTION OF ZERO PHONON TRANSITION
IN
THE DECAY OF ^{60}CO TO ^{60}NI
4+
2+
347
1173
2+
1332
0+
$^{60}_{28}$Ni
X5
X10
X20
X31
X20
X10
X5

Meyer - Fig. 62